Global three-dimensional modelling of minor constituents in the middle atmosphere including the hydrogen escape flux

Dissertation

am Leibniz-Institut für Atmosphärenphysik in Kühlungsborn
zur Erlangung der Doktorwürde
der Mathematisch–Naturwissenschaftlichen Fakultät
der Universität Rostock

von
Ulrich Körner

30. November 2001

Contents

1 Introduction **1**
- 1.1 Radiation and the Greenhouse Effect . . . 2
- 1.2 Middle Atmosphere Modelling . . . 3

2 Basic Description of the Model **6**
- 2.1 Introduction . . . 6
- 2.2 Brief Description of COMMA . . . 7
  - 2.2.1 New Features of COMMA-IAP . . . 8
  - 2.2.2 The Important Process of Gravity Wave Saturation and Breaking 8
- 2.3 Description of the CTM . . . 8
  - 2.3.1 Chemistry Module . . . 9
  - 2.3.2 Revised Concepts of the Model . . . 10
- 2.4 Program Development of the CTM . . . 11
- 2.5 Height of Isobaric Surfaces in the Mesosphere . . . 12

3 Chemistry **14**
- 3.1 Elementary Reaction Kinetics . . . 14
  - 3.1.1 First Order Process . . . 15
  - 3.1.2 Second Order Process . . . 15
  - 3.1.3 Steady State . . . 16
  - 3.1.4 Unimolecular Reactions . . . 17
  - 3.1.5 Termolecular Reactions . . . 18
  - 3.1.6 Thermodynamic Considerations . . . 19
- 3.2 Calculation Concepts . . . 20
  - 3.2.1 Explicit Euler Method . . . 21
  - 3.2.2 Implicit Euler Method . . . 22
  - 3.2.3 Implicit Method with Quadratic Loss Term . . . 23
  - 3.2.4 The Concept of Chemical Families . . . 24
- 3.3 Impact of Dynamics on Chemistry . . . 25
- 3.4 Chemical Reactions and Rate Constants . . . 27

3.5 Photodissociation 32

4 Transport **33**
4.1 Modelling of Transport Processes 33
4.2 Advection Schemes 35
4.2.1 Euler Forward Differencing 35
4.2.2 Upwind Differencing Scheme 35
4.2.3 Smolarkiewicz Scheme 36
4.3 Summary of Transport 39
4.3.1 Interesting Schemes for Further Development 40

5 Diffusion **41**
5.1 Barometric Law and Scale Height 41
5.2 Vertical Stability 42
5.3 Vertical Mixing of the Atmosphere 43
5.3.1 Modelling of the Turbulent Mixing 43
5.3.2 Modelling of the Molecular Diffusion 44
5.4 Calculation Concepts 45
5.4.1 Eddy Diffusion 45
5.4.2 Molecular Diffusion 47
5.5 Discretization of the Diffusion Equation 51
5.5.1 Explicit or Implicit Solution? 51
5.5.2 Solution of the Implicit Scheme 52
5.5.3 Implicit Scheme for the Complete Diffusion Equation 55
5.6 Calculation Concept for the Fluxes 56

6 Data from COMMA-IAP **58**

7 CTM-Results of Important Constituents **63**
7.1 Water Vapour and the Hydrogen Constituents 63
7.1.1 Water Vapour Correlated Phenomena 65
7.1.2 Water Vapour Measurements 66
7.1.3 Modelling Results 68
7.2 Ozone and the Oxygen Constituents 77

8 Flux Calculation for Hydrogen Constituents **82**
8.1 Introduction 82
8.2 Atmospheric Escape 83
8.3 Boundary Conditions 84
8.4 Results 85
8.5 Total Hydrogen in the Middle Atmosphere 89

9 Chemical Heating **90**
9.1 Introduction 90
9.2 Modelling Results 91

10 Summary **94**
10.1 Summary 94
10.2 Future Tasks with the CTM 94

List of Figures

2.1 Geometric heights and isobaric surfaces in the mesosphere 13

3.1 Methane decomposition by $O(^1D)$ 31

6.1 Latitudinal section of the zonally averaged temperature 59
6.2 Latitudinal section of the zonally averaged zonal wind 60
6.3 Latitudinal section of the zonally averaged meridional wind 61
6.4 Latitudinal section of the zonally averaged vertical wind 61
6.5 Seasonal section of the zonally averaged vertical wind at 72.5° N . . . 62

7.1 Height profile of hydrogen constituents at 2.5° N 64
7.2 Latitudinal section of H_2O with isobaric surfaces 69
7.3 Surface section of H_2O at 88 km height 70
7.4 Microwave water vapour measurements 71
7.5 Seasonal section of H_2O at 72.5° N 73
7.6 Seasonal section of H_2 at 72.5° N 73
7.7 Seasonal section of H_2O at 2.5° N 74
7.8 Seasonal section of H_2 at 2.5° N 74
7.9 Seasonal section of the total characteristic transport time for H_2O . . 75
7.10 Latitudinal section of the total characteristic transport time for H_2O 75
7.11 Seasonal section of the effective characteristic chemical time for H_2O . 76
7.12 Latitudinal section of the effective characteristic chemical time for H_2O 76
7.13 Height profile of oxygen constituents at 2.5° N 79
7.14 Latitudinal section of O at solstice, 12LT 80
7.15 Latitudinal section of O at solstice, 24LT 80
7.16 Latitudinal section of O_3 at solstice, 12LT 81
7.17 Latitudinal section of O_3 at solstice, 24LT 81

8.1 Sensitivity study of eddy diffusion coefficients 86
8.2 Total hydrogen, standard K_{zz} profile 87
8.3 Hydrogen fluxes, standard K_{zz} profile 87

8.4 Total hydrogen, decreased K_{zz} profile 87
8.5 Hydrogen fluxes, decreased K_{zz} profile 87
8.6 Total hydrogen, increased K_{zz} profile 88
8.7 Hydrogen fluxes, increased K_{zz} profile 88

9.1 Latitudinal section of chemical heating at solstice, 12LT 93
9.2 Latitudinal section of chemical heating at solstice, 24LT 93

Chapter 1

Introduction

Water makes the Earth unique. Life, the climate and the weather all exist as they do because gaseous, liquid and solid forms of water can coexist on the planet. The oceans, the ice masses, the clouds and the humidity of the atmosphere all play major roles in climate and weather [*Peixoto and Oort*, 1996].

The composition of the atmosphere is a key determinant of Earth's climate. The interaction of atmospheric gases with radiant energy modulates the flow of energy through the climate system. The mass of the atmosphere ($5.14\ 10^{18}$ kg) is about three orders in magnitude smaller than the mass of the ocean ($1.39\ 10^{21}$ kg) which is about three orders smaller than the mass of the solid earth ($5.98\ 10^{24}$ kg). The atmospheric gases that are important for the absorption and emission of radiant energy comprise less than 1 % of the atmosphere's mass. These include water vapour ($3.3\ 10^{-3}$ of the atmosphere's total mass), carbon dioxide ($5.3\ 10^{-4}$), and ozone ($6.42\ 10^{-7}$), in order of importance for surface temperature, followed by methane, nitrous oxide, and a host of other minor species [*Hartmann*, 1994].

These two citations show the immense relevance of water and water vapour on earth and in the atmosphere. A detailed knowledge about the distribution of water vapour in the atmosphere is essential for atmospheric and climate science.

There is a significant increase in the number and quality of stratospheric water vapour measurements in the last 25 years. Global observations were possible with the advent of satellite technique. The stated accuracy of most of the in situ and remote instruments cluster within a ± 10 % range. Additional effort, however, is necessary in the stratosphere and especially in the mesosphere.

In the foreword of the SPARC (Stratospheric Processes and their Role in Climate) assessment of upper tropospheric and stratospheric water vapour [*Kley et al.*, 2000] the editors write: Considering the fundamental role of water vapour in climate, and the scarcity of information concerning its distribution, variability and long-term evolution, the need for such an assessment was recognized by the SPARC Scientific

Steering Group. The lack of knowledge on water vapour also leads to a large uncertainty in the prediction of climate change.

The lack of knowledge on water vapour in the mesosphere is comparable or even worse because the important microwave observations are limited to about 85 km in altitude. At a distinct height Noctilucent Clouds (NLCs) are observed and small changes in the temperature and the water vapour distribution have influence on the cloud formation.

1.1 Radiation and the Greenhouse Effect

What makes the gases H_2O, CO_2, and O_3 so important for the surface temperature and the heat balance of the atmosphere?

At wavelengths in the infrared over 4 μm the terrestrial emissions dominate the solar input. For the emission temperature of the earth of ≈ 255 K the emission peaks at around 10 μm, while the emission peak of the sun lies at around 0.6 μm. Looking at the black body emission spectra for both, the emitted energy at 4 μm is very small compared to the emitted energies at the peaks of both spectra, so that solar and terrestrial radiation can be seen as two separate entities.

Water vapour is a non-linear molecule with a complex vibration-rotation spectrum. It has a permanent dipole moment and therefore pure rotation bands and in addition vibration-rotation bands (vibrational transitions usually involve a change in the rotational energy). Water vapour has an important vibration-rotation band ν_2 near 6.3 μm, and a densely spaced band of pure rotational lines at about 12 μm which strongly absorbs terrestrial emission. Between these wavelength regions there is an interval with relatively weak absorption called the water vapour window where longwave radiation can pass relatively freely through the atmosphere. In the middle of this window sits the ν_3 band (9.6 μm) of ozone. These two absorption features make the troposphere nearly opaque to longwave radiation.

Carbon dioxide is a linear molecule with a relatively simple absorption spectrum. It has no permanent dipole moment and has no pure rotational transitions. During vibrational transitions the CO_2 molecule develops temporary dipole moments so that rotational transitions can accompany a vibrational transition. By the combination of possible vibrational and rotational transitions the molecule can absorb or emit photons at a large number of closely spaced frequencies which declares the term absorption band. The ν_3 band (4.3 μm) is strong but has a marginal influence because both solar and terrestrial emissions are weak. The ν_2 band (15 μm) is important for the energy budget of the earth because it is located close to the peak wavelength of the terrestrial emission.

For the middle atmosphere, the most important trace gases from a thermal point of view are ozone, carbon dioxide and water vapour in the order of their importance.

In the middle atmosphere the primary energy loss is due to radiative emission in the ν_2 band of CO_2 at 15 μm. The primary heat input occurs via absorption by ozone which produces the increase in temperature in the stratosphere.

The atmospheric green house effect leads to higher temperature than the emission temperature of the earth. The absorbed solar radiation is compensated by the radiation emitted from the earth as a black body with a certain temperature. Heat, in the form of infrared radiation, that would normally be dissipated to outer space, is absorbed by atmospheric constituents like H_2O, CO_2 and CH_4, leading to heating of the earth's lower atmosphere. When the atmospheric concentrations of some of these species increases (for example CO_2 and other by anthropogenic activity), the potential for altering the earth's climate is given.

1.2 Middle Atmosphere Modelling

The main interest in modelling the dynamic and chemistry of the middle atmosphere is focused on the stratospheric ozone layer and related problems. There are several research groups in Germany working on this field (Hamburg, Berlin, Mainz, Karlsruhe, and München). The mesosphere is included as an upper model domain and the sensitive mesopause region is excluded. Many excellent scientific papers and books exist about the middle atmosphere, but here just one reference is given with 31 pages of reference to papers and literature about atmospheric research [*Brasseur et al.*, 1999].

The focus of this work is the distribution of the minor constituents (including water vapour and ozone) in the region of the mesosphere and lower thermosphere (MLT-region), according to the main research fields of the Institute of Atmospheric Physics in Kühlungsborn where observations are mainly located in the mesospheric height region. The IAP is operating lidar and radar devices in Kühlungsborn, Andoya (Northern Norway), and part time of the year a transportable lidar in a container on mount Teide at Tenerife, or at Longyearbyen on Svalbard (Northern Norway). NLCs and PMSEs (Polar Mesospheric Summer Echoes) are observed, both by lidar and radar [*von Zahn and Bremer*, 1999], [*Alpers et al.*, 2000].

One point of interest in the understanding of NLC and PMSE observations is the basic distribution of water vapour in 80–90 km altitude. Micro wave measurements by *Seele and Hartogh* [1999] at Andoya go slightly higher than 80 km and lidar detection in the typical NLC height of 82–84 km allows estimates for water vapour but there is still need for modelling of the distribution and annual variation of water vapour mixing ratios, especially for northern summer conditions, which can be compared with the observed mixing ratios.

There are some two-dimensional models, including the mesospheric height range, from *Brasseur et al.* [1990], *Yang et al.* [1991], *Jackman et al.* [1991], *Garcia et al.* [1992], *Ko et al.* [1993], and *Summers et al.* [1997a]. Two-dimensional models,

however, if using the diurnal average of the dissociation rates, are not able to calculate the distribution of constituents with lifetimes comparable to 1 day.

There are also some three-dimensional models including the mesosphere and lower thermosphere (MLT). The model of *Arnold and Robinson* [1998] has a height range from 10 to 140 km. *Brasseur and de Baets* [1986], *Richmond et al.* [1992], and *Roble and Ridley* [1994] are modelling dynamics and chemistry of the thermosphere. The model of *Roble and Ridley* [1994] has a height range from 30–500 km.

For the calculation of the diurnal average water vapour distribution, there would be no need for a three-dimensional model. The lidar observations, however, give precise height information about NLC detection all over the day. The diurnal variation of the received signal raises the interest in a three-dimensional time dependent model, if the vertical resolution is small enough.

Each model has an upper boundary with boundary conditions of Dirichlet- or von Neumann type. The model results at the boundary region are in general less realistic than in the inner domain because the model is forced in some way to these values. The question is to find a suitable height for the upper boundary. ECHAM4-MA, a version of the successful ECHAM model in Hamburg is extended up to 0.01 hp (approx. 80 km). In the height region from 75–105 km momentum from breaking gravity waves is deposited. From the viewpoint of atmospheric dynamics the pressure of 0.01 hp as the upper boundary makes it difficult to get realistic wind fields in the upper model domain. For modelling of the mesosphere the upper boundary has to be above the height region of breaking gravity waves.

The chemistry of the mesosphere is strongly determined by hydrogen species and thus by water vapour as the main source of the odd-hydrogens like OH, HO_2, and H. The catalytic destruction of ozone in the mesosphere is mainly controlled by hydrogen species. Two of the hydrogen species, H and H_2, have very small molecular weights compared to the molecular weight of the surrounding air. The physical process of molecular diffusion has therefore to be included yet in the upper mesosphere. For a complete view on the hydrogen fluxes, however, the molecular diffusion of all hydrogen species has to be calculated at all atmospheric heights. The hydrogen bearing species with the highest mixing ratios have all a smaller molecular weight than air. An upwards directed flux of hydrogen follows until the sum of the mixing ratios increases with height and a compensating downwards directed flux results in the balance of the fluxes. If there is any sink for hydrogen like the escape flux of hydrogen to space a constant flux in global, long-term average at all heights should be the consequence. A spatial and temporal averaging may be necessary to consider possible atmospheric storage effects.

The aim of this work was the modelling of the minor constituents of the mesosphere. One precondition was a dynamic model whose upper boundary was not below 120 km. Observations of NLCs and PMSEs reinforced the interest in the distribution

of water vapour because certain amounts of water vapour seemed to be necessary for the formation of these phenomena. The long-term microwave measurements delivered valuable water vapour mixing ratios at the same location where the lidar and radar observations were obtained. The observational data allowed an excellent evaluation of both, the dynamic model and the model of chemistry and transport, at high latitudes.

However, both models are global three-dimensional models and the results from one model feed the supplementary model. The world wide interaction of both models, for example by chemical heating, allows no strong focusing of parametrizations on the polar latitudes.

Two important questions evolved during the work with the chemistry transport model. The answers should be given by the model results.

- Does the model produce a realistic distribution of water vapour and other constituents?

- How precise will be the calculation of the fluxes of the hydrogen constituents, as a kind of evaluation of the conservation of number density in chemistry and of the formulation of molecular diffusion in the grid structure of the dynamic model?

Chapter 2

Basic Description of the Model

2.1 Introduction

A Chemistry-Transport-Model (CTM), conceived for the height region from 45 km up to 150 km, is used to investigate the distribution of minor constituents especially in the mesosphere and mesopause region. The whole modeling domain consists of two coupled parts.

The dynamics part COMMA-IAP is a further development of the model COMMA described by *Jakobs et al.* [1986], *Berger and Dameris* [1993], *Ebel et al.* [1995], *Kremp et al.* [1999] or *Berger and von Zahn* [1999]. It is based on a model, developed by *Klinker* [1981] and *Rose* [1983]. COMMA stands for Cologne Model of the Middle Atmosphere and IAP for Institute of Atmospheric Physics in Kühlungsborn where the further development of the model focuses on the dynamics and thermal structure of the mesosphere and especially on the mesopause region.

The chemistry part of the model is based on a model described by *Sonnemann et al.* [1998a]. So far, the models are not coupled interactively. The CTM uses the data of wind speed, temperature and pressure from COMMA-IAP in order to compute concentrations of minor atmospheric constituents (including advective and diffusive transport). COMMA-IAP uses the mixing ratios of the calculated species to compute the radiative fluxes (UV+IR) and the heating rates by exothermic chemical reactions. The chemistry-transport model uses the same grid resolution as COMMA-IAP and a main advantage of the model consists in the height resolution of 1.15 km, or 118 grid points from ground level to the top of the model at 135 km in log-pressure coordinates with a fixed scale height of 7 km. The latitudinal resolution is 36 grid points from south pole to north pole. The grid resolution in zonal direction can be varied between 16 and 64 grid points to allow fast model runs (CPU-time) during parameter tests, and to have more precise runs when the model is well tuned.

The initial conditions result from a one year run of the dynamic model with fixed

absorber profiles for chemical heating, and absorption of radiation in the UV (H_2O, O_3, O_2), and IR (CO_2, O_3, NO, O and H_2O). There is data output of horizontal and vertical wind speed, temperature, and pressure altitude every ten days from the entire grid. The data from this run are fed into the CTM which gives the 3-dimensional distribution of the minor constituents. The diurnal variation is obtained by shifting these data around the grid. By this procedure the amount of saved data can be kept small. Iterations with these new profiles are made by feeding back the data from the chemistry module into the dynamic model. An interactive coupling of both models should be the next step. The release of heat from some important exothermic reactions provides a significant amount of heat into the mesopause region. The mean heating rates are included in the dynamic model, but a full coupling should give better results for the heating with regards to the structure of the mesopause with two distinctive layers [*von Zahn et al.*, 1996].

2.2 Brief Description of COMMA

COMMA is a hydrostatic global Eulerian grid point model integrating the set of nonlinear primitive atmospheric equations in flux form. The model extends from the ground to the mean thermosphere (0–150 km). A smoothed topography is included as a lower boundary condition of the geopotential. The vertical resolution is $\triangle z = 1.15$ km. The horizontal resolution is 5° in latitude versus 22.5° or 5.625° in longitude. This corresponds to 36 steps in meridional direction versus 16 or 64 steps in zonal direction. The spatial resolution requires a time step of 225 s using a combined leapfrog and Euler-backward scheme.

COMMA takes into account radiation calculations which provide the radiative cooling and heating rates to drive the diabatic circulation of the model atmosphere. Parametrizations of the solar absorption in the UV and partly in the visible range consider the contributions of ozone and molecular oxygen as absorber in the middle atmosphere and thermosphere. The values of the solar fluxes and absorption cross sections are taken from the paper by *Strobel* [1978]. The actual energy available from direct solar heating is scaled by the stored potential chemical energy and the energy loss due to airglow emission according to *Mlynczak and Solomon* [1993]. Absorption of solar radiation by tropospheric water vapour and carbon dioxide in the near infrared range is calculated according to *Lacis and Hansen* [1974] and *Liou* [1980]. The cooling rates by terrestrial radiative flux divergences are computed by the use of parametrizations of water vapour [*Liou*, 1980], ozone [*Fomichev and Shved*, 1985], carbon dioxide [*Ramanathan et al.*, 1983], and atomic oxygen and nitric oxide in the lower thermosphere regions [*Kockarts*, 1980]. Further details about COMMA can be read in the paper by *Jakobs et al.* [1986], *Berger and Dameris* [1993], *Ebel et al.* [1995], *Kremp et al.* [1999].

2.2.1 New Features of COMMA-IAP

The upgrade of COMMA to COMMA-IAP is first documented in the paper by *Berger and von Zahn* [1999] and has been done for studies of mesopause processes, where a high vertical resolution is necessary.

The new characteristics are:

- Carbon dioxide is now specified through variable mixing ratios of CO_2 in order to compute the greenhouse effect instead of the former constant mixing ratio of 360 ppmv in the lower and middle atmosphere and a decreasing mixing ratio above 85 km altitude according to the paper by *Fomichev et al.* [1998].
- The cooling rates due to CO_2 are computed using parametrizations of *Kutepov and Fomichev* [1993] and *Fomichev et al.* [1998], including effects from nonlocal thermodynamic equilibrium conditions (NLTE).
- Chemical heating due to exothermic chemical reactions lead to heat deposition in the upper mesosphere and lower thermosphere [*Mlynczak and Solomon*, 1993], [*Sonnemann et al.*, 1998a].

The detailed calculation of chemical heating and infrared cooling rates needs a consistent 3-dimensional data set of important minor constituents of the middle atmosphere which is produced by the CTM in the height range of 45–150 km. In regions below 45 km the distribution of ozone and water vapour as the most important absorber are given by climatological Nimbus 7 data e.g. [*Frederick et al.*, 1983].

2.2.2 The Important Process of Gravity Wave Saturation and Breaking

The gravity wave parametrization is based on the work of *Holten and Zhu* [1984]. At each time step the actual gravity wave momentum deposition near critical and breaking levels is computed. A family of gravity waves with horizontal phase velocities of 5, 25, and 50 $\mathrm{m\,s^{-1}}$ is propagating simultaneously in four directions (0, $\pi/2$, π, and $3\pi/2$). The estimated gravity wave diffusion coefficient K_{zz} is used as the actual eddy diffusion parameter for the vertical eddy transport of heat, for the cooling due to the divergence of the vertical eddy heat flux and for the heating from dissipation of turbulent gravity wave energy (choosing a Prandtl number $P_r = 3$).

2.3 Description of the CTM

The chemistry model was first described by *Sonnemann et al.* [1984], and *Fichtelmann and Sonnemann* [1989]. It was developed as a one dimensional model for small

cpu-time consumption. The lower boundary was at 30 km, the upper boundary at 200 km. The stiff ODE (Ordinary Differential Equation) system of the chemistry was solved by a family concept where constituents with fast exchange reactions are grouped together. Vertical diffusion was taken into account. The model allowed the calculation of the diurnal variation of ozone and the hydrogen radicals, due to a small time step. The hydrogen radicals control the catalytic ozone destruction in the upper mesosphere. The radiation code considered the EUV and X-ray spectrum of the solar radiation which reflects the main focus on the mesosphere and lower thermosphere. The model was further developed into a three dimensional model to give a more realistic picture of mesospheric phenomena [*Sonnemann et al.*, 1995]. Wind speed and temperature data for this model were taken from COMMA. Further papers [*Sonnemann et al.*, 1998a], [*Sonnemann et al.*, 1998b], and [*Kremp et al.*, 1999] show the development of the model.

Particularly within the mesopause region, which is characterized by strong gradients of the mixing ratios of the most important minor constituents, the smoothing caused by the discretization of the relatively coarse grid (numerical diffusion) was too strong. With the requirements of a finer grid resolution especially of the vertical coordinate from 24 to 118 levels the needed cpu-time becomes a problem on the available workstations of the IAP. Model runs were limited to about a month of model time and sensitivity studies and testing of new parametrizations were cpu-time devouring. Therefore, the decision was made to rewrite large parts of the model.

2.3.1 Chemistry Module

Elemental parts of the chemistry:

- The chemistry module consists of 19 constituents: H, OH, HO_2, H_2O_2, H_2, H_2O, CH_4, O, $O(^1D)$, O_3, N, NO, NO_2, NO_3, N_2O, Cl, ClO, Br, BrO.
- Constituents subjected to advective and diffusive transport are: HX, OX, NX, H_2, H_2O, CH_4, N_2O.
- The reaction scheme includes 55 chemical reactions.
- 13 photodissociation rates reflect the diurnal variation of the daylight dependent reactions.
- The chemical families are:

$$\begin{aligned} \mathrm{HX} &= \mathrm{H} + \mathrm{OH} + \mathrm{HO_2} + 2\,\mathrm{H_2O_2} \\ \mathrm{OX} &= \mathrm{O} + \mathrm{O(^1D)} + \mathrm{O_3} \\ \mathrm{NX} &= \mathrm{N} + \mathrm{NO} + \mathrm{NO_2} + \mathrm{NO_3} \\ \mathrm{ClX} &= \mathrm{Cl} + \mathrm{ClO} \\ \mathrm{BrX} &= \mathrm{Br} + \mathrm{BrO} \end{aligned}$$

(The halogen families are normally switched off and only used for sensitivity studies of catalytic mesospheric ozone decomposition which occurs mainly by hydrogen reactions.)

The standard calculation concept for the constituents is now the semi implicit scheme. It avoids instability and is mass conserving to a sufficient degree for the constituents with large characteristic times compared with the time step. The short lived constituents are included in the chemical families and are standardized to the family mixing ratio. The families have to have long enough characteristic times, too. Quadratic loss processes occur often in families. They are linearised by Taylor expansion and included in the semi-implicit scheme. The mixing ratios of the major constituents O_2 and N_2 are taken from *U. S. Standard Atmosphere* [1976]. The actual number density of each constituent used for the calculation of chemical reactions is obtained by using the actual temperature of the grid point, the pressure level and the ideal gas law. The temperature influences the chemical turnover not only by the temperature dependent reaction rates but also by the number density of the constituents. The strongest influence of this feature is on the three body reactions like the recombination of atomic oxygen, because the temperature has not only a quadratic but a cubic effect on the chemical turnover of the reaction.

2.3.2 Revised Concepts of the Model

The following major concepts in the CTM have been revised compared to the former model.

- Implicit calculation of the molecular diffusion allows a larger time step with enhanced precision. The upper 20 km of the model domain required a very small time step using the explicit Euler scheme or the Crank-Nicholson scheme.

- The families in the chemistry are solved as a fully implicit subsystem including quadratic loss processes. The full implicit solution is mass conserving and needs no standardization of the members by the family concentration. The result is a higher precision of the distribution of the constituents in the chemical families, especially where two major constituents have a characteristic time of the same order.

- The transport is calculated highly vectorized either by the upwind-scheme or by the Smolarkiewicz-scheme with one correction step, which is done by the upwind-scheme again using an anti-diffusion velocity in order to correct the strong numerical diffusion of the upwind-scheme.

Much larger time steps can be used now for a quick check of new parametrizations without causing instable behaviour. Model runs over several years give a realistic distribution of the annual variation of water vapour and other constituents. Some results are shown in *Körner and Sonnemann* [2001]. One particular feature of the rewritten model is the high precision of the calculation of the hydrogen fluxes which requires a consistent formulation of the model in the modules diffusion and chemistry. In a model run with switched off advective transport the global average flux balance of the hydrogen constituents is nearly constant over the entire height range (fluctuations of less than 5 %) at a value of about 3 10^8 $cm^{-2}s^{-1}$ which is equivalent to the hydrogen escape to space. The results considering advective transport have not this high precision. This can be caused by the transport scheme or by too long time intervals in the exchange of data between COMMA-IAP and the CTM. Further development of the advective transport and the coupling of both models should improve the accuracy of these calculations.

2.4 Program Development of the CTM

The CTM was first developed on a HP workstation. The needed cpu-time amounted to about 4 h per calculated day in the model. The long-term objective was the ability to do model runs over several years. Three major steps increased the speed of the program by an order in magnitude, each:

- The change from the workstation to the NEC-SX4.
- The improvement of the degree of vectorization from about 100 Mflops up to around 950 Mflops, at a theoretical capacity of 1800 Mflops for this computer. Careful storage management of the variables was necessary. Slightly more than 1000 Mflops were possible but only at the cost of four times more main storage use of the cpu.
- The implementation of implicit calculation in diffusive transport and chemistry together with a larger time step. The precision of the entire program was improved in spite of the larger time step.

The needed cpu-time per model day in a standard run with a time step of 450 s is now reduced to about ten seconds. A four times larger time step can be chosen for a quick overlook on new parametrizations. The limit is at about 2700 s by the Courant-Friedrichs-Lewy condition in the transport module. A large time step, however, enhances the diffusivity of the algorithm.

The first long term model runs showed a smoothing of tracer gradients which increased strongly after the first year. Main parts of the program had to be checked

for a better internal consistency. The temperature at each grid point changes now the number density of the air according to the ideal gas law and the diffusion coefficients are calculated by using the actual temperature.

The calculation of the turnover by chemical reactions is done in units of number density (particles cm^{-3}) at the grid points, whereby the calculations of the advective transport and the molecular- and eddy diffusion are done in units of mixing ratio for reason of better consistency with the dynamic model COMMA-IAP and thereby increased precision. At each time step a transformation from mixing ratio to number density and back is done before and after the calculation in the chemistry module. Details about the individual modules can be found in the corresponding chapters.

2.5 Height of Isobaric Surfaces in the Mesosphere

The model calculations are made on isobaric surfaces according to the pressure levels of the model COMMA-IAP. Many observational data, however, like lidar data, radar data, microwave measurements and satellite data are presented on a geometric scale. In the troposphere and stratosphere pressure and geometric height are in a nearly fixed relation to each other. In the mesosphere especially under solstice conditions this is not valid. Figure 2.1 shows the height variation of the isobaric surfaces versus a geometric scale. For the surface of 0.01 hp ($\sim$ 80 km) the variation is about 10 km. The strong temperature difference in the underlying atmospheric column between summer and winter hemisphere results in a contraction or an expansion, respectively, of the atmospheric column. There should be no fixed scaling between pressure level and geometric height when the latitude varies in plots about mesospheric phenomena.

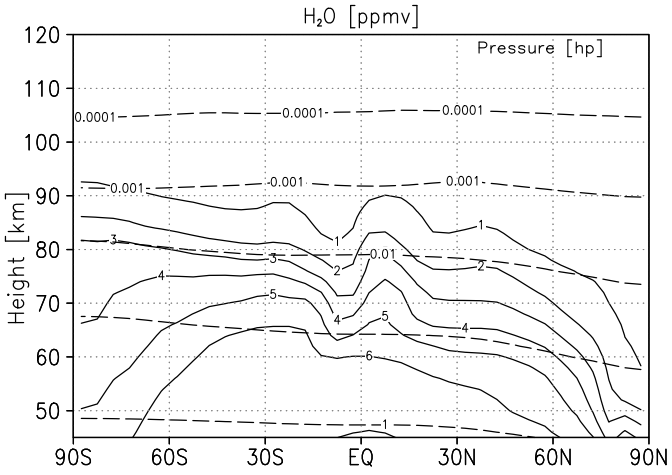

Figure 2.1: Water vapour [ppmv] (solid lines) at southern summer solstice with isobaric surfaces [hp] (dashed lines).

Chapter 3

Chemistry

3.1 Elementary Reaction Kinetics

The chemistry of atmospheres consists of many elementary reaction steps involving atoms, radicals, excited states and ions as reactants and products. Laboratory investigations of the reactions are necessary. Methods such as flash photolysis and flow techniques have provided much information about reaction kinetics. Organizations such as NASA and the National Bureau of Standards (NBS) evaluate critically kinetic data for use in atmospheric chemistry. However, the laboratory data often cannot be obtained under conditions identical to those present in an atmosphere. Extrapolation of the laboratory results, based on a believable theory for the concerned process, may be used in interpreting atmospheric chemistry.

The reaction, $\mathrm{A} + \mathrm{B} \rightarrow \textit{products}$, proceeds with a rate proportional to the concentrations raised to some power. The change of the concentration of constituent A, [A], may be written as

$$\frac{\mathrm{d}[\mathrm{A}]}{\mathrm{d}t} = -k[\mathrm{A}]^{\alpha}[\mathrm{B}]^{\beta} \quad . \tag{3.1}$$

The powers α and β are the order of reaction with respect to A and B, and $\alpha + \beta$ is the overall order. The constant of proportionality, k, is the rate coefficient. The molecularity of a reaction is the number of reactant molecules written in the stoichiometric equation. Thus order is an experimental quantity, molecularity an arbitrary theoretical one. An elementary reaction step is conceived as one that cannot be split into any chemically simpler process. For truly elementary steps, order and molecularity are in general identical, adopted from *Wayne* [1991].

For simple reactions (reactions with few elementary steps) the total order is between 0 and 4 in most cases. The order of the single components varies mostly between 0 and 2. The following example from *Atkins* [1986] shows that the order of a reaction is not necessary an integer. The reaction of $\mathrm{H_2} + \mathrm{Br_2} \rightarrow 2\,\mathrm{HBr}$ is stoi-

chiometric simple but cannot be classified because the equation for the speed of the reaction is

$$\frac{\mathrm{d[HBr]}}{\mathrm{d}t} \;=\; k\;\frac{[\mathrm{H_2}][\mathrm{Br_2}]^{3/2}}{[\mathrm{Br_2}]+\mathrm{k'[HBr]}} \quad . \tag{3.2}$$

In general, the equation for the speed of a reaction can only obtained by experiment and cannot derived from the reaction formula.

In the middle atmosphere, however, most chemical reactions are of second or third order. A short look on the solution of the ordinary differential equations is now given to get a basic understanding of the simplifications which are made with the numeric solution of the finite difference equations.

3.1.1 First Order Process

A first order process is the decay of a molecule into two parts

$$\mathrm{A} \;\longrightarrow\; \mathrm{C} \;+\; \mathrm{D} \quad , \tag{3.3}$$

with the rate constant

$$k\,[\mathrm{A}] \;=\; -\frac{\mathrm{d[A]}}{\mathrm{d}t} \;=\; \frac{\mathrm{d[C]}}{\mathrm{d}t} \;=\; \frac{\mathrm{d[D]}}{\mathrm{d}t} \quad . \tag{3.4}$$

The time dependent solution for an initial concentration $[\mathrm{A}] = [\mathrm{A_0}]$ is

$$[\mathrm{A}] \;=\; [\mathrm{A_0}]\exp(-kt) \quad . \tag{3.5}$$

The required time for a decrease to $1/e$ of the initial value is therefore equal to $1/k$, if this was the only reaction process. This is the standard definition of the chemical lifetime of a species. The concept of lifetime is important for atmospheric applications because species with short lifetimes compared to the transport time scales are not affected by transport processes in a first order approximation. The distribution of chemically long lived species, however, depends mainly on transport processes. For some species like ozone in the stratosphere or water vapour in the mesosphere the lifetime from the loss process results in a much shorter lifetime compared to a lifetime definition which takes the production processes into account. The products of the photodissociation can form back the original species very fast so that the dependence on transport processes can be stronger than expected, see the discussion of water vapour lifetime in section 7.1.3.

3.1.2 Second Order Process

A bimolecular or second order process can be described by

$$\mathrm{A} \;+\; \mathrm{B} \;\longrightarrow \mathrm{C} \;+\; \mathrm{D} \quad , \tag{3.6}$$

with the rate constant

$$k\,[\mathrm{A}][\mathrm{B}] \;=\; \frac{\mathrm{d}[\mathrm{C}]}{\mathrm{d}t} \;=\; \frac{\mathrm{d}[\mathrm{D}]}{\mathrm{d}t} \;=\; -\frac{\mathrm{d}[\mathrm{A}]}{\mathrm{d}t} \;=\; -\frac{\mathrm{d}[\mathrm{B}]}{\mathrm{d}t} \quad . \tag{3.7}$$

If $[\mathrm{A}] \ll [\mathrm{B}]$, the second order process can be treated as a pseudo first order process because the concentration of species B stays nearly constant during the reaction of both species. Equation 3.6 then gives the simple solution

$$[\mathrm{A}] \;\approx\; [\mathrm{A}_0]\exp(-k[\mathrm{B}]t) \quad . \tag{3.8}$$

The lifetime from the loss process is

$$\tau_{\mathrm{A}} \;=\; \frac{1}{k[\mathrm{B}]} \quad . \tag{3.9}$$

The pseudo first order treatment is widely used in atmospheric chemistry. However, $[A] \ll [B]$ is not valid in general in the atmosphere. The reaction of ozone with atomic oxygen, $\mathrm{O} + \mathrm{O}_3 \rightarrow 2\ \mathrm{O}_2$, shows a mixing ratio of the same order of both constituents at about 60 km altitude. For the reaction

$$\mathrm{A} \;+\; \mathrm{A} \;+\; \mathrm{M} \;\longrightarrow\; \mathrm{C} \;+\; \mathrm{M} \quad , \tag{3.10}$$

which can serve as a general case of the situation just described, the loss process has a quadratic dependence on [A]. *Shimazaki* [1985] calls this a β-type loss process. A pseudo first order calculation would give less realistic results. This behaviour is important for a reaction like

$$\mathrm{O} \;+\; \mathrm{O} \;+\; \mathrm{M} \;\longrightarrow\; \mathrm{O}_2 \;+\; \mathrm{M} \quad , \tag{3.11}$$

and for the family concept, where several constituents with fast exchange reactions are grouped together and β-type loss processes in a family occur, see the family concept in subsection 3.2.4.

3.1.3 Steady State

In a complex system like the atmosphere, a species can be removed and produced by several processes simultaneously.

$$\frac{\mathrm{d}[\mathrm{A}]}{\mathrm{d}t} \;=\; -k_1[\mathrm{A}][\mathrm{B}_1] - k_2[\mathrm{A}][\mathrm{B}_2] - \cdots \;+ k_n[\mathrm{C}][\mathrm{D}] + \cdots \tag{3.12}$$

$$\frac{\mathrm{d}[\mathrm{A}]}{\mathrm{d}t} \;=\; -\sum_i L_i\ [\mathrm{A}] + \sum_i P_i \tag{3.13}$$

L stands for a loss process of species A, and P for a production process. The characteristic chemical time is normally based on the loss processes although it is often useful to look on the production rate, too. The distribution of a constituent may be influenced seriously by transport processes if the production processes are of the same order as the loss processes. Examples for this behaviour are ozone in the stratosphere and water vapour in the mesosphere.

$$\tau_{\mathrm{A}} \;=\; \frac{1}{k_1[\mathrm{B}_1] + k_2[\mathrm{B}_2]} + \cdots \;=\; \frac{1}{\sum\limits_i L_i} \tag{3.14}$$

If the chemical lifetime is short compared to transport time scales and if the reaction rates and all other species are assumed to be nearly constant over the time scale considered, photochemical stationary or steady state can be assumed, meaning

$$\frac{\mathrm{d}[\mathrm{A}]}{\mathrm{d}t} \;=\; 0 \;=\; \sum_i P_i - [\mathrm{A}] \sum_i L_i \qquad \Leftrightarrow \tag{3.15}$$

$$[\mathrm{A}] \;=\; \frac{\sum\limits_i P_i}{\sum\limits_i L_i} \;=\; \tau_{\mathrm{A}} \sum_i P_i \;=\; \frac{k_n[\mathrm{C}][\mathrm{D}] + \cdots}{k_1[\mathrm{B}_1] + k_2[\mathrm{B}_2] + \cdots} \qquad . \tag{3.16}$$

The approximation of steady state processes is intensely used along with the family concept, discussed in subsection 3.2.4.

3.1.4 Unimolecular Reactions

Several gas phase reactions show a reaction kinetic of first order. It is supposed that they have a unimolecular reaction step which determines the speed of the reaction. The theory of this reaction mechanism was first proposed by *Lindemann* [1922].

activation:	k_a	$\mathrm{A} + \mathrm{M}$	$\longrightarrow$	$\mathrm{A}^* + \mathrm{M}$
deactivation:	k_d	$\mathrm{A}^* + \mathrm{M}$	$\longrightarrow$	$\mathrm{A} + \mathrm{M}$
reaction:	k_r	$\mathrm{A}^* + \mathrm{M}$	$\longrightarrow$	$\mathrm{B} + \mathrm{C}$

A molecule is first activated by collision with other molecules (k_a), but can also be deactivated by quenching (k_d) or decompose into parts (k_r). The rate of decomposition is

$$\frac{\mathrm{d}[\mathrm{A}]}{\mathrm{d}t} \;=\; -k_r\,[\mathrm{A}^*] \quad . \tag{3.17}$$

The steady state concentration of A^* is

$$\frac{d[A^*]}{\mathrm{d}t} \;=\; 0 \;=\; k_a[A][M] - (k_d[M] + k_r)[A^*] \quad , \tag{3.18}$$

which is equivalent to

$$[\mathrm{A}^*] \;=\; \frac{k_a[\mathrm{A}][\mathrm{M}]}{k_d[\mathrm{M}] + k_r} \quad , \tag{3.19}$$

and for the decomposition of A follows

$$\frac{\mathrm{d}[\mathrm{A}]}{\mathrm{d}t} \;=\; -k_r \, \frac{k_a[\mathrm{A}][\mathrm{M}]}{k_d[\mathrm{M}] + k_r} \quad . \tag{3.20}$$

At high pressures the rate of deactivation is greater than the rate of decomposition or $k_d[\mathrm{M}] \gg k_r$. The high pressure limit is therefore the first order process

$$\frac{\mathrm{d}[\mathrm{A}]}{\mathrm{d}t} \;\approx\; -k_r \, \frac{k_a[\mathrm{A}]}{k_d} \quad . \tag{3.21}$$

At low enough pressure the rate of decomposition is the main loss process for A^*. $k_d[\mathrm{M}] \ll k_r$ is valid and the low pressure limit is

$$\frac{\mathrm{d}[\mathrm{A}]}{\mathrm{d}t} \;\approx\; -k_a \, [\mathrm{A}][\mathrm{M}] \quad , \tag{3.22}$$

which is a reaction of second order. At moderate pressure this reaction is neither first nor second order and the pressure dependence has to be carefully parametrized, if the activated molecule should not be an additional constituent of the system. The thermal decomposition of $\mathrm{N_2O_5}$,

$$\mathrm{N_2O_5} \longrightarrow \mathrm{NO_2} \;+\; \mathrm{NO_3} \tag{3.23}$$

is an important stratospheric reaction which is of intermediate order at stratospheric pressures.

3.1.5 Termolecular Reactions

Some reactions of two molecules or atoms can proceed more easily by the presence of a third body. An example is the reaction $\mathrm{O} + \mathrm{O_2} + \mathrm{M} \rightarrow \mathrm{O_3} + \mathrm{M}$. The probability for a collision of all three particles is quite small, so that in general the reaction can be understood according to the activated complex theory of the unimolecular reaction. Two particles interact in an initial step to an activated complex which would decompose back to the reactants if not a second interaction deactivates and stabilizes the new complex.

activation:	k_a	$\mathrm{A} + \mathrm{B}$	$\longrightarrow$	C^*
deactivation:	k_d	$\mathrm{C}^* + \mathrm{M}$	$\longrightarrow$	$\mathrm{C} + \mathrm{M}$
unimolecular:	k_u	C^*	$\longrightarrow$	$\mathrm{A} + \mathrm{B}$

This process is the reverse process to the unimolecular decay. The formation rate of C is given by

$$\frac{\mathrm{d[C]}}{\mathrm{d}t} \;=\; k_d[\mathrm{C^*}][\mathrm{M}] \;=\; k_d[\mathrm{M}]\,\frac{k_a[\mathrm{A}][\mathrm{B}]}{k_d[\mathrm{M}]+k_u} \quad . \tag{3.24}$$

For the low pressure limit $k_u \gg k_d[\mathrm{M}]$ the result is the third order reaction

$$\frac{\mathrm{d[C]}}{\mathrm{d}t} \;\approx\; k_d\frac{k_a}{k_u}[\mathrm{A}][\mathrm{B}][\mathrm{M}] \quad . \tag{3.25}$$

The high pressure limit $k_u \ll k_d[\mathrm{M}]$ gives the reaction of second order

$$\frac{\mathrm{d[C]}}{\mathrm{d}t} \;\approx\; k_a[\mathrm{A}][\mathrm{B}] \quad . \tag{3.26}$$

In the data of chemical kinetics from *DeMore et al.* [1994] and in similar publications the rate constants for termolecular reactions are given in the form

$$k_0(\mathrm{T}) \;=\; k_0^{300}\,(\mathrm{T}/300)^{-n}\ \mathrm{cm^6\,molecule^{-2}\,s^{-1}} \quad , \tag{3.27}$$

where k_0^{300} has been adjusted for air as third body. The reaction $\mathrm{O+O_2+M \rightarrow O_3+M}$ has no additional entry for the pressure dependency, which means that this reaction is calculated as a reaction of third order. When pressure fall-off correlations are necessary, an additional entry gives the limiting high pressure rate constant in a similar form:

$$k_\infty(\mathrm{T}) \;=\; k_\infty^{300}\,(\mathrm{T}/300)^{-m}\ \mathrm{cm^3\,molecule^{-1}\,s^{-1}} \quad . \tag{3.28}$$

The reaction has to be calculated as a pseudo second order reaction with an effective reaction rate

$$k([\mathrm{M}],\mathrm{T}) \;=\; \left(\frac{k_0(\mathrm{T})[\mathrm{M}]}{1+\left(\dfrac{k_0(\mathrm{T})[\mathrm{M}]}{k_\infty(\mathrm{T})}\right)}\right) 0.6^{\left\{1+\left[\log_{10}\left(\dfrac{k_0(\mathrm{T})[\mathrm{M}]}{k_\infty(\mathrm{T})}\right)\right]^2\right\}^{-1}} \quad . \tag{3.29}$$

3.1.6 Thermodynamic Considerations

Chemical reactions in general can be exothermic or endothermic. An exothermic reaction librates heat to the surrounding, an endothermic reaction can proceed if the required energy is provided by an external source, such as a photon for a photolysis reaction. In the exothermic case, the chemical bonds represent more internal energy before the reaction happens than afterwards. This is expressed in the concept of enthalpy. A substance in its most stable form is assigned a zero enthalpy of formation. A second important point is the entropy, which represents the disorder or randomness

of a particular process. The *Gibbs* free energy of a reaction includes both the enthalpy and entropy and is defined as

$$\Delta G \;=\; \Delta H \;-\; T\,\Delta S \quad , \tag{3.30}$$

with ΔG is the *Gibbs* free energy, ΔH is the enthalpy, T is the temperature, and ΔS is the entropy. For a general reaction

$$\mathrm{A} \;+\; \mathrm{B} \longrightarrow \mathrm{C} \;+\; \mathrm{D} \quad , \tag{3.31}$$

the *Gibbs* free energy of the reaction is

$$\Delta G_R \;=\; \Delta G[\mathrm{C}] + \Delta G[\mathrm{D}] - \Delta G[\mathrm{A}] - \Delta G[\mathrm{B}] \quad . \tag{3.32}$$

If ΔG_R is negative, then the reaction can proceed spontaneously. The use of these thermodynamic data allows the evaluation of the feasibility of proposed chemical reactions, which have perhaps never been studied in a laboratory. *Brasseur and Solomon* [1986] showed a table with thermodynamic data of several atmospheric species and gave two examples on how to deal with these data. The first example is the reaction

$$\mathrm{NO_3} \;+\; \mathrm{H_2O} \longrightarrow \mathrm{HNO_3} \;+\; \mathrm{OH} \quad , \tag{3.33}$$

which looks as if it could occur but gives a positive *Gibbs* free energy. The reaction is therefore thermodynamically impossible without an external source of energy in the atmosphere. The external energy needed for an endothermic reaction can be provided by a photon. The photolysis of molecular oxygen, as an example, needs an amount of energy that corresponds to a photon wavelength of $\lambda \leq 240\,nm$. The second example is the reaction

$$\mathrm{O} \;+\; \mathrm{O_2} \;+\; \mathrm{M} \longrightarrow \mathrm{O_3} \;+\; \mathrm{M} \quad , \tag{3.34}$$

which is known to be exothermic and serves as an important source of heat in the upper part of the middle atmosphere. This is one of the reactions which release heat into the entire middle atmosphere and thus have influence on the structure of the mesopause. The release of heat by chemical reactions is often called *chemical heating* and has been taken into account by several scientists, who work on modelling of the mesosphere, as will be discussed in chapter 9.

3.2 Calculation Concepts

The process of chemistry in the atmosphere has to be simplified to get a mathematical expression by a system of ordinary differential equations (ODEs). As discussed before reactions of second order are usually treated as pseudo first order reactions. This is

not a good approximation for reactions which have two constituents with number densities of the same order. The reaction $O + O + M \rightarrow O_2 + M$ is an example for a reaction with a quadratic loss process. *Shimazaki* [1985] used a linearization by Taylor expansion , see subsection 3.2.3, which gives an enhancement in precision for several reactions.

The most serious problem, however, is the variation of the rate constants of the ODE system over several orders of magnitude which leeds to a so called stiff system of ODEs. For stiff systems the explicit Runge-Kutta methods, which are widely used in solving ODEs, are not suitable because they are restricted in stability. The simplest explicit Runge-Kutta method is the explicit Euler method. It is often used in atmospheric chemistry together with the family concept. Although the family concept weakens the problem of stability, great care has to be taken about the time step in order to avoid instability. Implicit methods are favourized in general for the solution of stiff systems because they have much better stability properties. A very precise method is the scheme of *Gear* [1971]. It is computational expensive and therefore not commonly used in three-dimensional modelling but sometimes for zero- or one-dimensional tracer studies. In this work a partitioning concept is used. The long-lived constituents are solved singly by the implicit scheme. The short-lived constituents are included in chemical families which are solved as fully implicit subsystems. This compromise incorporates a precise solution at moderate need of cpu-time. *Press et al.* [1990] give a short overlook on higher-order methods for stiff systems:

- Generalizations of the Runge-Kutta method, of which the most useful are the Rosenbrock methods. The first practical implementation of these ideas was by Kaps and Rentrop, and so these methods are also called Kaps-Rentrop methods.

- Generalizations of the Bulirsch-Stoer method, in particular a semi-implicit extrapolation method due to Bader and Deuflhard.

- Predictor-corrector methods, most of which are descendants of Gear's backward differentiation method.

3.2.1 Explicit Euler Method

The change of the number density of each constituent is generally expressed in terms of production and loss by chemical reactions with other constituents.

$$\frac{\partial n_i}{\partial t} = \sum_j P_j - \sum_j L_j n_i \tag{3.35}$$

The simplest numerical scheme to solve equation 3.35 is the explicit Euler method.

$$n_i^{t+\Delta t} = n_i^t + \left(\sum_j P_j - \sum_j L_j n_i^t \right) \cdot \Delta t \tag{3.36}$$

Equation 3.36 is the straight discretization of Equation 3.35. The explicit method is computational cheap and mass conserving but not positive definite which means that a negative concentration may result if the time step is too large and the loss rate overbalances the production rate. The time step is restricted in order to avoid negative values in the solution. The time step should not be larger than 1/5 of the time constant of the fastest loss process in the set of equations. As an example, the quenching process for $O(^1D)$ results in a time constant of about 10^{-8} s in the stratosphere. The use of the family concept replaces the time constant of the fast processes by the time constant of the family but the restriction is still severe. The explicit method is therefore not a good choice for the modelling of seasonal variations of components, or model runs over several model years.

3.2.2 Implicit Euler Method

The implicit or backward Euler method is the simplest of the implicit Runge-Kutta methods and gives a numerically stable and positive definite solution. It allows therefore the use of a much larger time step. However, the solution is no longer mass conserving if the scheme is used singly for each component of the system which is here called the semi-implicit method. The mass conservation i.e. for family members should be done by using the family concentration for the normalization of the members.

$$n_i^{t+\Delta t} = n_i^t + \left(\sum_j P_j - \sum_j L_j n_i^{t+\Delta t} \right) \Delta t \tag{3.37}$$

$$n_i^{t+\Delta t} = \frac{n_i^t + \sum_j P_j \Delta t}{1 + \sum_j L_j \Delta t} \tag{3.38}$$

The loss rate can be replaced by the inverse of the chemical life time ($\tau = 1/\sum_j L_j$). The index for the component is omitted in the following equations.

$$n^{t+\Delta t} = \frac{n^t + P\Delta t}{1 + L\Delta t} = \frac{\tau n^t + \tau P \Delta t}{\tau + \Delta t} \tag{3.39}$$

For $\Delta t \gg \tau$, the solution converges against the steady state solution $n = P/L$.

$$n^{t+\Delta t} \approx \frac{\tau}{\Delta t} n^t + \tau P \approx \tau P = \frac{P}{L} \tag{3.40}$$

For $\Delta t \ll \tau$, the solution converges against the solution of the explicit method.

$$n^{t+\Delta t} = n^t + \frac{(\tau P - n^t)\Delta t}{\tau + \Delta t} \approx n^t + \frac{(\tau P - n^t)\Delta t}{\tau} = n^t + (P - Ln^t)\Delta t \tag{3.41}$$

For $\Delta t \approx \tau$, the result is.

$$n^{t+\Delta t} \approx \frac{n^t + P\Delta t}{2} \tag{3.42}$$

Although this method is not mass conserving, it gives a smooth solution at each time step and should therefore not lead to numerical oscillations of the solution of the whole system. The implicit method can be used in a mass conserving manner, if all components of the system are solved simultaneously. At each grid point a linearized algebraic system then has to be solved, which has as many variables as the number of constituents in the system. Even with highly developed system routines and modern supercomputers, this method is computational expensive. A compromise, chosen in this work, is to compute the families as full implicit subsystems and to compute the long-lived constituents singly implicit. This results in a more accurate solution of the family members without the need of normalization compared with the single implicit solution.

3.2.3 Implicit Method with Quadratic Loss Term

Compared with the implicit solution described in the previous subsection, a loss term which is proportional to the square of the number density, $\widehat{L}\, n^2$, is added.

$$n_i^{t+\Delta t} = n_i^t + \left(\sum_j P_j - \sum_j L_j n_i^{t+\Delta t} - \sum_j \widehat{L}_j \left(n_i^{t+\Delta t}\right)^2 \right) \Delta t \tag{3.43}$$

For the solution of this equation the quadratic term may be linearized by Taylor expansion. The index for the component is omitted again in the following equations.

$$\left(n^{t+\Delta t}\right)^2 = 2n^t n^{t+\Delta t} - \left(n^t\right)^2 \tag{3.44}$$

Equation 3.43 is then linear in $n^{t+\Delta t}$

$$n^{t+\Delta t} = n^t + \left(P - Ln^{t+\Delta t} - \widehat{L} \left(2n^{t+\Delta t} n^t - \left(n^t\right)^2 \right) \right) \Delta t \tag{3.45}$$

and can be transformed into

$$n^{t+\Delta t} = \frac{n^t + \left(P + \widehat{L}\, (n^t)^2 \right) \Delta t}{1 + \left(L + 2\widehat{L}\, n^t \right) \Delta t} \quad . \tag{3.46}$$

3.2.4 The Concept of Chemical Families

Using the explicit Euler method, the calculation of some constituents of the atmospheric chemistry requires an extreme short time step compared with the desired modelling time of years. The characteristic time of $O(^1D)$ is about 10^{-7} s at an altitude of 30 km. This constituent is not the problem because $O(^1D)$ can be set into chemical equilibrium. Ozone, however, has a characteristic time of about 10^2 s in the mesosphere which would require a time step of about 20 s using the explicit Euler method. Although the implicit method has better stability properties, the time step should not be very much larger because the precision of the solution would decrease otherwise. Much more difficult is the case of atomic hydrogen. The characteristic time at 60 km is about one second, at 100 km it is about a day.

The popular solution for this problem is the concept of chemical families. Some constituents with fast exchange reactions among one another are grouped into a so called family. The odd-oxygen family in the described CTM, for example, consists of $O(^1D)$, $O(^3P)$, and O_3. At each time step, the change of the family as a whole is calculated and then, with the assumption of steady state for the $n-1$ most short-lived components of the family, the number density of the family is divided into the number density of the members.

This allows the use of a much larger time step because the restriction of the time step is now the characteristic time of the family. In general, good results are obtained by use of the family concept, but some problems still remain. The partitioning of the family cannot be fixed because reaction rates and therefore characteristic times derived from loss rates, are changing with temperature, pressure (three body reactions), and radiative conditions. The component with the largest lifetime in a family can change, and therefore, the characteristic times have to be checked. But, if the two largest characteristic times in the family are nearly equal, an oscillating behaviour can occur.

One possibility is to solve each component of the family singly with the implicit Euler method and use the family concentration only for the normalization of the number density. For short-lived components this is like steady state calculation and for long-lived it is like Euler explicit, as described before. The smooth transition between both cases, however, avoids an if-construct in the inner loop of chemistry, which allows a much better vectorization of the chemistry. The β-type loss behaviour can be included into the calculation of the family and into the calculation of single components.

The next improvement step is, to solve the equations for the family members fully implicit. This concept is shown in the book of *Shimazaki* [1985]. The chemical components are solved with the implicit Euler-method. For the members of a family the equations are solved simultaneously, so that hydrogen is conserved for the hydrogen family and so on. The non-linear terms are linearized by Taylor expansion. This

method gives a continuous partitioning of the families even in regions where two major components of a family have a lifetime of the same order of magnitude. For small subsystems the required additional cpu-time is acceptable, but, with the included β-type loss processes better results for the partitioning of families are obtained. The calculation of the fluxes of the hydrogen components will show the quality of this concept.

A fully implicit calculation of all components would be a further improvement, but much more cpu-time would be needed, even with sparse matrix library-subroutines which are available for the most modern supercomputer.

3.3 Impact of Dynamics on Chemistry

If only advective transport and chemical reactions are taken into account, the continuity equation for a single species with number density n_i is

$$\frac{\partial n_i}{\partial t} = \sum_j P_j - \sum_j L_j n_i - \nabla \cdot (\vec{v} \cdot n_i) \quad . \tag{3.47}$$

To decide which process is of main influence in an atmospheric region, it is useful to compare the characteristic times.

For the estimation of the characteristic transport time in the considered grid direction, the gradient of the distribution of the species i is required. If, for example, the vertical distribution can be described by the scale height H_i, where z is the altitude and $n_{i,0}$ is the number density at the lowest height level ($z_0 = 0$), the number density is

$$n_i = n_{i,0}\, e^{-z/H_i} \quad , \tag{3.48}$$

and the derivative is

$$\frac{\partial n_i}{\partial z} = -\frac{1}{H_i}\, n_{i,0}\, e^{-z/H_i} = -\frac{n_i}{H_i} \quad . \tag{3.49}$$

If the idealized case of a constant vertical transport and vanishing zonal and meridional wind is supposed, the continuity equation reduces to

$$\frac{\partial n_i}{\partial t} = -\frac{\partial}{\partial z}(n_i\, w) = \frac{w}{H_i}\, n_i \quad , \tag{3.50}$$

with

$$n_{i,t} = n_{i,t_0} \exp\left(\frac{w}{H_i}\, t\right) \quad . \tag{3.51}$$

The term $\tau_w = H_i/w$ expresses the characteristic time for the vertical advection. Time constants in meridional and zonal direction can be derived analogous. The according

gradients, however, are much more difficult to derive because more measurements in vertical direction exist. Assuming a length scale of 1000 km in the horizontal directions and a typical zonal wind speed of 10 - 100m/s, the characteristic time τ_u is about a day in the middle atmosphere. The mean meridional transport in the stratosphere has a time scale τ_v of months. The time scale in the mesosphere is in the order of days due to the higher speed of the mean meridional wind.

In general, *Brasseur and Solomon* [1986] distinguish three cases which characterize the influence of dynamics and chemistry on the distribution of a tracer.

$\tau_{chem} \ll \tau_{dyn}$: In this case the species will be in photochemical equilibrium and advective transport has no direct influence on the distribution. An indirect influence by interaction with species of longer life times, or a change in temperature for temperature dependent reaction rate constants, can occur and change the distribution of the constituent.

$\tau_{chem} \gg \tau_{dyn}$: The advective transport is responsible for the distribution of the constituent. For example, N_2O has a τ_{chem} in the order of years in the lower stratosphere and a τ_u in the order of days. This results in a constant mixing ratio in zonal direction.

$\tau_{chem} \approx \tau_{dyn}$: The distribution of the species depends critically on both, dynamics and chemistry.

3.4 Chemical Reactions and Rate Constants

The set of chemical reactions is based on the paper by *Fichtelmann and Sonnemann* [1989]. The scheme consists mainly of the oxygen, hydrogen and nitrogen reactions. The few carbon reactions are used for the parametrization of the methane decomposition by $O(^1D)$ according to the graph in figure 3.1, taken from the paper of *Sonnemann et al.* [1998a]. The chlorine and bromine reactions were used for sensitivity studies of the odd oxygen destruction in the mesosphere. ClX and BrX were set to a constant, height depending mixing ratio for these calculations.

The scheme includes the rates of interaction of neutral atoms and molecules for the mesosphere and lower thermosphere. This reduced scheme, compared with schemes for stratospheric chemistry, would not give a state of the art distribution for ozone. An ozone climatology [*Pawson et al.*, 1998] is therefore implemented for the lower mesospheric height region as a boundary condition. This is helpful to get reasonable transfer rates between the hydrogen constituents. The reactions of plasma components are not included, although they are important for the NOX chemistry in the thermosphere. For a 3-dimensional model however, with a high spatial resolution in vertical direction, a cut has to be made somewhere for the reason of needed cpu-time.

The reaction rate set is compared with the set in *Brasseur and Solomon* [1986]. Reaction rates which are not updated by new publications have the abbreviation "BS" in the last column. The updated rates have an "D90" for *DeMore et al.* [1990], "D92" for *DeMore et al.* [1992], "D94" for*DeMore et al.* [1994], or "AT" for *Atkinson et al.* [1992], although there are only small changes mostly. The presentation of the rate constants is like in the book of *Brasseur and Solomon* [1986] in order to allow an easy comparison of the used reactions. Additional reactions (the name of the rate constant begins with r) from the scheme of *Fichtelmann and Sonnemann* [1989] are included although some of the rates are small compared to other reactions of the same group.

Oxygen (O_x) Reactions

k_1	$O + O + M$	$\longrightarrow$	$O_2 + M$	$4.7(-33)\,(300/T)^{2.0}$	BS
k_2	$O + O_2 + M$	$\longrightarrow$	$O_3 + M$	$6.0(-34)\,(300/T)^{2.3}$	BS
k_3	$O + O_3$	$\longrightarrow$	$2\,O_2$	$8.0(-12)\exp(-2600/T)$	BS
k_{4a}	$O(^1D) + N_2$	$\longrightarrow$	$O(^3P) + N_2$	$1.8(-11)\exp(110/T)$	D94
k_{4b}	$O(^1D) + O_2$	$\longrightarrow$	$O(^3P) + O_2$	$3.2(-11)\exp(70/T)$	D94
k_7	$O(^1D) + O_3$	$\longrightarrow$	$2\,O_2$	$1.2(-10)$	BS
k_8	$O(^1D) + O_3$	$\longrightarrow$	$O_2 + 2\,O$	$1.2(-10)$	BS

Hydrogen (HO_x) Reactions

a_{1a}	$H_2O + O(^1D)$	$\longrightarrow$	$2\,OH$	$2.2(-10)$	BS
a_{3a}	$H_2 + O(^1D)$	$\longrightarrow$	$H + OH$	$1.0(-10)$	BS
a_1	$H + O_2 + M$	$\longrightarrow$	$HO_2 + M$	$5.7(-32)\,(300/T)^{1.6}$	D94
a_2	$H + O_3$	$\longrightarrow$	$OH + O_2$	$1.4(-10)\exp(470/T)$	BS
a_5	$OH + O$	$\longrightarrow$	$H + O_2$	$2.2(-11)\exp(120/T)$	D94
a_6	$OH + O_3$	$\longrightarrow$	$HO_2 + O_2$	$1.6(-12)\exp(-940/T)$	BS
a_{6b}	$HO_2 + O_3$	$\longrightarrow$	$OH + 2\,O_2$	$1.1(-14)\exp(-500/T)$	D94
a_7	$HO_2 + O$	$\longrightarrow$	$OH + O_2$	$3.0(-11)\exp(200/T)$	BS
a_{16}	$2\,OH$	$\longrightarrow$	$H_2O + O$	$4.2(-12)\exp(-240/T)$	D94
a_{17}	$OH + HO_2$	$\longrightarrow$	$H_2O + O_2$	$4.8(-11)\exp(250/T)$	D94
a_{19}	$OH + H_2$	$\longrightarrow$	$H_2O + H$	$5.5(-12)\exp(-2000/T)$	D94
a_{23a}	$H + HO_2$	$\longrightarrow$	$2\,OH$	$7.2(-11)$	AT
a_{23b}	$H + HO_2$	$\longrightarrow$	$H_2 + O_2$	$5.6(-12)$	AT
a_{23c}	$H + HO_2$	$\longrightarrow$	$H_2O + O$	$2.4(-12)$	AT
a_{26}	$HO_2 + NO$	$\longrightarrow$	$OH + NO_2$	$3.7(-12)\exp(240/T)$	BS
a_{27}	$2\,HO_2$	$\longrightarrow$	$H_2O_2 + O_2$	$2.3(-13)\exp(600/T)$	D94
a_{30}	$H_2O_2 + OH$	$\longrightarrow$	$H_2O + HO_2$	$2.9(-12)\exp(-160/T)$	D94
a_{31}	$H_2O_2 + O$	$\longrightarrow$	$OH + HO_2$	$1.4(-12)\exp(-2000/T)$	BS
r_{65}	$N + OH$	$\longrightarrow$	$NO + H$	$3.8(-11)\exp(85/T)$	AT
r_{74}	$H + NO_2$	$\longrightarrow$	$NO + OH$	$4.0(-10)\exp(-340/T)$	D92
r_{83}	$H + OH + N_2$	$\longrightarrow$	$H_2O + N_2$	$1.4(-24)\,(1/T)^{2.6}$	D90
r_{95}	$2\,OH + M$	$\longrightarrow$	$H_2O_2 + M$	$6.9(-31)\,(300/T)^{0.8}$	D90
r_{100}	$2\,HO_2 + M$	$\longrightarrow$	$H_2O_2 + O_2 + M$	$1.7(-33)\exp(1000/T)$	D90

Nitrogen (NO_x) Reactions

b_3	$NO_2 + O$	$\longrightarrow$	$NO + O_2$	$6.5(-12)\exp(120/T)$	D94
b_4	$NO + O_3$	$\longrightarrow$	$NO_2 + O_2$	$2.0(-12)\exp(-1400/T)$	D94
b_5	$N + NO_2$	$\longrightarrow$	$N_2O + O$	$3.0(-12)$	BS
b_6	$N + NO$	$\longrightarrow$	$N_2 + O$	$3.4(-11)$	BS
b_7	$N + O_2$	$\longrightarrow$	$NO + O$	$4.4(-12)\exp(-3220/T)$	BS
b_9	$NO_2 + O_3$	$\longrightarrow$	$NO_3 + O_2$	$1.2(-13)\exp(-2450/T)$	BS
b_{11}	$NO_3 + NO$	$\longrightarrow$	$2\,NO_2$	$1.3(-11)\exp(250/T)$	BS
b_{15}	$NO_3 + O$	$\longrightarrow$	$NO_2 + O_2$	$1.0(-11)$	BS
b_{38}	$N_2O + O(^1D)$	$\longrightarrow$	$N_2 + O_2$	$4.9(-11)$	BS
b_{39}	$N_2O + O(^1D)$	$\longrightarrow$	$2\,NO$	$6.7(-11)$	BS
r_{15}	$O + NO + M$	$\longrightarrow$	$NO_2 + M$	$9.0(-32)\,(300/T)^{1.5}$	D94
r_{19}	$O + NO_2 + M$	$\longrightarrow$	$NO_3 + M$	$9.0(-32)\,(300/T)^{2}$	D94
r_{53}	$O_3 + N$	$\longrightarrow$	$NO + O_2$	$1.0(-16)$	D90

Carbon Reactions

c_{1a}	$CH_4 + O(^1D)$	$\longrightarrow$	$CH_3 + OH$	$1.4(-10)$	BS
c_{1b}	$CH_4 + O(^1D)$	$\longrightarrow$	$CH_2O + H_2$	$1.4(-11)$	BS
c_2	$CH_4 + OH$	$\longrightarrow$	$CH_3 + H_2O$	$2.65(-12)\exp(-1800/T)$	D94

Chlorine and Bromine Reactions

d_2	$Cl + O_3$	$\longrightarrow$	$ClO + O_2$	$2.8(-11)\exp(-257/T)$	BS
d_3	$ClO + O$	$\longrightarrow$	$Cl + O_2$	$4.7(-11)\exp(-50/T)$	BS
d_4	$ClO + NO$	$\longrightarrow$	$Cl + NO_2$	$6.2(-12)\exp(294/T)$	BS
e_2	$Br + O_3$	$\longrightarrow$	$BrO + O_2$	$1.4(-11)\exp(-755/T)$	BS
e_3	$BrO + O$	$\longrightarrow$	$Br + O_2$	$3.0(-11)$	BS
e_4	$BrO + NO$	$\longrightarrow$	$Br + NO_2$	$8.7(-12)\exp(265/T)$	BS
e_{4b}	$BrO + OH$	$\longrightarrow$	$Br + HO_2$	$1.0(-11)$	BS
e_5	$BrO + ClO$	$\longrightarrow$	$Br + Cl + O_2$	$3.0(-11)$	BS
e_6	$BrO + BrO$	$\longrightarrow$	$2\,Br + O_2$	$6.0(-14)\exp(150/T)$	BS

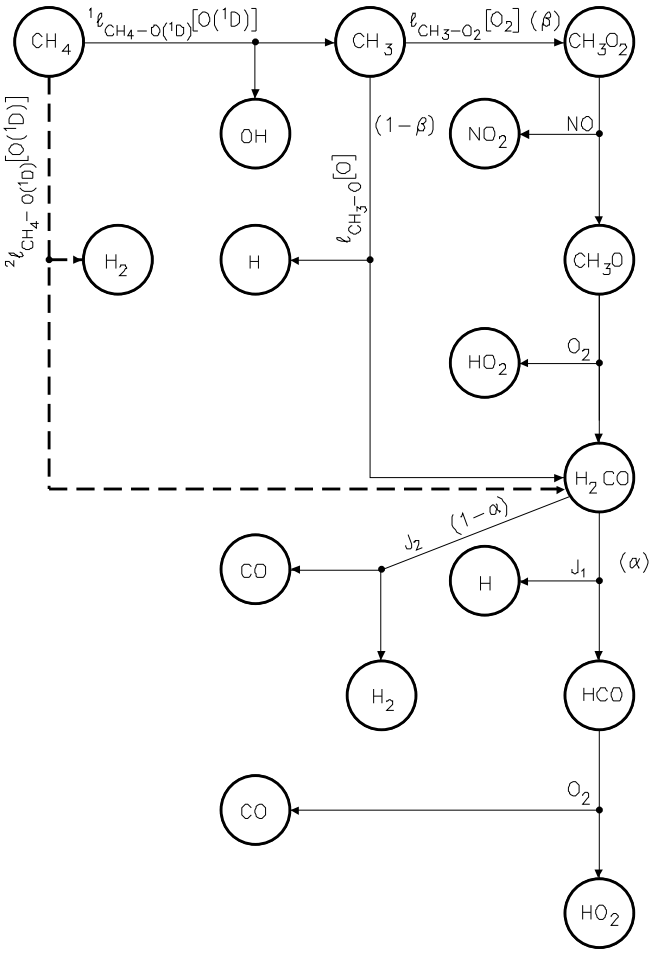

H	OH	HO_2	H_{odd}	H_2	O	O_{odd}	NO	NO_2	N_{odd}	CO
$1-\beta+\alpha$	1	$\beta+\alpha$	$2+2\alpha$	$1-\alpha$	$\beta-1$	$-2+\beta$	$-\beta$	β	0	1

Gain or Loss in Units of ${}^1\ell_{CH_4-O(^1D)}[CH_4][O(^1D)]$ (solid line graph only)

Branching rates: $\alpha = \frac{J_1}{J_1+J_2}$; $\beta = \frac{\ell_{CH_3-O_2}[O_2][M]}{\ell_{CH_3-O_2}[O_2][M]+\ell_{CH_3-O}[O]}$

Figure 3.1: Graph of the methane decomposition by $O(^1D)$ from the paper by *Sonnemann et al.* [1998a].

3.5 Photodissociation

The main part of the diurnal variation in chemistry results from the change of the zenith angle of the sun on the grid and the depending photodissociation of certain molecules. The used radiation code is the same as in the paper by *Sonnemann et al.* [1998a]. The code was primarily developed by *Fichtelmann and Sonnemann* [1989] for use in mesospheric and thermospheric modelling and considers the EUV and X-ray spectrum of the solar radiation. The lower mesospheric rates were revised by Kremp, a co-author of the paper by *Sonnemann et al.* [1998a]. She implemented a code developed by *Röth* [1992] for stratospheric modelling. The annual variation due to the eccentricity of the earth's orbit is approximated by a sine function with an amplitude of 3.5 % of the calculated rates, which means an absolute variation of 7 % between summer and winter. The radiation code is running offline, which means that it uses fixed absorber concentrations for the calculation of the photodissociation rates.

The rates in a model run are taken from the precalculated library and the actual rates depend on the zenith-angle of the sun at the grid points. The zenith-angle is rounded to integer yielding the index for the library. Due to the small variations in the mesosphere of the photolysis rates of the minor constituents this is an useful first approximation. Modelling the stratospheric photolysis, scientists have to deal much more with reflection by clouds and scattering of radiation. Between 300 and 800 nm an enhancement factor of the radiation intensity greater than unity is calculated depending on surface albedo and multiple scattering [*Brasseur and Solomon*, 1986]. The described procedure saves cpu-time but for an interactive coupling with the dynamic module it should be revised and the actual absorber concentrations should be used.

Reconsidering water vapour at mesospheric heights the cyclical variation over longer periods (e.g. 11-year cycle of the sun) in Lyman-α should be implemented also, because the probability of NLC-observation seems to be anti-correlated with the solar activity. Right now this effect can only be parametrized by a rough scaling of the Lyman-α related dissociation rates for the purpose of sensitivity studies.

Chapter 4

Transport

4.1 Modelling of Transport Processes

For the modelling of the distribution of the minor constituents, the advective transport is an important process for chemically long-lived trace gases. The equation to be solved is the continuity equation describing the advection of a non-diffusive quantity in a flow field.

$$\frac{\partial \psi}{\partial t} \; + \; \nabla \cdot (\vec{v}\psi) \; = \; 0 \quad , \tag{4.1}$$

with the non-diffusive scalar quantity $\psi(x, y, z, t)$, the velocity vector $\vec{v} = (u, v, w)$, and the independent space and time variables x, y, z, t. For atmospheric transport x and y are expressed by spherical coordinates and u and v are the velocity components in the according direction of the spherical coordinate system. The change of the quantity per time interval in a grid box must be equal to the flux through the boundaries, if there are no sources and sinks (theorem of Gauss). Equation (4.1) can be transformed into

$$\frac{\partial \psi}{\partial t} \; + \; \vec{v} \cdot \nabla \psi \; + \; \psi \, \nabla \cdot \vec{v} \; = \; 0 \quad . \tag{4.2}$$

For an incompressible fluid the divergence of the wind speed is equal to zero ($\nabla \cdot \vec{v} = 0$) which simplifies equation 4.2. For a compressible fluid like the atmosphere a similar simplification $\nabla \cdot (\rho \vec{v}) = 0$ can be achieved by the use of log-pressure coordinates, as used in COMMA-IAP. The vertical velocity w is calculated in COMMA-IAP according to the hydrostatic law

$$\frac{1}{r \cos\phi} \frac{\partial}{\partial \phi}(v \cos\phi) \; + \; \frac{1}{r \cos\phi} \frac{\partial u}{\partial \lambda} \; + \; \frac{1}{\rho_0} \frac{\partial}{\partial z}(\rho_0 w) \; = \; 0 \quad , \tag{4.3}$$

with $\rho_0(z) = \rho_s \exp(-z/H)$, where $\rho_{s(urface)}$ is the density at $z = 0$. For description in detail see the book by *Holton* [1992] and the Ph.D. thesis by *Berger* [1994]. Equation

(4.2) is reduced to

$$\frac{\partial \psi}{\partial t} + \vec{v} \cdot \nabla \psi = 0 \quad . \tag{4.4}$$

The density is set as independent of temperature, although in the real atmosphere there is a relation between pressure and density according to the ideal gas law

$$\rho = p \cdot \frac{m}{kT} \quad . \tag{4.5}$$

If an air parcel at a level of constant pressure is heated up by radiation, the air expands and a divergent flow follows as long as the expansion process takes place. This process would have to be included in Equation (4.3) if the density ρ would depend on temperature. The formulation of Equation (4.3) however is equivalent to $\nabla \cdot \rho \vec{v} = 0$, and so Equation (4.4) is for the advective transport equivalent to Equation (4.1) and can be used for the calculation of advective transport by the use of mixing ratios.

For the one-dimensional case the Equation (4.4) is reduced to

$$\frac{\partial \psi}{\partial t} + u \frac{\partial \psi}{\partial x} = 0 \quad . \tag{4.6}$$

It can be shown that for all initial values

$$\psi(x, t_0) = \zeta(x) \tag{4.7}$$

a general solution exists [*Haltiner and Williams*, 1980]

$$\psi(x, t) = \zeta(x - ut) \quad . \tag{4.8}$$

This is equivalent to a wave that propagates in the positive x-direction. The lines $x - ut = constant$ are called the characteristics of the advection equation.
However, for a real atmosphere no analytic solution of this equation exists. Numerical advective schemes have to be used, to calculate the transport effects. These schemes have to fulfil the following requirements for the transport of a chemical tracer:

stability: the solution should converge against finite values over a long integration period

positive definiteness: there should be no negative concentrations or mixing ratios in the solution

mass conserving: there should be no sources or sinks due to the advection algorithm

monotonicity: the advection scheme should not produce new extrema in the distribution of constituents

small numerical diffusion: gradients should be conserved and not be smoothed very much with time

low cpu-time consumption: the needed cpu-time per constituent should be small because several constituents have to be transported in the CTM

4.2 Advection Schemes

4.2.1 Euler Forward Differencing

A simple scheme to solve Equation (4.6) is the so called Euler forward differencing. It is first order in time and second order in space by centered differencing. ψ_j^n is the value of ψ at time step n and grid point j.

$$\frac{\psi_j^{n+1} - \psi_j^n}{\Delta t} = -u_j^n \left(\frac{\psi_{j+1}^n - \psi_{j-1}^n}{2\Delta x} \right) \tag{4.9}$$

Quantities at time step $n+1$ are calculated only by quantities at time step n. The authors of the book *Numerical Recipes* [*Press et al.*, 1990] write about this scheme: "It's a fine example of an algorithm that is easy to derive, takes little storage, and executes quickly. Too bad it doesn't work!" It is an unstable method, which can be used only to study waves for a short fraction of one oscillation period, see the chapter about partial differential equations for more details.

4.2.2 Upwind Differencing Scheme

There is a variety of different advection schemes with different advantages and disadvantages. The simplest way to model transport properties more realistic than it can be done with the forward Euler method, is the usage of the so called upwind differencing scheme.

$$\frac{\psi_j^{n+1} - \psi_j^n}{\Delta t} = -u_j^n \begin{cases} \dfrac{\psi_j^n - \psi_{j-1}^n}{\Delta x}, & u_j^n > 0 \\ \dfrac{\psi_{j+1}^n - \psi_j^n}{\Delta x}, & u_j^n < 0 \end{cases} \tag{4.10}$$

This scheme is only first order, both in time and space. Why does it work better than the Euler forward differencing?

The stability analysis yields a stable behaviour of the solution, if the CFL (Courant-Friedrichs-Lewy) condition [*Courant et al.*, 1928]

$$\frac{|v|\ \Delta t}{\Delta x} \ \leq \ 1 \tag{4.11}$$

is fulfilled. With a maximum allowed velocity of $|v| = \Delta x/\Delta t$, the upwind scheme produces an advective shift of the quantities of one grid cell length in the direction of the flow, never producing negative values. The Euler forward scheme, however, can produce negative values even for smaller velocities, if the gradients are steep enough.

4.2.3 Smolarkiewicz Scheme

The upwind scheme has one major disadvantage. It produces enhanced numerical diffusion, or in other words, the spatial gradients in the distribution of a constituent are smoothed quickly. On the other hand, this scheme is fast, mass conserving, and positive definite. This led scientists to the approach of building up an advective scheme on the basis of the upwind scheme with less numerical diffusion. One successful approach is the scheme of *Smolarkiewicz* [1983]. His approach starts with the general advection equation in one dimension

$$\frac{\partial \psi}{\partial t} + \frac{\partial}{\partial x}(u\psi) \ = \ 0 \quad , \tag{4.12}$$

and uses a staggered grid for the upwind scheme:

$$\psi_j^{n+1} \ = \ \psi_j^n - \left[F(\psi_j^n, \psi_{j+1}^n, u_{j+1/2}^n) - F(\psi_{j-1}^n, \psi_j^n, u_{j-1/2}^n)\right] \quad , \tag{4.13}$$

with

$$F(\psi_j, \psi_{j+1}, u) \ = \ \frac{\Delta t}{2\Delta x}\left[(u + |u|)\psi_j + (u - |u|)\psi_{j+1}\right] \quad . \tag{4.14}$$

Δt and Δx are the time and space increments. The fluxes F are defined at the same staggered grid points as the velocity values. To reduce numerical diffusion, Smolarkiewicz expands ψ_j^{n+1} , ψ_{j+1}^n , and ψ_{j-1}^n in a second order Taylor sum about the point (x_j, t^n) for the case of uniform flow ($u = constant$).

$$\begin{aligned}
\psi(t + \Delta t) &= \psi(t) + \Delta t \frac{\partial \psi}{\partial t} + \frac{\Delta t^2}{2}\frac{\partial^2 \psi}{\partial t^2} + \ldots \\
u\psi(x + \Delta x) &= u\psi(x) + \Delta x \frac{\partial (u\psi)}{\partial x} + \frac{\Delta t^2}{2}\frac{\partial^2 (u\psi)}{\partial t^2} + \ldots \\
u\psi(x - \Delta x) &= u\psi(x) - \Delta x \frac{\partial (u\psi)}{\partial x} + \frac{\Delta t^2}{2}\frac{\partial^2 (u\psi)}{\partial t^2} - \ldots
\end{aligned} \tag{4.15}$$

The advection equation

$$\frac{\partial \psi}{\partial t} = -\frac{\partial}{\partial x}(u\psi) \tag{4.16}$$

gives for the first order Taylor sum

$$\frac{\psi_j^{n+1} - \psi_j^n}{\Delta t} = -\frac{1}{\Delta x} \begin{cases} u\psi_j^n - u\psi_{j-1}^n \,, & u_j^n > 0 \\ u\psi_{j+1}^n - u\psi_j^n \,, & u_j^n < 0 \end{cases} \,, \tag{4.17}$$

and for the second order Taylor sum, with the use of

$$\frac{\partial^2 \psi}{\partial t^2} = \frac{\partial}{\partial t} u \frac{\partial \psi}{\partial x} = u \frac{\partial}{\partial x} u \frac{\partial \psi}{\partial x} = \frac{\partial}{\partial x} u^2 \frac{\partial \psi}{\partial x} - u \frac{\partial \psi}{\partial x} \underbrace{\frac{\partial u}{\partial x}}_{=0} \tag{4.18}$$

and

$$\frac{\partial^2 (u\psi)}{\partial x^2} = \frac{\partial}{\partial x}\left(u \frac{\partial \psi}{\partial x} \right) + \frac{\partial}{\partial x}\left(\psi \underbrace{\frac{\partial u}{\partial x}}_{=0} \right) \tag{4.19}$$

Equation (4.16) expresses

$$\frac{\psi^{n+1} - \psi^n}{\Delta t} = \frac{\partial \psi}{\partial t} + \frac{\Delta t}{2} \frac{\partial^2 \psi}{\partial t^2} \approx \frac{\partial \psi}{\partial t} + \frac{\partial}{\partial x}\left(\frac{1}{2} \Delta t u^2 \frac{\partial \psi}{\partial x} \right) \tag{4.20}$$

and

$$\left.\begin{aligned} -\frac{u(\psi_{j+1} - \psi_j)}{\Delta x} &= -\frac{\partial (u\psi)}{\partial x} - \frac{\Delta x}{2} \frac{\partial^2 (u\psi)}{\partial x^2} \quad , \quad u < 0 \\ -\frac{u(\psi_j - \psi_{j-1})}{\Delta x} &= -\frac{\partial (u\psi)}{\partial x} + \frac{\Delta x}{2} \frac{\partial^2 (u\psi)}{\partial x^2} \quad , \quad u > 0 \end{aligned}\right\} \approx -\frac{\partial (u\psi)}{\partial x} + \frac{\Delta x}{2} \frac{\partial}{\partial x}\left(|u| \frac{\partial \psi}{\partial x} \right) \quad . \tag{4.21}$$

The resulting equation which is represented by the second order Taylor sum of the formulation of the upwind scheme, for $u = constant$, is

$$\frac{\partial \psi}{\partial t} = -\frac{\partial (u\psi)}{\partial x} + \frac{1}{2} \frac{\partial}{\partial x}\left[(\Delta x |u| - \Delta t u^2) \frac{\partial \psi}{\partial x} \right] \quad . \tag{4.22}$$

Equation 4.22 is equivalent to

$$\frac{\partial \psi}{\partial t} + \frac{\partial (u\psi)}{\partial x} = \frac{\partial}{\partial x}\left(K_{diff} \frac{\partial \psi}{\partial x} \right) \quad , \tag{4.23}$$

with the diffusion coefficient $K_{diff} = \frac{1}{2}(\Delta x|u| - \Delta t u^2)$. For $\Delta x \to 0$, and $\Delta t \to 0$, Equation(4.23) approaches Equation(4.12), but in a normal computational process scheme (4.10) with finite Δt and Δx approximates better an advection equation with an additional diffusive term. This diffusion term, however, is important for the stability of the scheme and cannot simply be subtracted. The diffusion process and the equation that describes it, are irreversible.

The main idea of Smolarkiewicz is, to reverse the effect of the diffusion equation in time, by the use of the upwind scheme again. The diffusion equation can be written as

$$\frac{\partial \psi}{\partial t} = \frac{\partial}{\partial x}\left(K_{diff}\frac{\partial \psi}{\partial x}\right) \quad , \tag{4.24}$$

and reversion in time means to calculate

$$\frac{\partial \psi}{\partial t} = -\frac{\partial}{\partial x}\Big(u_d \psi\Big) \quad , \tag{4.25}$$

where

$$u_d = \begin{cases} -\dfrac{K_{diff}}{\psi}\dfrac{\partial \psi}{\partial x} \, , & \text{if} \quad \psi > 0 \\ \\ 0 \, , & \text{if} \quad \psi = 0 \end{cases} \quad . \tag{4.26}$$

With the definition of the anti-diffusion velocity $\tilde{u}$,

$$\tilde{u} = \begin{cases} -u_d \, , & \text{if} \quad \psi > 0 \\ 0 \, , & \text{if} \quad \psi = 0 \end{cases} \quad , \tag{4.27}$$

the reversal in time can be simulated by the use of the upwind scheme. The resulting scheme then has two steps. The first is

$$\psi_j^* = \psi_j^n - \left[F(\psi_j^n, \psi_{j+1}^n, u_{j+1/2}^n) - F(\psi_{j-1}^n, \psi_j^n, u_{j-1/2}^n)\right] \quad , \tag{4.28}$$

the second is

$$\psi_j^{n+1} = \psi_j^* - \left[F(\psi_j^*, \psi_{j+1}^*, \tilde{u}_{j+1/2}) - F(\psi_{j-1}^*, \psi_j^*, \tilde{u}_{j-1/2})\right] \quad , \tag{4.29}$$

with

$$\tilde{u}_{j+1/2} = \frac{(|u_{j+1/2}|\Delta x - \Delta t u_{j+1/2}^2)(\psi_{j+1}^* - \psi_j^*)}{(\psi_j^* + \psi_{j+1}^* + \epsilon)\Delta x} \quad . \tag{4.30}$$

F is defined as before, and ϵ is a small value, just to ensure $\tilde{u} = 0$ when $\psi_{j+1}^* = \psi_j^* = 0$.

Because the correction step is just another upwind step, the stability of the scheme is guaranteed again by the CFL condition. And, like the upwind scheme, it is positive definite and mass conserving. For three dimensional calculations, the scheme can be

used by operator splitting. Smolarkiewicz writes in his paper, that the implicit cross-space partial derivative terms in the multidimensional formulation of his scheme are not compensated, but in the "time splitting" form, *Smolarkiewicz* [1983]. Therefore the corrective step may be repeated for better accuracy. An important point, however, is the fact that u is supposed to be constant in the derivation of the scheme. In a three dimensional model the wind components may have significant fluctuations and the scheme then will not be of second order accuracy.

Additional, some arguments follow which give a better understanding of how the concept of anti-diffusion velocity works. Outgoing from Equation (4.30), the anti-diffusion velocity $\tilde{u}$ is equal to zero for $|u| = \Delta x/\Delta t$, which is the maximum velocity acceptable for the CFL condition. For this velocity a mixing ratio at a grid point is shifted one grid cell length in the direction of the velocity. A correction in any direction would not give an improvement in accuracy . For this extreme case the upwind scheme produces no diffusion and the anti-diffusion correction works well because the result is not changed by the correction step. Another extreme case, e.g., when the gradient of the distribution is large, $\psi_{j+1} \gg \psi_j$, the mixing ratio term of the anti-diffusion velocity is close to unity,

$$\frac{\psi_{j+1} - \psi_j}{\psi_{j+1} + \psi_j + \epsilon} \leq 1 \quad . \tag{4.31}$$

If the velocity is small ($u \ll \Delta x/\Delta t$), combined with a large gradient, the diffusion effect is large and the anti-diffusion velocity is nearly equal to the velocity used in the first step of the calculations,

$$\tilde{u} \;\leq\; u \quad . \tag{4.32}$$

The anti-diffusion velocity for two grid points involved, x_j and x_{j+1}, is always directed from the lower to the higher value of the mixing ratio and thus working against the diffusive smoothing.

4.3 Summary of Transport

The scheme of Smolarkiewicz is easy to implement, computational fast, and gives good results, but for regions with high wind speed and large fluctuations, like the upper mesosphere, there is still a significant amount of smoothing due to numerical diffusion. For chemical active species with relatively short lifetimes compared to a typical transport timescale, this effect can be neglected. For long-lived constituents, however, a less diffusive transport scheme would be useful, if mass conservation and the other criteria are fulfilled in the same quality.

4.3.1 Interesting Schemes for Further Development

A very interesting scheme is presented by *Bott* [1989], with a further improvement given in a subsequent paper [*Bott*, 1992]. *Günther* [1995] compares in his Ph.D. thesis several transport schemes. Among them are three versions of Smolarkiewicz and Bott. The simplest versions of both authors are about comparable, with slightly better results for the Bott scheme and less cpu-time consumption of the Smolarkiewicz scheme. Several other schemes are tested, like semi Lagrangian schemes and a scheme provided by Prather [*Prather*, 1986]. But, the semi Lagrangian schemes have in general a problem with the mass conservation, which is a real disadvantage for the transport of a chemical tracer, and the scheme of Prather suffers from high CPU-time consumption.

So, the favourized schemes were those of Smolarkiewicz and Bott. In the two-dimensional tests, the results of the Bott schemes were the best compromise between accuracy, low numerical diffusion, and CPU-time consumption. However, in the one-dimensional description of the Smolarkiewicz scheme in the thesis of Günther, the calculation of the anti-diffusion velocity is too small by a factor of two, compared to the original formulation of Smolarkiewicz. If this is included in the source code of the test, the numerical diffusion will be enhanced.

For longtime model runs in this thesis the first run, after a parameter has been changed in the model, is always done with the upwind-scheme, because the needed cpu-time time is smaller by a factor of four compared to the Smolarkiewicz scheme with one correction step. The reason is that the upwind step can be vectorized very effectively with some precalculations used for each species to be transported. The correction step, however, needs more calculations in the inner loops, because the anti-diffusion velocity depends on the just calculated gradients of the constituents. The correction step of Smolarkiewicz can be done with a very similar structure in the source code, different from the use of the Bott scheme, which makes it to the favourized scheme in this CTM.

Another interesting candidate for the future is an algorithm presented in *Walcek and Aleksic* [1998] and *Walcek* [2000], which has a significantly improved conservation of gradients compared to the Bott scheme.

Chapter 5

Diffusion

5.1 Barometric Law and Scale Height

In a static atmosphere the pressure gradient at any level, $p(z)$, is balanced by the gravitational force on the air parcel

$$\frac{\mathrm{d}p}{\mathrm{d}z} = -\varrho\, g \ . \tag{5.1}$$

The equivalent integral form is the weight of the gas in a vertical column of unit cross section above that level

$$p(z) = \int_z^\infty \varrho(z')\, g(z')\, \mathrm{d}z' \ , \tag{5.2}$$

where $\varrho(z')$ is the density at height z', and $g(z')$ is the vertical acceleration due to gravity. According to the ideal gas law,

$$p = n\, k\, T = \varrho\, k\, T/m \ , \tag{5.3}$$

where n is the number density, k is Boltzmann's constant, T is the absolute temperature, and m is the mean molecular mass of the gas. Substituting for ϱ in Equation (5.1) and rearranging, one obtains

$$\frac{\mathrm{d}p}{p} = -\frac{mg}{kT}\,\mathrm{d}z = -\frac{\mathrm{d}z}{H} \ , \tag{5.4}$$

with $H = kT/mg$, called the atmospheric scale height. $H(z) = const.$ yields the simple form of the barometric law

$$p(z) = p(z_0)\ \exp\left(-\frac{z - z_0}{H}\right) \ . \tag{5.5}$$

In the real atmosphere with height dependent $H(z)$, the barometric law gives

$$p(z) = p(z_0)\ \exp\left(-\int_{z_0}^{z} \frac{1}{H(z')}\ \mathrm{d}z'\right)\ . \tag{5.6}$$

The height variation for m and g are small in the lower and middle atmosphere. Therefore H changes mainly with the change in T, and constant scale height means constant temperature in first approximation. The model COMMA-IAP includes a constant scale height of $H = 7\,\mathrm{km}$.

In the brief discussion of the barometric law, the atmosphere is treated as composed of a single gas of molecular mass equal to the mean molecular mass. Equation (5.1), together with the ideal gas law gives

$$\frac{\mathrm{d}p}{\mathrm{d}z} = -\varrho\, g = -n\, m\, g\ , \tag{5.7}$$

representing the balance between a pressure gradient force and the force of gravity.

5.2 Vertical Stability

In fact, the atmosphere is composed of a mixture of gases of different molecular masses m_i. If the forces are balanced for each constituent individually, Equation (5.7) becomes

$$\frac{\mathrm{d}p_i}{\mathrm{d}z} = -n_i\, m_i\, g\ , \tag{5.8}$$

where p_i is the partial pressure of constituent i, and n_i is the according number density. The sum of Equation (5.8) over all constituents gives Equation (5.7), since $p = \sum_i p_i$, $n = \sum_i n_i$, and $m = \sum_i n_i m_i / n$. The barometric law is satisfied in an atmosphere in which the forces of the individual constituents are balanced. The formulation of the diffusion processes in this work is based on the COMMA grid and its constant scale height of $H = 7\,\mathrm{km}$. The scale height of the constituents with small atomic weight is thus constant, too, but with a larger value of

$$H_i = H\,\frac{m}{m_i}\ , \quad H_i = \frac{kT}{m_i g}\ , \tag{5.9}$$

leading to a partial pressure of

$$p_i(z) = p_i(z_0)\ \exp\left(-\frac{z - z_0}{H_i}\right)\ . \tag{5.10}$$

Light gases like atomic and molecular hydrogen have large scale heights, whereas heavy gases like N_2O and O_3 have small scale heights. Therefore the density of the

heavy constituents decrease more rapidly with altitude than the density of the light constituents, and the mean molecular mass decreases with increasing height. This phenomenon of gravitational separation is observed in the heterosphere above about 100 km, but not in the underlying homosphere. Since gravitational forces on different constituents are as different below 100 km as above, the absence of gravitational separation in the homosphere requires some explanations.

If we imagine an initially homogeneous atmosphere with constant mixing ratios for all constituents independent of altitude and allow then gravity to act on the different constituents, the atmosphere will move towards a condition of gravitational separation. The different constituents will diffuse through one another and the relative motion carries on till pressure gradient and gravitational forces on each constituent are balanced as in Equation (5.8). When this balance exists, the atmosphere is said to be in diffusive equilibrium.

The relative motion of the different constituents is inhibited by collisions between them. Collisions are frequent at low altitudes where densities are high and are infrequent at high altitudes. Diffusion is therefore fast at high altitudes and slow at low altitudes. This explains the heterosphere at high altitude, but which processes explain the homosphere?

5.3 Vertical Mixing of the Atmosphere

Vertical mixing occurs by large scale convective transport, small scale turbulent mixing, and molecular diffusion. The small scale turbulent mixing cannot be resolved by the grid structure of the model.It is therefore parametrized by the concept of *eddy diffusion.*

In the stratosphere vertical mixing is slow, but even faster than separation by molecular diffusion. In the mesosphere, vertical mixing occurs fast and is still faster than the increasing molecular diffusion. In the thermosphere, above the height region where gravity waves break, separation of constituents by molecular diffusion is faster than mixing by vertical motion of the atmosphere and the heterosphere begins.

5.3.1 Modelling of the Turbulent Mixing

The atmospheric motion can be seen as a large number of eddys of different size in horizontal and also in vertical direction. This leads to the phenomenon that each model with different grid size and different filter procedures for the dynamic variables needs a different parametrization for the not resolved scale of turbulent mixing. The eddy diffusion coefficient is used to get realistic results for the vertical mixing.

For a one-dimensional model the eddy diffusion coefficient is a scalar, for a two-dimensional model it is a tensor with four components, and for a three-dimensional

model it should be a tensor with nine components.

In this CTM the eddy diffusion is calculated only with an one-dimensional eddy diffusion coefficient for the vertical coordinate. The three-dimensional wind data, provided by COMMA-IAP, have a greater variability in wind speed than typical data of a two-dimensional model. A part of the atmospheric mixing which must be parametrized by eddy diffusion in other models, is done by the three-dimensional advective transport with the diffusive Smolarkiewicz scheme.

It is easy to lose sight of the fact that the oversimplified model that is eddy diffusion must be used with care and a great deal of auxiliary physical insight, see the section by Hunten in the book *McCormac* [1975].

The parametrization of the eddy diffusion is often used to get a realistic distribution of long lived species in CTMs. This works best for chemically inactive constituents. An early model with incorporated eddy diffusion was formulated by *Colegrove et al.* [1965]. *Strobel et al.* [1987] used different values for the eddy diffusion coefficient, depending on whether a constituent is chemically active or not. The chemical passive constituents are just moved up and down by small scale eddys or gravity waves, while the active ones, like atomic oxygen or atomic hydrogen, are very effectively transported downwards into regions, where the recombination rates or loss rates are much higher. This is valid in general for termolecular loss processes with air molecules as third particles. The reaction rate increases with the increase of the number density of the surrounding air. If an air parcel is moved downwards, the loss rate for atomic oxygen is higher than before. When the parcel moves back to the place where it originated, the content of atomic oxygen has decreased. A chemical inactive tracer would not change its mixing ratio during this movement.

5.3.2 Modelling of the Molecular Diffusion

Hunten [*McCormac*, 1975] points out, that the molecular diffusion becomes important at about 90 km and dominant above 100 km. For light molecules, especially H_2 and H_2O, it should not be neglected at any height [*Hunten*, 1973], [*Hunten and Strobel*, 1974]. The flux of total-H above the tropopause is accurately conserved and is equal to the escape flux.

To get the result of a constant flux of total-H in a time dependent three- dimensional CTM, the calculation has to be highly accurate. The conservation of total-H in the chemistry and the partitioning of the hydrogen-family has to be fulfilled. Additional, the advective transport of the long lived tracer has to be accurate, too. It is allowed to be diffusive, but not dispersive, and the velocity components should be divergence free. To achieve this precision in the diffusion processes the following derivation was made.

5.4 Calculation Concepts

5.4.1 Eddy Diffusion

The *U. S. Standard Atmosphere* [1976], Equation (6), gives an expression for the vertical flux of the molecules of an individual gas species according to *Colegrove et al.* [1965]. In terms of the i th gas species, this expression is

$$\begin{aligned} n_i \cdot v_i \;\; &+ \;\; D_i \cdot \left(\frac{\mathrm{d}n_i}{\mathrm{d}z} + \frac{n_i \cdot (1+\alpha_i)}{T} \cdot \frac{\mathrm{d}T}{\mathrm{d}z} + \frac{g \cdot n_i \cdot M_i}{R^* \cdot T} \right) \\ &+ \;\; K \cdot \left(\frac{\mathrm{d}n_i}{\mathrm{d}z} + \frac{n_i}{T} \cdot \frac{\mathrm{d}T}{\mathrm{d}z} + \frac{g \cdot n_i \cdot M}{R^* \cdot T} \right) \;\; = \;\; 0 \quad , \end{aligned} \tag{5.11}$$

where R^* is the universal gas constant (R^* is equal to $k \cdot N_a$, where k is Boltzmann's constant and N_a Avogadro's constant), D_i the height-dependent molecular diffusion coefficient of the i'th species diffusing through N_2, α_i the thermal diffusion coefficient of the i'th species, M_i the molecular weight of the gas through which the i'th species is diffusing (see table 3 in *U. S. Standard Atmosphere* [1976], for the major species N_2, M has the value of 28.0134 kg/kmol), and K the height-dependent eddy diffusion coefficient.

This equation is formulated for the number density of the minor species in a geometric coordinate system. The easiest way seems to be the use of the number density of the species and the value of $\mathrm{d}z$ from the dynamic model to calculate the diffusion effects. However, this would not be very precise if the dynamic model uses log-pressure coordinates. The evaluation of the geopotential gives a temperature dependent geometric height for grid points with the same pressure meaning a temperature dependent $\mathrm{d}z$ in geometric coordinates, too. Additional, the exponential height dependence of the number density of the air is the underlying height dependence for each species.

At each grid point of the CTM the number density of the air changes with temperature according to the ideal gas law. The calculation of diffusive fluxes should be done in terms of the mixing ratios of the constituents in order to get a better accuracy. For the calculations of the chemistry module, the number density of the air is important for the termolecular reactions. A change in temperature results in a change of the production and loss rates for several constituents. The molecular diffusion coefficient is dependent on both, temperature and number density of the air.

Calculations in terms of mixing ratios avoids the side effects of the exponential function in derivations. The use of $\mathrm{d}z$ from log-pressure coordinates requires to make the same assumptions for the height dependency of the number density of the air. The derivation for the calculation in mixing ratios and $\mathrm{d}z$ from log-pressure coordinates

is shown for the eddy diffusion and for the molecular diffusion which is a bit more complex. Both is combined and solved in the model by implicit Euler differencing and the use of the Thomas algorithm, described subsequently.

The calculation of temperature and wind speed by COMMA-IAP is done under the assumption that the atmosphere is in diffusive equilibrium by the use of log-pressure coordinates. For diffusive equilibrium the flux induced by eddy diffusion for the number density of the air is

$$\Phi_k \;=\; -K \underbrace{\left(\frac{\partial n}{\partial z} + n\left(\frac{1}{H} + \frac{\partial \ln T}{\partial z}\right)\right)}_{=0} \;=\; 0 \qquad . \tag{5.12}$$

With a non zero eddy coefficient, the underbraced term has to be zero. This is an equivalent formulation to the use of log-pressure coordinates as used in COMMA-IAP.

$$p \;=\; p_0\, e^{-z/H} \qquad\qquad H = const.,\; z_0 = 0 \tag{5.13}$$

With the ideal gas law we get the height- and temperature-dependent number density of the air

$$p = nkT \qquad \Longleftrightarrow \qquad n = \frac{p}{kT} = \frac{p_0\, e^{-z/H}}{kT} \; . \tag{5.14}$$

Differentiation of the number density yields

$$\frac{1}{n}\frac{\partial n}{\partial z} \;=\; -\left(\frac{1}{H} + \frac{1}{T}\frac{\partial T}{\partial z}\right) \qquad \Longleftrightarrow \qquad \frac{\partial \ln n}{\partial z} \;=\; -\left(\frac{1}{H} + \frac{\partial \ln T}{\partial z}\right) \; . \tag{5.15}$$

Equation (5.12) can be transformed into the change of the number density per unit time by the use of Fick's law.

$$\boxed{\frac{\partial n}{\partial t} \;=\; -\frac{\partial}{\partial z}\left(\Phi_k\right) \;=\; \frac{\partial}{\partial z}\left(K\left(\frac{\partial n}{\partial z} + n\left(\frac{1}{H} + \frac{\partial \ln T}{\partial z}\right)\right)\right)} \tag{5.16}$$

These two terms are equivalent to the zero value for the underbraced term in equation 5.12. A constant scale height and the ideal gas law taken into account means the same as the assumption of a zero flux for the number density of the air by eddy diffusion. This is important for the analytic simplification of the diffusion equation.

The equation for the calculation of the eddy diffusion of the i'th constituent in terms of mixing ratio f_i can be derived.

$$n_i = n f_i \qquad \Longrightarrow \qquad \frac{\partial n_i}{\partial z} = n\,\frac{\partial f_i}{\partial z} + f_i\,\frac{\partial n}{\partial z} \tag{5.17}$$

$$\Phi_{k,i} = -K\left(\frac{\partial n_i}{\partial z} + n_i\left(\frac{1}{H} + \frac{\partial \ln T}{\partial z}\right)\right) \tag{5.18}$$

$$\frac{\partial n_i}{\partial t} = n\,\frac{\partial f_i}{\partial t} + f_i\,\frac{\partial n}{\partial t} = -\frac{\partial}{\partial z}\left(\Phi_{k,i}\right) \tag{5.19}$$

$$n\,\frac{\partial f_i}{\partial t} + f_i\,\frac{\partial n}{\partial t} = \frac{\partial}{\partial z}\left(K\left(n\frac{\partial f_i}{\partial z} + f_i\frac{\partial n}{\partial z} + n\,f_i\left(\frac{1}{H} + \frac{\partial \ln T}{\partial z}\right)\right)\right) \tag{5.20}$$

$$\begin{aligned} n\frac{\partial f_i}{\partial t} + \underbrace{f_i\frac{\partial n}{\partial t}}_{1} = {} & \frac{\partial}{\partial z}\left(Kn\frac{\partial f_i}{\partial z}\right) + \underbrace{f_i\frac{\partial}{\partial z}\left(K\left(\frac{\partial n}{\partial z} + n\left(\frac{1}{H} + \frac{\partial \ln T}{\partial z}\right)\right)\right)}_{1} \\ & + \frac{\partial f_i}{\partial z}K\underbrace{\left(\frac{\partial n}{\partial z} + n\left(\frac{1}{H} + \frac{\partial \ln T}{\partial z}\right)\right)}_{=0} \end{aligned} \tag{5.21}$$

The terms underbraced with 1 are equivalent to the diffusion of the air multiplied with the mixing ratio of the i'th constituent, and they equalize each other because the air is assumed to be in diffusive equilibrium. The third underbraced term is equal to zero according to Equation (5.12). The remaining terms are

$$n\frac{\partial f_i}{\partial t} = n\frac{\partial f_i}{\partial z}\frac{\partial K}{\partial z} + K\frac{\partial f_i}{\partial z}\frac{\partial n}{\partial z} + Kn\frac{\partial^2 f_i}{\partial z^2} \quad . \tag{5.22}$$

$$\boxed{\frac{\partial f_i}{\partial t} = K\frac{\partial^2 f_i}{\partial z^2} + \frac{\partial f_i}{\partial z}\left(\frac{\partial K}{\partial z} + K\frac{1}{n}\frac{\partial n}{\partial z}\right)} \tag{5.23}$$

With Equation (5.12) the resulting equation, which is used to calculate the effect of the eddy diffusion, is

$$\boxed{\frac{\partial f_i}{\partial t} = K\frac{\partial^2 f_i}{\partial z^2} + \frac{\partial f_i}{\partial z}\left(\frac{\partial K}{\partial z} - K\left(\frac{1}{H} + \frac{\partial \ln T}{\partial z}\right)\right)} \quad . \tag{5.24}$$

5.4.2 Molecular Diffusion

To yield a similar expression for the molecular diffusion a slightly more complicated transformation has to be done. The flux for the i'th gas species can be written

according *U. S. Standard Atmosphere* [1976]

$$\Phi_{D,i} = -D_i \left(\frac{\partial n_i}{\partial z} + n_i \left(\frac{1}{H_i} + (1+\alpha_i) \frac{\partial \ln T}{\partial z} \right) \right) \quad . \tag{5.25}$$

The individual scale height for each component can be expressed in terms of the constant scale height

$$H = \frac{R^* T}{Mg} = \frac{kT}{mg} \qquad , \qquad H_i = \frac{kT}{m_i g} = H \frac{m}{m_i} \quad . \tag{5.26}$$

M is the mass of one mole of air molecules, m the average mass of a single molecule.

The molecular diffusion coefficients are proportional to the temperature, and inverse proportional to the number density of the air. The species Dependent coefficients a_i and β_i (table 5.1) are taken from *U. S. Standard Atmosphere* [1976].

$$D_i = a_i \frac{T^{\beta_i}}{n} = \frac{\hat{D}_i}{n} \tag{5.27}$$

The equipartition law of the kinetic theory of heat says that $\overline{\frac{m}{2}u^2} = \frac{3}{2}kT$. At

gas	α_i (dimensionless)	a_i ($\mathrm{m^{-1}\,s^{-1}}$)	β_i (dimensionless)
O	0.0	$6.986 \cdot 10^{20}$	0.750
O_2	0.0	$4.836 \cdot 10^{20}$	0.750
H	-0.25	$3.305 \cdot 10^{21}$	0.500

Table 5.1: Species dependent constants required in the function of the molecular diffusion coefficient (*U. S. Standard Atmosphere* [1976])

constant temperature this is equivalent to $\overline{u^2} \sim \frac{1}{m}$. This gives the possibility to derive the appropriate values for other molecules from the table of the *U. S. Standard Atmosphere* [1976], because the root mean square of the velocity is proportional to the molecular diffusion coefficient. The coefficient $a(\mathrm{H_2})$ is calculated from the value $a(\mathrm{H})$, all other components are calculated from the values of $a(\mathrm{O})$ and $a(\mathrm{O_2})$, depending on which molecular weight is closer to the molecular weight of the component. $D(\mathrm{H_2})$ gets the same temperature dependence as $D(\mathrm{H})$.

$$a(\mathrm{H_2}) = a(\mathrm{H}) \sqrt{\frac{m(\mathrm{H})}{m(\mathrm{H_2})}} \quad , \qquad a(\mathrm{H_2O}) = a(\mathrm{O}) \sqrt{\frac{m(\mathrm{O})}{m(\mathrm{H_2O})}} \tag{5.28}$$

The z-derivative of the diffusion coefficient can be expressed in terms of the z-derivative of the temperature. This needs less cpu time for calculation and gives a reduction for the terms of the molecular diffusion. The Equation (5.29) is needed for the Equations (5.37) to (5.41).

$$\frac{\partial \hat{D}_i}{\partial z} = \beta_i \hat{D}_i \frac{\partial \ln T}{\partial z} \tag{5.29}$$

Now the molecular diffusion will be transformed analogous to the eddy diffusion.

$$\Phi_{D,i} = -D_i \left(\frac{\partial n_i}{\partial z} + n_i \left(\frac{1}{H} + \frac{\partial \ln T}{\partial z} \right) + n_i \left(\frac{1}{H} \left(\frac{m_i}{m} - 1 \right) + \alpha_i \frac{\partial \ln T}{\partial z} \right) \right) \tag{5.30}$$

$$\Phi_{D,i} = \Phi_{D_1,i} + \Phi_{D_2,i} \tag{5.31}$$

$$\Phi_{D_1,i} = -D_i \left(\frac{\partial n_i}{\partial z} + n_i \left(\frac{1}{H} + \frac{\partial \ln T}{\partial z} \right) \right) \tag{5.32}$$

$$\Phi_{D_2,i} = -D_i \; n_i \left(\frac{1}{H} \left(\frac{m_i}{m} - 1 \right) + \alpha_i \frac{\partial \ln T}{\partial z} \right) \tag{5.33}$$

The flux component $\Phi_{D_1,i}$ has the same mathematical structure as the flux resulting from the eddy diffusion.

$$\boxed{\frac{\partial n_i}{\partial t} = -\frac{\partial}{\partial z} \left(\Phi_{D_1,i} + \Phi_{D_2,i} \right)} \tag{5.34}$$

$$\boxed{\frac{\partial f_i}{\partial t} = D_i \frac{\partial^2 f_i}{\partial z^2} + \frac{\partial f_i}{\partial z} \left(\frac{\partial D_i}{\partial z} - D_i \left(\frac{1}{H} + \frac{\partial \ln T}{\partial z} \right) \right) - \frac{1}{n} \frac{\partial}{\partial z} \left(\Phi_{D_2,i} \right)} \tag{5.35}$$

Some precalculations are needed to get the z-derivative of the flux term $\Phi_{D_2,i}$.

$$F_i(T) = \frac{1}{H} \left(\frac{m_i}{m} - 1 \right) + \alpha_i \frac{\partial \ln T}{\partial z} \tag{5.36}$$

$$\begin{aligned}
-\frac{1}{n} \frac{\partial}{\partial z} \left(\Phi_{D_2,i} \right) &= \frac{1}{n} \frac{\partial}{\partial z} \left(D_i n_i F_i(T) \right) = \frac{1}{n} \frac{\partial}{\partial z} \left(D_i n f_i F_i(T) \right) \\
&= \frac{1}{n} \left(\frac{\partial f_i}{\partial z} D_i n F_i(T) + f_i \frac{\partial}{\partial z} \left(D_i n F_i(T) \right) \right) \\
&= \frac{\partial f_i}{\partial z} \left(D_i F_i(T) \right) + f_i \frac{1}{n} \frac{\partial}{\partial z} \left(D_i n F_i(T) \right) \\
&= \frac{\partial f_i}{\partial z} D_i \left(\frac{1}{H} \left(\frac{m_i}{m} - 1 \right) + \alpha_i \frac{\partial \ln T}{\partial z} \right) + f_i \frac{1}{n} \frac{\partial}{\partial z} \left(\hat{D}_i F_i(T) \right)
\end{aligned} \tag{5.37}$$

$$\begin{aligned}\frac{\partial}{\partial z}\left(\hat{D}_i F_i(T)\right) &= F_i(T)\frac{\partial \hat{D}_i}{\partial z} + \hat{D}_i \frac{\partial F_i(T)}{\partial z} \\ &= \beta_i \hat{D}_i F_i(T)\frac{\partial \ln T}{\partial z} + \hat{D}_i \alpha_i \frac{\partial}{\partial z}\left(\frac{\partial \ln T}{\partial z}\right) \end{aligned} \tag{5.38}$$

$$\frac{\partial}{\partial z}\left(\frac{\partial \ln T}{\partial z}\right) = \frac{1}{T}\frac{\partial^2 T}{\partial z^2} - \left(\frac{1}{T}\frac{\partial T}{\partial z}\right)^2 \tag{5.39}$$

$$\boxed{-\frac{1}{n}\frac{\partial}{\partial z}\left(\Phi_{D_2,i}\right) = \frac{\partial f_i}{\partial z} D_i F_i(T) + f_i D_i \left(\beta_i \frac{\partial \ln T}{\partial z} F_i(T) + \alpha_i \frac{\partial}{\partial z}\left(\frac{\partial \ln T}{\partial z}\right)\right)} \tag{5.40}$$

$$\begin{aligned}\frac{\partial D_i}{\partial z} &= \frac{\partial}{\partial z}\left(\frac{\hat{D}_i}{n}\right) = \frac{1}{n}\frac{\partial \hat{D}_i}{\partial z} + \hat{D}_i \frac{\partial}{\partial z}\left(\frac{1}{n}\right) \\ &= \frac{1}{n}\beta_i \hat{D}_i \frac{\partial \ln T}{\partial z} + \hat{D}_i \frac{1}{n}\left(\frac{1}{H} + \frac{\partial \ln T}{\partial z}\right) \\ &= \beta_i D_i \frac{\partial \ln T}{\partial z} + D_i \left(\frac{1}{H} + \frac{\partial \ln T}{\partial z}\right) \end{aligned} \tag{5.41}$$

$$\boxed{\frac{\partial D_i}{\partial z} = D_i \left((1+\beta_i)\frac{\partial \ln T}{\partial z} + \frac{1}{H}\right)} \tag{5.42}$$

The Equation (5.42) will be inserted into Equation(5.35). The terms are now added up to get a suitable structure.

$$\begin{aligned}\frac{\partial f_i}{\partial t} &= \frac{\partial^2 f_i}{\partial z^2} D_i \\ &\quad + \frac{\partial f_i}{\partial z}\left(D_i\left((1+\beta_i)\frac{\partial \ln T}{\partial z} + \frac{1}{H}\right) - D_i\left(\frac{1}{H} + \frac{\partial \ln T}{\partial z}\right) + D_i F_i(T)\right) \\ &\quad + f_i D_i \left(\beta_i \frac{\partial \ln T}{\partial z} F_i(T) + \alpha_i \frac{\partial}{\partial z}\left(\frac{\partial \ln T}{\partial z}\right)\right) \end{aligned} \tag{5.43}$$

$$\begin{aligned}\frac{\partial f_i}{\partial t} &= \frac{\partial^2 f_i}{\partial z^2} D_i + \frac{\partial f_i}{\partial z} D_i \left(\beta_i \frac{\partial \ln T}{\partial z} + F_i(T) \right) \\ &\quad + f_i D_i \left(\beta_i \frac{\partial \ln T}{\partial z} F_i(T) + \alpha_i \frac{\partial}{\partial z} \left(\frac{\partial \ln T}{\partial z} \right) \right)\end{aligned} \tag{5.44}$$

All terms of the Equations (5.24) and (5.44) are added up now. They can be solved with the implicit Thomas algorithm as described in *Morton and Mayers* [1994]. The structure of Equation (5.45) allows very few calculations of z-derivatives and results in an accurate calculation of the diffusion terms. Additional, it allows a maximum of precalculation for the terms of the innermost loops, and therefore a fast computer code with a high degree of vectorization.

$$\begin{aligned}\frac{\partial f_i}{\partial t} &= \frac{\partial^2 f_i}{\partial z^2} \left(K + D_i \right) \\ &\quad + \frac{\partial f_i}{\partial z} \left(\frac{\partial K}{\partial z} - K \left(\frac{1}{H} + \frac{\partial \ln T}{\partial z} \right) + D_i \left(\beta_i \frac{\partial \ln T}{\partial z} + F_i(T) \right) \right) \\ &\quad + f_i \; D_i \left(\beta_i \frac{\partial \ln T}{\partial z} F_i(T) + \alpha_i \frac{\partial}{\partial z} \left(\frac{\partial \ln T}{\partial z} \right) \right)\end{aligned} \tag{5.45}$$

5.5 Discretization of the Diffusion Equation

5.5.1 Explicit or Implicit Solution?

First of all, an explicit scheme for a reduced diffusion equation shall be discussed.

$$\frac{\partial f}{\partial t} = D \; \frac{\partial^2 f}{\partial z^2} \tag{5.46}$$

The discretization (the upper index is for the time step, the lower index for a one-dimensional grid) yields

$$\frac{f_j^{n+1} - f_j^n}{\Delta t} = D \; \frac{f_{j+1}^n - 2 f_j^n + f_{j-1}^n}{\Delta z^2} \quad , \tag{5.47}$$

and the new mixing ratio is

$$f_j^{n+1} = f_j^n + \frac{D \Delta t}{\Delta z^2} \left(f_{j+1}^n - 2 f_j^n + f_{j-1}^n \right) \quad . \tag{5.48}$$

If $D\,\Delta t/\Delta z^2 > 1/2$, then f_j^{n+1} can have a negative value, in the worst case. The time step therefore must fulfil the requirement $\Delta t \leq \Delta z^2/2D$, to keep the system stable. For $\Delta z \approx 1100\,\mathrm{m}$ and $D \approx 10^5\,\mathrm{m^2\,s^{-1}}$ at the upper boundary, follows

$$\Delta t \;\leq\; \frac{1.21 \cdot 10^6\,\mathrm{m^2}}{2 \cdot 10^5\,\mathrm{m^2\,s^{-1}}} \;\approx\; 6\,\mathrm{s} \quad . \tag{5.49}$$

This means that the calculation of the diffusion at the upper boundary needs a very small time step for reason of stability. Normally, a ten times larger time step would be stable, because there are no steep gradients to expect at the upper boundary. At a height of about 110 km the diffusion coefficient is about two orders in magnitude smaller, so the stability limit for the time step would be about 600 s for the explicit method. This behaviour shows that an implicit scheme would be more reasonable to solve the diffusion equation, because there is not such a severe stability restruction. Both schemes have first order accuracy in time and second order accuracy in space. The reduced equation formulated with the implicit method, means, to replace the forward time difference by the backward time difference, the space difference remains the same.

$$\frac{f_j^{n+1} - f_j^n}{\Delta t} \;=\; D\,\frac{f_{j+1}^{n+1} - 2f_j^{n+1} + f_{j-1}^{n+1}}{\Delta z^2} \tag{5.50}$$

With $r = \frac{\Delta t}{\Delta z^2}\,D$, the equation gives

$$-r f_{j-1}^{n+1} + (1+2r) f_j^{n+1} - r f_{j+1}^{n+1} \;=\; f_j^n \quad . \tag{5.51}$$

The implicit scheme is not so easy to solve as the explicit scheme. It involves three unknown values at the time level $n+1$, and the value of f_j^{n+1} cannot be calculated immediately since the equation involves the two neighbouring values f_{j+1}^{n+1} and f_{j-1}^{n+1}, which are unknown, too. If j has the values $1, 2, \ldots, (J-1)$ a system of $J-1$ linear equations with $J-1$ unknowns $f_j^{n+1}, j = 1, 2, \ldots, J-1$ has to be solved. Instead of a separate trivial formula for each of the unknowns in the explicit scheme, the system of equations must be solved to give the values simultaneously. The first and the last of these equations, corresponding to $j = 1$ and $j = J-1$, incorporate the known values of f_0^{n+1} and f_J^{n+1} given by the boundary conditions. Fixed values means boundary conditions of Dirichlet type, while a flux boundary condition, known as von Neumann type, means to fix the derivation at the boundary, $(\frac{f_J - f_{J-1}}{\Delta z}) = const.$. The number of unknown values in the equation system remains the same, independent of the type of boundary conditions.

5.5.2 Solution of the Implicit Scheme

LU-Decomposition

The system of equations to be solved is tridiagonal. Equation number j involves only unknowns with numbers $j-1, j$ and $j+1$, so that non-zero matrix elements are only

on the diagonal and in the positions to the left and to the right of the diagonal.

To solve a system of linear equations, there exist ready to use subroutines for almost every computer. But, for the number of $n_{surf} = 36 * 16$ or $n_{surf} = 36 * 64$ grid points on the surface of the earth, each time step of the model requires n_{surf} calls of this subroutine. Each call commonly starts a so called LU decomposition, where $\mathbf{L}$ stands for a lower triangle matrix, and $\mathbf{U}$ stands for an upper diagonal matrix.

$$\mathbf{A} \cdot \vec{x} = (\mathbf{L} \cdot \mathbf{U}) \cdot \vec{x} = \mathbf{L} \cdot (\mathbf{U} \cdot \vec{x}) = \vec{b} \tag{5.52}$$

Solving first for the vector $\vec{y}$

$$\mathbf{L} \cdot \vec{y} = \vec{b} \quad , \tag{5.53}$$

and then for the vector $\vec{x}$

$$\mathbf{U} \cdot \vec{x} = \vec{y} \quad . \tag{5.54}$$

Each right hand side $\vec{b}$ needs N^2 (N is the number of involved grid points) executions of an inner loop containing one multiplication and one addition. This method is more effective than to calculate the inverse matrix $\mathbf{A^{-1}}$ of the problem. If there is a special subroutine for tridiagonal systems, this works comparable to the Thomas algorithm, and the number of operations is in the order of N. For a detailed description see the book 'Numerical Recipes' by [*Press et al.*, 1990].

CPU-Time Consumption and Vectorization

For a grid with three dimensions, using a subroutine from a library, the vectorization is done on the dimension where the decomposition is calculated. Depending on the number of grid points, it can be favourable for a vertical diffusion process, to have the vectorization done on the horizontal dimensions of the grid. An effective way to do this, by the disadvantage of the need of more memory on the computer, is the use of the Thomas algorithm, which needs 3(addition) + 3(multiplication) +2(division) operations per mesh point. One division operation takes about the same cpu-time as three multiplication operations, but even with this weighting, the Thomas algorithm needs a factor of 10 less calculations than the general LU decomposition, with 118 grid points in vertical direction. For a powerful vectorization, each variable with one index of the now described Thomas algorithm is a matrix with three indices, and the vectorization can be done on the indices which are not involved in the decomposition.

Technical Remark about Vectorization

The memory of the NEC-SX4 is organized in a certain number of banks. The cpu cannot access the same memory bank in two consecutive access steps. At least one access on a different bank has to occur or a wait cycle happens which increases the

needed time for the program. If the vectorization is done in the innermost loop for three nested loops and three-dimensional variables, it has usually a stride of one and bank conflict should be no problem. A vectorization over the outer loops often results in an even stride. The worst cases for the stride are the higher powers of two. The dimension of the variables in the CTM are (16, 36, 118). A vectorization over the first two indices would result in a stride of 118 for the memory access. Additional needed local variables in the module should then eventually have the dimension (16, 36, 119) which would result in an uneven stride for these variables. It depends on the number of additional needed local variables and the occurrences of bank conflicts but the minimizing of bank conflicts may give a significant enhancement of the speed. However, these memory considerations are not valid for cache-based machines.

The Thomas Algorithm

A tridiagonal system in general has the form

$$-a_j f_{j-1}^{n+1} + b_j f_j^{n+1} - c_j f_{j+1}^{n+1} = f_j^n \ , \quad j = 1, 2, \ldots, J-1 \quad , \tag{5.55}$$

with

$$f_0 = const. \ , \quad f_J = const. \tag{5.56}$$

for Dirichlet boundary condition at all time steps. The coefficients a_j, b_j and c_j, and the right hand side f_j^n are given, and it is assumed that they satisfy the conditions

$$a_j > 0, \quad b_j > 0, \quad c_j > 0, \tag{5.57}$$

$$b_j > a_j + c_j > 0 \quad . \tag{5.58}$$

For the reduced diffusion equation with $a = D \frac{\Delta t}{\Delta z^2}$, $b = 1 + 2a$ and $c = a$, the conditions are satisfied. These conditions ensure that the matrix is *diagonally dominant*, with the diagonal element in each row at least as large as the sum of the absolute values of the other elements. The Thomas algorithm now reduces the system of equations to upper triangular form, by eliminating the term f_{j-1}^{n+1} in each of the equations. Suppose that the first k of equations (5.55) have been reduced to

$$f_j^{n+1} - d_j f_{j+1}^{n+1} = e_j \ , \quad j = 1, 2, \ldots, k \quad , \tag{5.59}$$

The last of these equations is

$$f_k^{n+1} - d_j f_{k+1}^{n+1} = e_k \ , \tag{5.60}$$

and the next equation in its original form is

$$-a_{k+1} f_k^{n+1} + b_{k+1} f_{k+1}^{n+1} - c_{k+1} f_{k+2}^{n+1} = f_{k+1}^n \quad . \tag{5.61}$$

The elimination of f_k^{n+1} from these two equations gives a new equation for f_{k+1}^{n+1} and f_{k+2}^{n+1},

$$f_{k+1}^{n+1} - \frac{c_{k+1}}{b_{k+1} - a_{k+1}d_k} f_{k+2}^{n+1} = \frac{f_{k+1}^n + a_{k+1}e_k}{b_{k+1} - a_{k+1}d_k} \tag{5.62}$$

Comparing equation (5.62) with equation (5.59) shows that the coefficients d_j and e_j can be obtained from the recurrence relations

$$d_j = \frac{c_j}{b_j - a_j d_{j-1}} , \quad e_j = \frac{f_j^n + a_j e_{j-1}}{b_j - a_j d_{j-1}} , \quad j = 1, 2, \ldots, J-1 \quad . \tag{5.63}$$

For the fixed boundary f_0 in equation (5.55) for $j = 1$, the initial values

$$d_0 = 0 , \quad \text{and} \quad e_0 = f_0 , \tag{5.64}$$

follow. The values of a_j, d_j, and the denominator of Equation (5.63) can be precalculated. They change only with a change in the diffusion coefficients, for example by change of the temperature. The values of e_j have to be calculated new at each time step, because the known mixing ratios f_j^n are involved. Nevertheless, a further reduction of the needed cpu-time is possible by doing these precalculations. The values of the unknown f_j^{n+1} are obtained by the use of Equation (5.60). Beginning with the known value f_J, the values of f_{J-1}^{n+1}, f_{J-2}^{n+1}, ..., f_1^{n+1} are calculated. The use of the recurrence relation in Equation (5.60) might be unstable if $|d_j| > 1$. The conditions for diagonal dominance, however, prevent this with an initial value of $|d_0| < 1$, which is fulfilled by $d_0 = 0$.

5.5.3 Implicit Scheme for the Complete Diffusion Equation

The complete diffusion equation according to Equation (5.45) can be written as

$$\frac{\partial f}{\partial t} = \frac{\partial^2 f}{\partial z^2} g_1(z) + \frac{\partial f}{\partial z} g_2(z) + g_3(z) \quad , \tag{5.65}$$

with

$$\begin{aligned} g_1 &= \left(D + K \right) \quad , \\ g_2 &= \left(\frac{\partial K}{\partial z} - K \left(\frac{1}{H} + \frac{\partial \ln T}{\partial z} \right) + D \left(\beta \frac{\partial \ln T}{\partial z} + F(T) \right) \right) \quad , \\ g_3 &= D \left(\beta \frac{\partial \ln T}{\partial z} F(T) + \alpha \frac{\partial}{\partial z} \left(\frac{\partial \ln T}{\partial z} \right) \right) \quad . \end{aligned} \tag{5.66}$$

The discretization yields

$$r_1 = \frac{\Delta t}{\Delta z^2} g_1 \quad , \qquad r_2 = \frac{\Delta t}{2\Delta z} g_2 \quad , and \qquad r_3 = \Delta t g_3 \quad , \tag{5.67}$$

and, inserted in Equation (5.55) gives

$$-(r_1 - r_2) f_{j-1}^{n+1} + (1 + 2r_1 + r_3) f_j^{n+1} - (r_1 + r_2) f_{j+1}^{n+1} = f_j^n \quad . \tag{5.68}$$

The coefficients for the calculation of the Thomas algorithm are

$$a = r_1 - r_2 \quad , \qquad b = 1 + 2r_1 + r_3 \quad , and \qquad c = r_1 + r_2 \quad . \tag{5.69}$$

All calculations of the diffusion equation are done with double precision. The described procedure allows a precise and fast calculation of the molecular- and eddy diffusion. The high quality of this formulation will be demonstrated by the results of the hydrogen escape flux calculation. The hydrogen escape flux, calculated at each height level in the model, is a very sensitive quantity to show unprecise calculations of the diffusion processes, the partitioning of the HX-family, and the calculation of advective transport.

5.6 Calculation Concept for the Fluxes of Minor Constituents

The calculation of the fluxes, especially for the hydrogen constituents, starts with the same equation from *U. S. Standard Atmosphere* [1976] as the calculation of the diffusion processes. The equation for the resulting flux from the eddy diffusion is

$$\Phi_{K,i} \;=\; -K \left(\frac{\partial n_i}{\partial z} + \frac{n_i}{T} \frac{\partial T}{\partial z} + \frac{n_i}{H} \right) \; . \tag{5.70}$$

With $n_i = n \cdot f_i$, the flux can be expressed in terms of the mixing ratio of the constituent.

$$\begin{aligned} \Phi_{K,i} &= -K \left(f_i \frac{\partial n}{\partial z} + n \frac{\partial f_i}{\partial z} + f_i \, n \left(\frac{\partial \ln T}{\partial z} + \frac{1}{H} \right) \right) \\ &= -n \, K \left(\frac{\partial f_i}{\partial z} + f_i \left(\underbrace{\frac{1}{n} \frac{\partial n}{\partial z} + \frac{\partial \ln T}{\partial z} + \frac{1}{H}}_{=0} \right) \right) \end{aligned} \tag{5.71}$$

$$\boxed{\Phi_{K,i} \;=\; -n \, K \, \frac{\partial f_i}{\partial z}} \tag{5.72}$$

The equation for the flux from the molecular diffusion is derived analogously.

$$\Phi_{D,i} = -D_i \left(\frac{\partial n_i}{\partial z} + \frac{n_i \cdot (1+\alpha_i)}{T} \frac{\partial T}{\partial z} + \frac{n_i}{H_i} \right) \tag{5.73}$$

$$\begin{aligned} \Phi_{D,i} &= -D_i \left(\frac{\partial n_i}{\partial z} + n_i \left(\frac{\partial \ln T}{\partial z} + \frac{1}{H} \right) + n_i \left(\frac{1}{H} \Big(\frac{m_i}{m} - 1 \Big) + \alpha_i \frac{\partial \ln T}{\partial z} \right) \right) \\ &= -n\, D_i \left(\frac{\partial f_i}{\partial z} + f_i \left(\frac{1}{H} \Big(\frac{m_i}{m} - 1 \Big) + \alpha_i \frac{\partial \ln T}{\partial z} \right) \right) \end{aligned} \tag{5.74}$$

With $D_i = \dfrac{\hat{D}_i}{n}$, and $\hat{D}_i = a_i \cdot T^{\beta_i}$ the flux is

$$\boxed{\Phi_{D,i} = -\hat{D}_i \left(\frac{\partial f_i}{\partial z} + f_i \left(\frac{1}{H} \Big(\frac{m_i}{m} - 1 \Big) + \alpha_i \frac{\partial \ln T}{\partial z} \right) \right)} \quad . \tag{5.75}$$

That means, the flux from the molecular diffusion is not dependent on the number density of the air. The sum of the diffusive fluxes is

$$\boxed{\Phi_{K,D,i} = -\frac{\partial f_i}{\partial z} \left(nK + \hat{D}_i \right) - f_i \hat{D}_i \left(\frac{1}{H} \left(\frac{m_i}{m} - 1 \right) + \alpha_i \frac{\partial \ln T}{\partial z} \right)} \quad . \tag{5.76}$$

Equation (5.76) shows, even if a constituent has a constant mixing ratio somewhere (the mixing ratio of H_2 in the stratosphere is nearly constant), there is a remaining positive flux for the light constituents depending on their molecular weight. This flux is independent on the number density of the air or the height level. This will be of some interest in the discussion of the total hydrogen flux.

The overall flux of a constituent, including the flux component from convective motion at a grid point, adds to

$$\boxed{\Phi_i = \Phi_{K,D,i} + f_i \cdot n \cdot w} \quad . \tag{5.77}$$

Chapter 6

Data from COMMA-IAP

COMMA-IAP provides the dynamic data for the CTM. For multiannual model runs a one year run of COMMA-IAP is the basis of the dynamic data. The current standard is to write out each constituent all ten days as a three-dimensional data field (at local midnight for the first index in longitude). Thereby, time variation is set equivalent to variation in longitude. Depending on the time step, the input fields in the CTM are shifted one grid point in longitude westward after some time steps.

For the version with 16 grid points in longitude, the maximum time step with this concept is 5400 s. With this time step a shift is necessary after each time step. A time step of 2700 s requires a shift after two time steps, and so on. The standard time step is 450 s, which requires a shift after 12 time steps. Using the 64 grid point version of COMMA-IAP, 450 s belongs to a shift of the input fields after three time steps. This concept saves storage as long as large data sets have to be precalculated for an iterative procedure with both models. For the full coupling of the models, the actual calculated values can easily be used as time and longitude dependent variables in the supplementing model.

The three wind components are needed in the advective transport module, the temperature is used in the calculation of the molecular diffusion and in the chemistry module. The data of the geopotential is used for the correlation of pressure level and geometric heights as briefly described in section 2.5. The long lived minor constituents of the mesosphere are strongly influenced by the advective transport. The following data from COMMA-IAP for northern summer solstice should give a rough understanding of typical structures of the mesosphere.

Figure 6.1 shows the latitudinal section of the zonally averaged temperature $\bar{T}$ during northern summer solstice. The grey beams indicate the height of the mesopause defined by the diurnal temperature minimum. The double structure of the mesopause is noticeable. The upper peak has a nearly constant value at the latitude range from 90° S to about 40° N. The lower peak of the summer mesopause rises with latitude

polewards. These modelling results [*Berger and von Zahn*, 1999] are in good agreement with the observations from lidar measurements on a voyage of the research vessel *Polarstern* from 71° S to 54° N, where a distinct jump in the mesopause altitude from 100 km down to 83 km happened near 25° N [*von Zahn et al.*, 1996].

The higher temperature of the mesosphere in the altitude range from the stratopause up to about 70 km expands the atmospheric column and leeds to the gradient of the isobaric surfaces versus geometric heights as shown in figure 2.1.

The three body reaction $O + O_2 + M \rightarrow O_3 + M$ which produces ozone is temperature dependent. Low temperature leeds to enhanced ozone production and the low temperature of the arctic summer mesopause influences the pattern of the secondary ozone maximum in this height region, see section 7.2. Figure 6.2 shows a high zonal

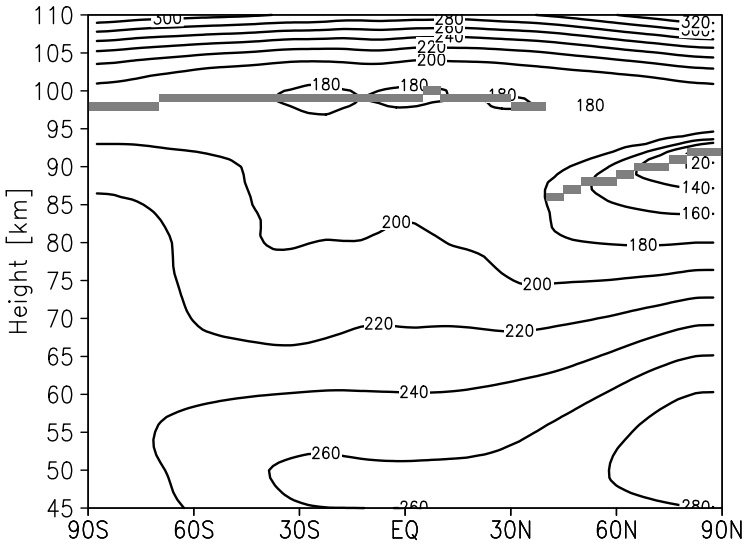

Figure 6.1: Latitudinal section of the zonally averaged temperature $\bar{T}$ [K] during northern summer solstice. The height of the mesopause is marked by grey beams.

velocity $\bar{u}$ of 50 m/s and more in large regions of the mesosphere inducing a fast mixing in zonal direction. Diurnal variations of constituents like ozone are influenced by the zonal shift with or against the rotation of the earth, see *Sonnemann et al.* [1999], and *Sonnemann* [2001].

A comparison of MF-radar wind observations with the model calculations can be found in *Kremp et al.* [1999]. The seasonal variation of the zonal wind basing on MF-radar observations in Juliusruh (1990-1997) show the pattern of a strong summer easterly wind jet of the mesosphere, a wind reversal above this domain, and a somewhat weaker eastward wind jet within the mesosphere in winter. The

comparison with the model data show that the model reflects the summer wind pattern quite well [*Kremp et al.*, 1999].

The zonally averaged meridional wind $\bar{v}$ in figure 6.3 at northern summer solstice is characterized by a general southward directed motion of a few meters per second. In the region of the cold summer mesopause a southward, downward directed pattern exceeds 5 m/s. Above this region a pattern of northward directed wind exist.

The according figure 6.4 shows the latitudinal section of the zonally averaged vertical wind during northern summer solstice. The upwind regime below the polar mesopause is noteworthy. It is a main cause for the distribution of water vapour at northern summer solstice. The vertical wind cells at lower latitudes influence strongly the distribution of the long lived constituents. The cell structure will be found again in the distribution of atomic oxygen in the upper mesosphere and lower thermosphere, see chapter 7.

In figure 6.5 a seasonal section of the zonally averaged vertical wind $\bar{w}$ at 72.5° N, close to the latitude of the ALOMAR observatory, is shown. The upwards directed vertical wind during summer causes the increase in the annual variation of the water vapour distribution. The two distinct levels of the mesopause height are demonstrated and the upwards directed vertical wind is highlighted.

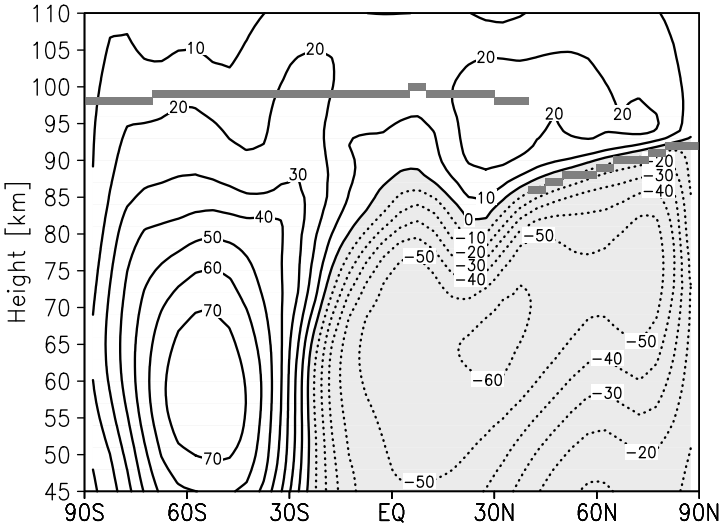

Figure 6.2: Latitudinal section of the zonally averaged zonal wind $\bar{u}$ [m/s] during northern summer solstice.

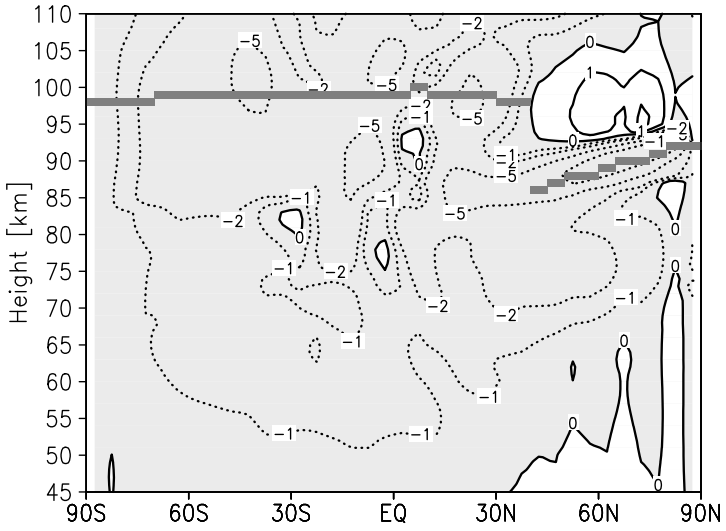

Figure 6.3: Latitudinal section of the zonally averaged meridional wind $\bar{v}$ [m/s] during northern summer solstice.

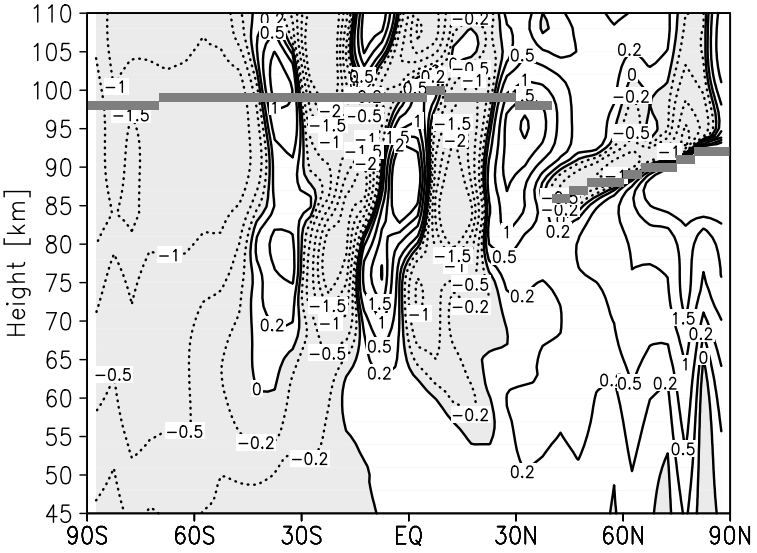

Figure 6.4: Latitudinal section of the zonally averaged vertical wind $\bar{w}$ [cm/s] during northern summer solstice. Within low latitudes vertical wind cells characterize the moving air.

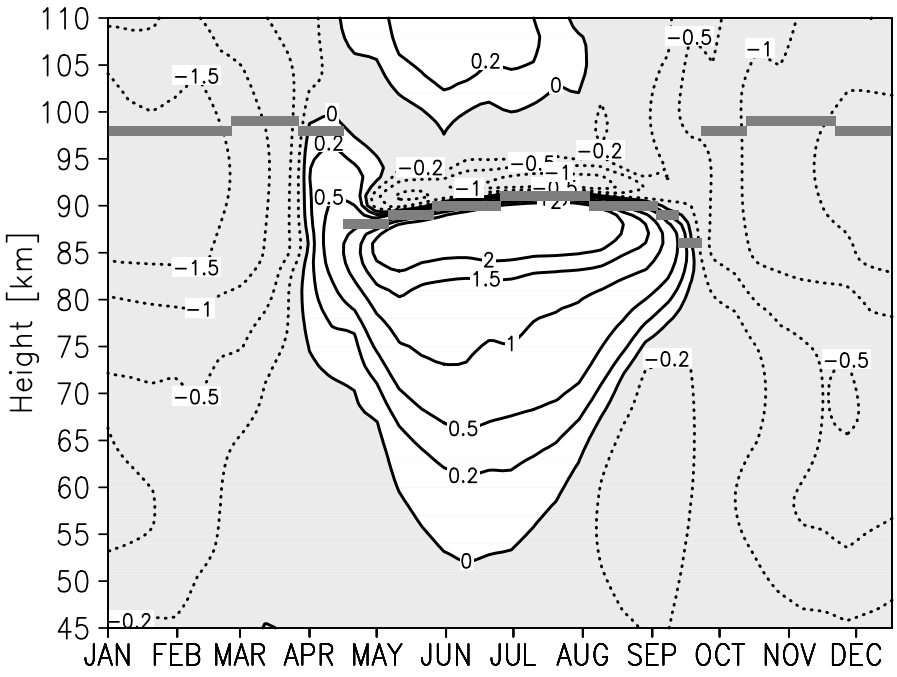

Figure 6.5: Seasonal section of the zonally averaged vertical wind $\bar{w}$ [cm/s] at 72.5° N. The grey beams indicate the height of the mesopause defined by the diurnal temperature minimum. The annual behaviour of the mesopause height with two distinct levels is demonstrated. Areas of downward directed wind are shaded.

Chapter 7

CTM-Results of Important Constituents of the Mesosphere and Lower Thermosphere

7.1 Water Vapour and the Hydrogen Constituents

Water vapour is an important constituent for the upper atmosphere. The relevance of water vapour for processes in the lower atmosphere is sufficiently known. The infrared absorption makes it to the most important green house gas of the troposphere. This influence is included in the dynamic model COMMA-IAP. The tidal waves excited by water vapour heating in the troposphere propagate up to the mesopause region and dissipate there.

Stratospheric Dryness

The troposphere is wet in contrast to the upper atmosphere and the cold tropopause acts as a trap for water vapour. The freeze drying process leaves about 4 ppmv at the tropopause height (in average 3.8 ppmv according to *Dessler and Kim* [1999]). The freeze drying only acts on H_2O, not on CH_4 or H_2 which is important for the amount of H_2O in the upper atmosphere. CH_4 is mainly oxidized to H_2O in the stratosphere. In *Gunson et al.* [1990] the total hydrogen at any altitude in the stratosphere is related to the sum of H_2O and $2\,CH_4$. This means at the same time, if there is an upward flux of CH_4 in global average larger than the equivalent escape flux of hydrogen to space, there must be a downward flux of H_2O in the stratosphere in global average. For more details about the fluxes of hydrogen constituents, see chapter 8.

Relative Water Vapour Maximum in the Lower Mesosphere

Figure 7.1 shows the typical number density of several hydrogen bearing constituents. The mixing ratios may roughly be estimated with the help of the lines of constant mixing ratio. The mixing ratio of H_2 in the stratosphere is nearly constant at a value of ≈ 0.5 ppmv. Total hydrogen is sometimes expressed by $H_{\mathrm{total}} = H_2O + 2\,CH_4 + H_2 = const$. This is valid up to about 80 km height until the mixing ratio of atomic hydrogen increases strongly and cannot be neglected in the sum of total hydrogen. In the upper mesosphere the concentration of CH_4 is small compared to the concentrations of H_2O or H_2. Variations in H_2O are therefore balanced by inverse variations in H_2. H_2O has a relative maximum mixing ratio in the middle atmosphere all over the year, but at different altitudes, depending on latitude and season.

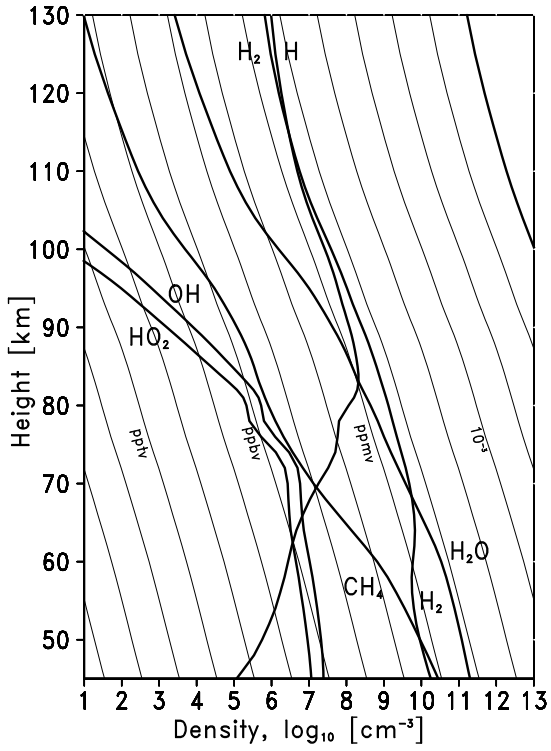

Figure 7.1: Height profile of different hydrogen bearing constituents at 2.5° N for the northern summer solstice, at noon. The thin lines represent levels of constant mixing ratio.

The Hydrogen Radicals

In the mesosphere the hydrogen radicals OH and H are mainly formed by photodissociation of H_2O by the solar Lyman-α radiation and radiation in the Schumann-Runge bands. The subsequent three body reaction of atomic hydrogen with molecular oxygen, $H+O_2+M \rightarrow HO_2+M$, forms the hydrogen radical HO_2. In the stratosphere the oxidation of H_2O by excited atomic oxygen $O(^1D)$ is more important than the photodissociation. The hydrogen radicals are the most efficient destroyer of odd-oxygen through catalytic cycles in the mesosphere. The formation of H_2 from H_2O requires the formation of hydrogen radicals, which have to be computed carefully in the chemistry module although they are only a small fraction in the total amount of hydrogen. Small deviations from mass conservation of the hydrogen radicals, however, could result in source- or sink terms for total hydrogen.

7.1.1 Water Vapour Correlated Phenomena

In the mesopause region there are some phenomena which are correlated to the concentration of water vapour. To understand these phenomena, a detailed knowledge of the climatology of water vapour is desirable.

- Noctilucent clouds (NLC), first discovered in 1885 (*Leslie* [1885] and *Jesse* [1885]), are optically thin clouds observed at altitudes between 80 and 85 km in summertime polewards of 50° latitude. For a review on the phenomenon of noctilucent clouds and observation history, see *Gadsden and Schröder* [1989].

- Polar mesospheric summer echoes (PSME) are another phenomenon of the high latitude summer mesopause. They were first discovered in 1979 as unexpectedly strong echoes obtained by a VHF-radar [*Balsley et al.*, 1980]. A review about PMSE has been written by *Cho and Röttger* [1997]. The simultaneous MST radar and electron density probe measurements by *Ulwick et al.* [1988] and the measurements of turbulence in the vicinity of PMSE by *Lübken et al.* [2001] should be noted in this context.

- The OH^*-layer, indicated by infrared airglow emission (500 nm–5 μm) in the Meinel bands, see *Makhlouf et al.* [1995] and *Sivjee* [1992]. Several night glow layers range from 85 km for OH to 97 km for the 557.7 nm line of atomic oxygen [*Meriwether*, 1989].

At ALOMAR and at the Andoya Rocket Range measurements with lidar, radar, and rocket borne instruments yield valuable data about temperature, wind, and the occurrence of NLC and PMSE in the polar mesosphere. The wind and temperature data are compared to the modelling results from COMMA-IAP [*Kremp et al.*, 1999],

[*Berger and von Zahn*, 1999]. The distribution of water vapour together with the temperature allows the calculation of the degree of supersaturation for water vapour which is correlated with the formation of NLCs and PMSEs. The modelling of the formation and the transport of icy particle layers in the high latitude mesopause region allows the detailed study of the NLC layer behaviour [*Berger and von Zahn*, 2002]. Information about atmospheric turbulence [*Lübken*, 2000] and modelling of electron density fluctuations [*Rapp and Lübken*, 2000] should give more information about the phenomenon PMSE. The aim of all this work is to get enhanced knowledge about the extreme polar mesosphere summer conditions.

7.1.2 Water Vapour Measurements

Responding to the importance of water vapour many papers have been written by scientists. An extended selection of observations of about the last two decades should be given here.

Water vapour observations in the mesosphere made by ground based microwave spectrometers have been done since about 1980 (see *Radford et al.* [1977], *Deguchi and Muhleman* [1982], *Bevilacqua et al.* [1985], *Tsou et al.* [1988], *Peter et al.* [1988], *Bevilacqua et al.* [1989], *Bevilacqua et al.* [1990], *Hartogh and Jarchow* [1995]). Airborne measurements have been done by *Peter et al.* [1988] or from MAS (Millimeter-wave Atmospheric Sounder) by *Bevilacqua et al.* [1996], and from space shuttle in the ATLAS-2 mission. A global coverage over annual time scales follows from an experiment on Nimbus 7 Limb Infrared Monitor of the Stratosphere (LIMS) which measured H_2O and NO_2 [*Kerridge and Remsberg*, 1989], from SAGE II and HALOE from UARS satellite (see *Russell et al.* [1993], *Harries et al.* [1996a], *Harries et al.* [1996b], *Summers et al.* [1996], *Summers et al.* [1997a], *Summers et al.* [1997b], *Siskind and Summers* [1998]), and from the Microwave Limb Sounder (MLS) [*Pumphrey and Harwood*, 1997].

The most surprising result was the high water vapour concentration in summer when the photodissociation acts strongest on H_2O in the mesosphere. In the winter hemisphere, however, the concentration was much lower (*Bevilacqua et al.* [1989], *Bevilacqua et al.* [1990]). These observations led to the position that the mean mesospheric circulation has an important influence on the water vapour distribution in the mesosphere which made it to a valuable tracer for atmospheric motion. Another important result was the maximum of the water vapour mixing ratio in the lower mesosphere.

Several water vapour observations with a millimeter-wave spectrometer have been made by Nedoluha and co-workers in the years since 1995, (*Nedoluha et al.* [1995], *Nedoluha et al.* [1996], *Nedoluha et al.* [1997], *Nedoluha et al.* [1998a], *Nedoluha et al.* [1998b], *Nedoluha et al.* [1999]). The first of the cited papers [*Nedoluha et al.*, 1995],

presents measurements of middle atmospheric water vapour mixing ratios using the ground-based Naval Research Laboratory water vapour millimeter-wave spectrometer (WVMS) instrument at the Jet Propulsion Laboratory Table Mountain Observatory (34.4° N, 117.7° W). The measurements covered a period from January 23, 1992, to October 13, 1992 and obtained a nearly continuous record of water vapour mixing ratios for altitudes from about 35 to 75 km. The mixing ratios generally peak between 55 and 65 km with a mixing ratio of about 6–7 ppmv. The highest peaks occurred in January, May, and October. This is not an evidence of a semiannual variation as would be to expect from the model calculations at these latitudes of this work, but it is far away from the annual variation at higher latitudes. The paper by *Nedoluha et al.* [1996], presents 3 years of nearly continuous measurements at the location of Table Mountain and Lauder, New Zealand (45.0° S, 169.7° E), at the National Institute of Water and Atmospheric Research (NIWA). They found a larger amplitude of the annual oscillation at 45.0° S than at 34.4° N, which is consistent with the higher latitude of the southern hemisphere site. The annual variation is expected to have a larger amplitude at higher latitudes due to the general circulation in the mesosphere. A semiannual cycle is particularly observed near 80 km altitude. The paper by *Nedoluha et al.* [1997] compares the observations from the WVMS instrument with five space based instruments. The annual variations measured by HALOE and WVMS show a marked similarity at the latitudes of the WVMS measurements at Table Mountain and at Lauder. The authors note that even small interannual variations in the amplitude of the seasonal cycles are consistent at Table Mountain. The profiles from the six instruments differ from the average calculated by using retrievals from all of the instruments less than one ppmv throughout most of the upper stratosphere and mesosphere. In 1998 the measurements from HALOE and WVMS had been extended up to seven years of nearly continuous measurements. The HALOE measurements in the equatorial region show trends for CH_4 and H_2O which are best explained with the used 2D model by a decrease in the tropical upward transport rate [*Nedoluha et al.*, 1998a]. The paper by *Nedoluha et al.* [1998b] compares again the HALOE and WVMS measurements at Table Mountain and at Lauder. The main issue are the observed trends of 0.129 ppmv/y (HALOE) and 0.148 ppmv/y (WVMS) in the 40–60 km height range. Measurements with the WVMS instrument at Mauna Loa, Hawaii (19.5° N, 204.4° E) started in March 1996. These observations are compared with the observations at Table Mountain and with the HALOE measurements by *Nedoluha et al.* [1999]. The relatively small seasonal variations, combined with the small amount of tropospheric water vapour above Mauna Loa, makes this an ideal site for the detection of multiyear variability in water vapour.

The most important observations for the purpose of comparison with the modelled water vapour distribution of this work are the microwave measurements by *Seele and Hartogh* [1999]. The observations were made at ALOMAR (Arctic Lidar Observatory

for Middle Atmospheric Research, Andoya, Norway, 69° N, 16° E), where also temperature observations by lidar and by falling spheres from rockets were made. A detailed description about microwave spectroscopy and the integration of the signal is given in the thesis of *Seele* [2000]. Seele and Hartogh used an average of 24 h of the measured signal at 22.235 GHz which confines the measurements to an altitude of about 80 km. An average over one week allows an retrieval of H_2O data up to 85 km. Above that height the measurement noise error and the influence of the a priori-profile (a first guess of the vertical distribution of H_2O which is needed for the inverting of the data) increase strongly. The microwave measurements at ALOMAR are carried on continuously since 1997. *Seele and Hartogh* [1999] found a pronounced annual cycle at northern high latitude with a maximum in the H_2O mixing ratio between May and September/October and a higher annual variability than at midlatitudes. There is no semiannual cycle at the northern high latitude.

A recent paper by *Summers et al.* [2001] reports the discovery of enhanced water vapour in the Arctic summer mesosphere made by utilizing two new techniques for remotely determining water vapour abundances. The first utilizes Middle Atmosphere High Resolution Spectrograph Investigation (MAHRSI) OH measurements as a proxy for water vapour. The second is a reanalysis of Halogen Occultation Experiment (HALOE) water vapour data with a technique to simultaneously determine polar mesospheric cloud (PMC) ice particle extinction along with the water vapour abundance. However, the use of the OH measurements as a proxy for water vapour needs the condition of photochemical equilibrium between odd-hydrogen and odd-oxygen species which may be not entirely fulfilled at 82–84 km altitude. Further investigation of this point with the CTM is desirable. The results of the enhanced water vapour at a level of 10–15 ppmv, coincident with the PMC region, are consistent with the indirect estimates of *von Cossart et al.* [1999] who gave an estimate of around 12 ppmv water vapour, if distributed over a narrow layer, contained in NLCs in the form of water ice.

7.1.3 Modelling Results

A model run of the CTM generates a 4-dimensional data set for each constituent. The grid structure has been described before. The time step of the data output is a multiple of the modelling time step. For multiannual model runs, usually 10 days, 15 days, or one month is chosen. The data on the pressure levels are interpolated to values on a geometric height scale by the use of the geopotential data. This allows a better comparison with lidar, radar or microwave data, which are represented on a geometric height scale.

Water Vapour and Molecular Hydrogen

In the mesosphere the isobaric levels between summer and winter hemisphere can show a height difference of up to 10 km, as shown in figure 7.2 . In the stratosphere the gradient of the isobaric surfaces versus the levels of constant altitude can be neglected. Figure 7.2 depicts the latitudinal section of water vapour at northern summer solstice. The supersaturation of water vapour at the polar mesopause is marked. A decrease of the mixing ratio from summer to winter is the mean situation at solstice due to advective transport. At low latitudes the circulation cells of up- and downwards moving air deform the isolines of water vapour mixing ratio.

Figure 7.3 shows the annual variation of water vapour at different latitudes. At high latitudes the annual variation dominates, at low latitudes the semiannual variation. Additionally, figure 7.3 contains areas which indicate the degree of supersaturation of H_2O according to the local distribution of water vapour and the temperature. The factor of supersaturation has been calculated according to an expression given by *Marti and Mauersberger* [1993]. The growth of ice particles needs a supersaturation greater than unity.

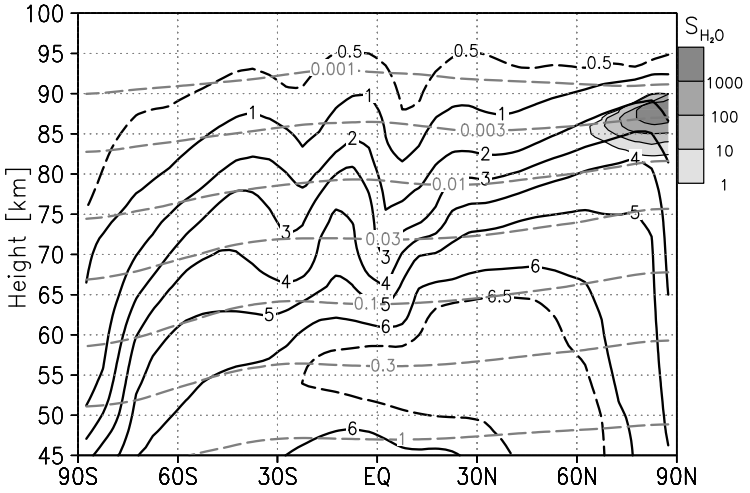

Figure 7.2: Latitudinal section of H_2O [ppmv] at northern summer solstice with isobaric surfaces (grey dashed) and supersaturation of water vapour (shaded areas).

The water vapour measurements in figure 7.4 [*Seele and Hartogh*, 1999] are in good agreement with the modelling results in figure 7.5. Both display the known seasonal variation at high latitudes. Highest values occur from May to September, lowest values from January to April. The increase in May is relatively steep compared to the decrease during autumn to winter. The summer maximum in the upper mesosphere occurs in the beginning of August. In larger heights the maximum is shifted to late

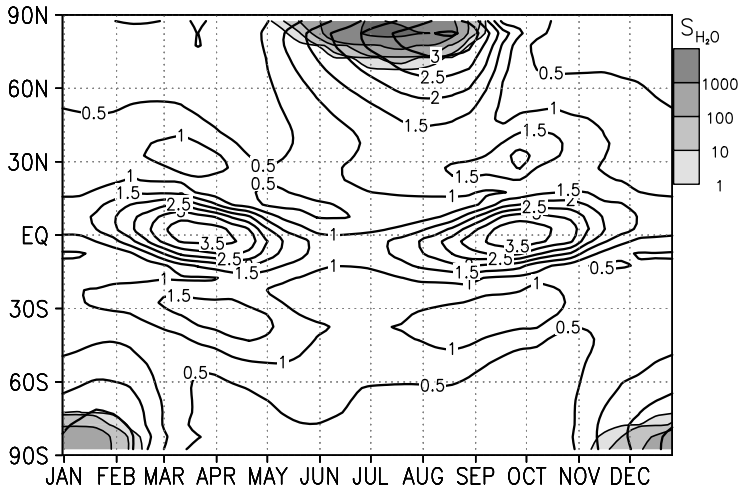

Figure 7.3: Annual variation of H_2O [ppmv] at 88 km height with supersaturation of water vapour (shaded areas).

August. During September and October an absolute maximum in the mixing ratio of 6.5–7 ppmv occurs in the upper stratosphere-lower mesosphere. All described features for the high latitude water vapour cycle agree well with the microwave observations of [*Seele and Hartogh*, 1999] in figure 7.4. They found the upper mesospheric mixing ratio maximum in August as well. The increase in May is somewhat steeper and the decrease after the summer maximum is a bit slower. The absolute amount of water vapour at the maximum in the model is about 1.5 ppmv lower, compared with the measurements. However, the Smolarkiewicz scheme, used for the advective transport, is quite diffusive, even with one correction step.

In the region, where the maximum in the water vapour distribution occurs, the recombination of hydrogen radicals form mainly H_2O to force these high mixing ratios. 8 ppmv of water vapour means that nearly all hydrogen is bound in this species. In the polar summer upwind regime few turbulent mixing occurs and the high water vapour mixing ratio seems to be possible. In this case a less diffusive transport scheme would be very important. It would give sharper gradients and a higher maximum value for water vapour in the model results.

Figure 7.6 depicts the distribution of H_2 according to figure 7.5. The inverse variation of H_2 compared with H_2O demonstrates the constant total hydrogen mixing ratio up to about 80 km. Above this height the part of atomic hydrogen in total hydrogen cannot be neglected.

The figures 7.7 and 7.8 are analogous to the figures 7.5 and 7.6 but at equatorial latitudes. The semiannual variation of both components is displayed and the validity

of constant total hydrogen can be assessed.

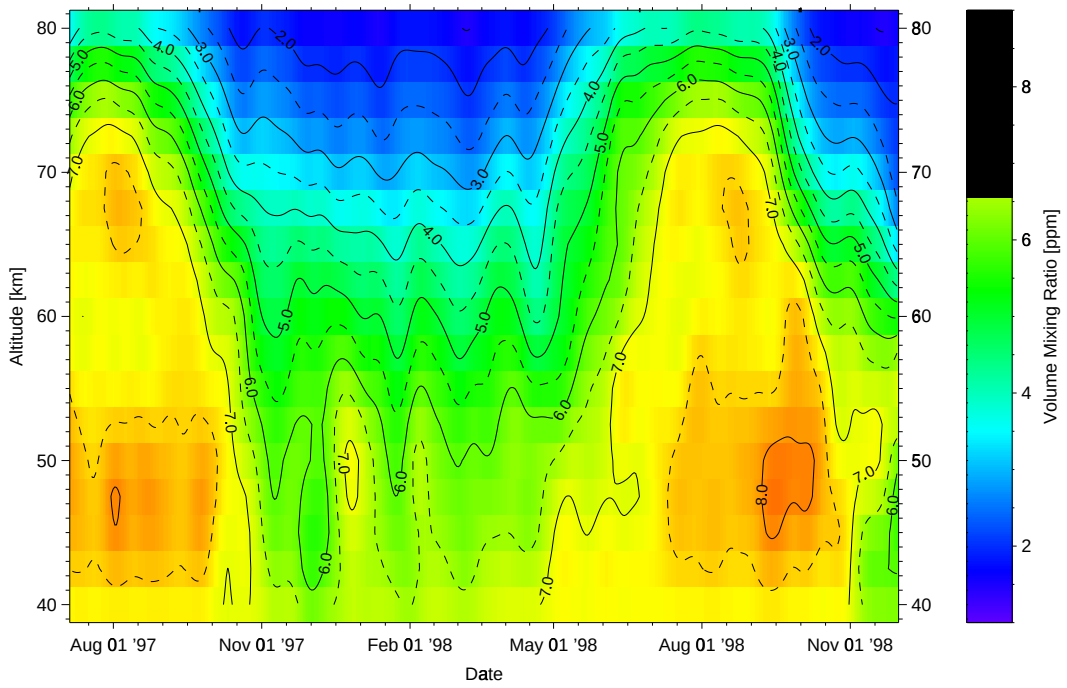

Figure 7.4: Microwave water vapour measurements at ALOMAR from *Seele and Hartogh* [1999].

Characteristic Times for Water Vapour

Different characteristic times can be calculated. The characteristic transport time includes the share of the characteristic diffusion time and the share of the characteristic time of the vertical wind. A characteristic time can be defined by the time a molecule needs to cover the distance of a scale height H, see the book of *Banks and Kockarts* [1973]. Generally, the characteristic time is a measure for the time scale in which the number density or mixing ratio of a constituent undergoes substantial changes. Characteristic times allow to assess the importance of one process compared to another.

$$\tau_T = \left(\tau_D^{-1} + \tau_w^{-1}\right)^{-1} = \frac{A \cdot H^2}{\left(\left(K + D_{H_2O}\right) + A \cdot H \cdot |w|\right)} \quad . \tag{7.1}$$

H is the atmospheric scale height, K is the eddy diffusion coefficient, D_{H_2O} is the molecular diffusion coefficient, $|w|$ is the absolute amount of the diurnal mean vertical wind and A is a constant chosen to unity, if the characteristic diffusion time has the form $\tau_{D_{H_2O}} = H^2 \;/\; (K + D_{H_2O})$, see discussion in the book of *Banks and Kockarts* [1973].

Figure 7.9 shows the seasonal section of the diurnally averaged total characteristic transport time of water vapour. The wind reversal during equinox enhances the characteristic transport time. In the upper domain the characteristic time decreases, determined by diffusion. Figure 7.10 shows a latitudinal section for northern summer solstice. There is an increase in the H_2O mixing ratio in the mesosphere during the summer months. In the lower mesosphere the characteristic transport time is in the order of months (10^7 s $\approx$ 4 month).

The second equation for comparison of the transport time scale with the chemical time scale is

$$\tau^*_{H_2O} \;=\; \left(\frac{L_{H_2O} - P_{H_2O}}{[\mathrm{H_2O}]} \right)^{-1} \quad . \tag{7.2}$$

L_{H_2O} is the absolute loss term, P_{H_2O} is the production of H_2O. Normally, the characteristic chemical time is expressed as $\tau_{H_2O} = [\mathrm{H_2O}]/L_{H_2O}$, but for the region of the water vapour maximum the production is in the order of the loss term and $\tau^*_{H_2O}$ gives a more realistic picture.

A similar situation exists in the stratosphere. The characteristic time for ozone is very much shorter than the characteristic time for odd oxygen, because ozone is immediately reproduced by reaction of atomic and molecular oxygen. The use of the measure $\tau^*_{O_3}$ from equation 7.2 would give a larger characteristic time if production and loss are nearly balanced and additional the information which process is dominant by the sign of τ^*. The characteristic time τ^* becomes a negative sign if the production term overbalances the loss term. One can argue about that, but it gives important information about interaction of transport and chemistry as shown in figures 7.11 and 7.12. The two isolated areas of strong production in figure 7.12 belong to circulation cells which move atomic and molecular hydrogen downward. The three body reaction $\mathrm{H + O_2 + M \rightarrow HO_2 + M}$ becomes more effective with decreasing height and thus the production of H_2O is enhanced. A large characteristic transport time (implicating low eddy diffusion) together with a non diffusive transport scheme may shift the H_2O maximum upwards, as published in *Harries et al.* [1996a], *Summers et al.* [1997a], and *Siskind and Summers* [1998] from HALOE data on the UARS satellite.

Above the mesopause region the loss of H_2O via photolysis is the dominating process, in the mesopause region production and loss processes are about equivalent, below 65 km altitude H_2O is effectively produced. In the polar night area exists a production of H_2O from downwards transported hydrogen which is not compensated by the slow loss processes.

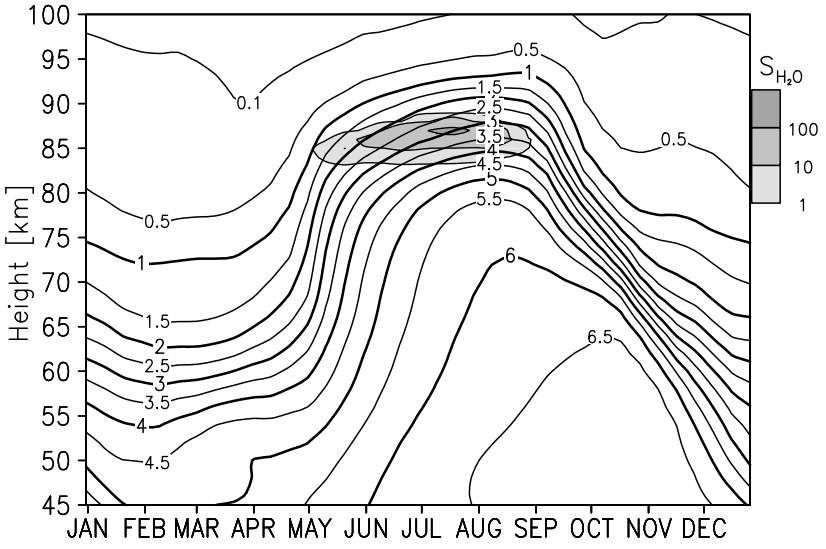

Figure 7.5: Seasonal section of H_2O [ppmv] at 72.5° N with supersaturation of water vapour (shaded areas).

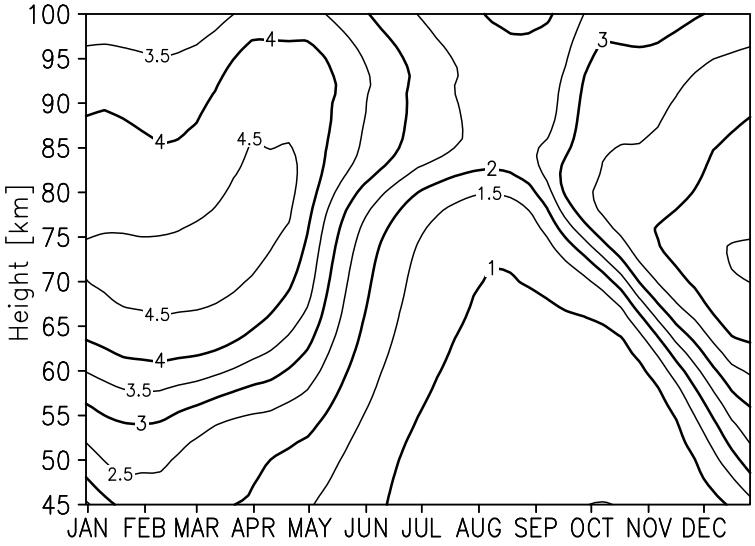

Figure 7.6: Seasonal section of H_2 [ppmv] at 72.5° N. This figure shows an inverse annual and latitudinal variation compared to figure 7.5. In the upper region the influence of atomic hydrogen dominates.

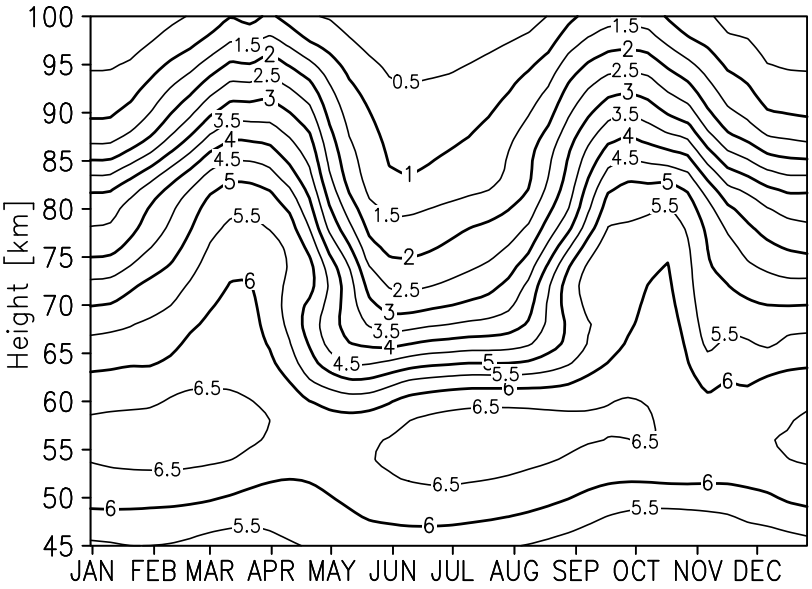

Figure 7.7: Seasonal section of H_2O [ppmv] at 2.5° N. In contrast to high latitudes (figure 7.5) a semiannual variation dominates in the equatorial region.

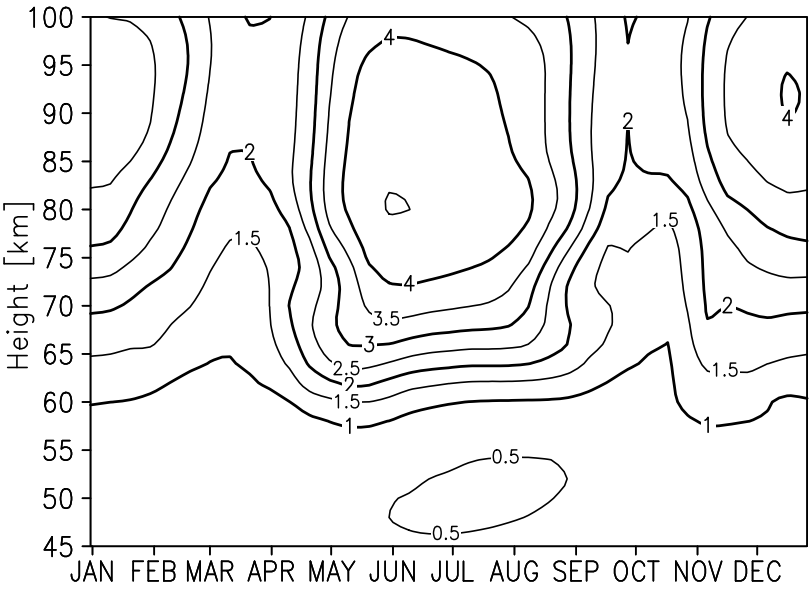

Figure 7.8: Seasonal section of H_2 [ppmv] at 2.5° N. This figure shows again the inverse variation of H_2O and H_2.

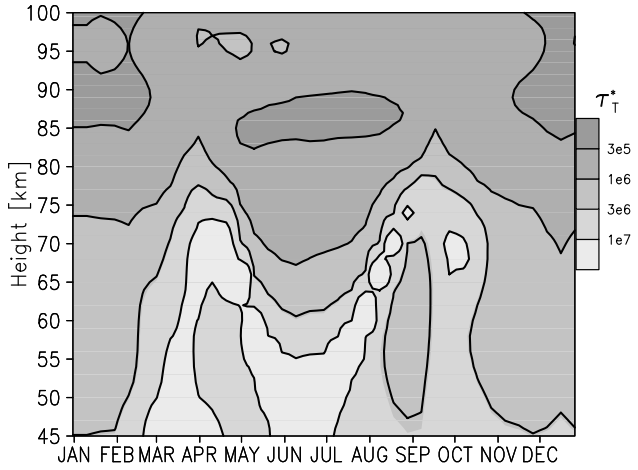

Figure 7.9: Seasonal section of the total characteristic transport time [s] for H_2O at 72.5° N computed according to equation 7.1. The wind reversal during equinox enhances the characteristic transport time.

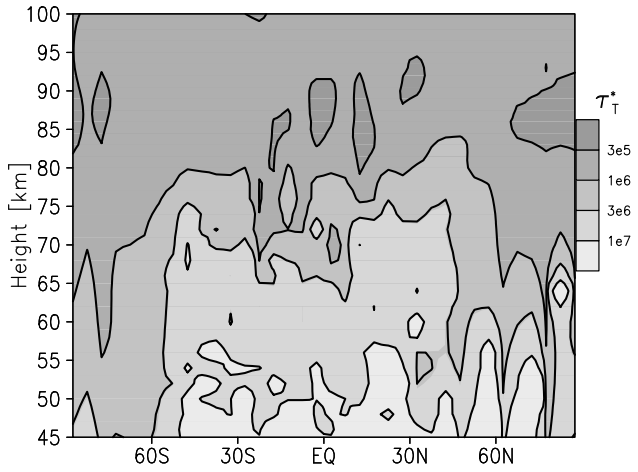

Figure 7.10: Latitudinal section of the total characteristic transport time [s] for H_2O for northern summer solstice computed according to equation 7.1. The marked cell patterns disappear as the characteristic time depends on the absolute value of the vertical wind.

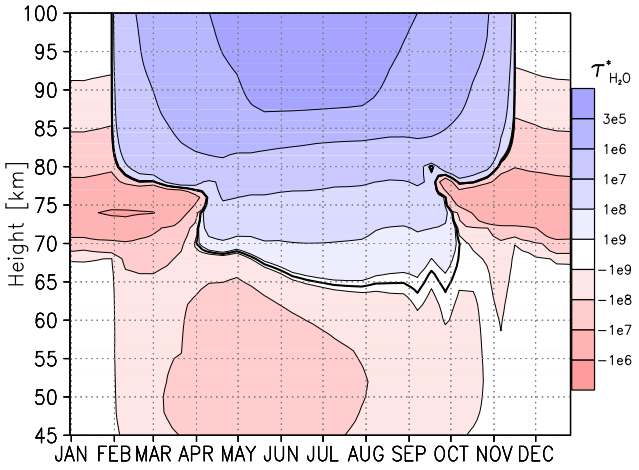

Figure 7.11: Seasonal section of the effective characteristic chemical time [s] for H_2O at 72.5° N computed according to equation 7.2. A negative characteristic (loss) time means that the production overbalances the loss of H_2O. There is no loss of H_2O during the polar night but a production due to the transport of atomic hydrogen from the thermosphere into the upper mesopause.

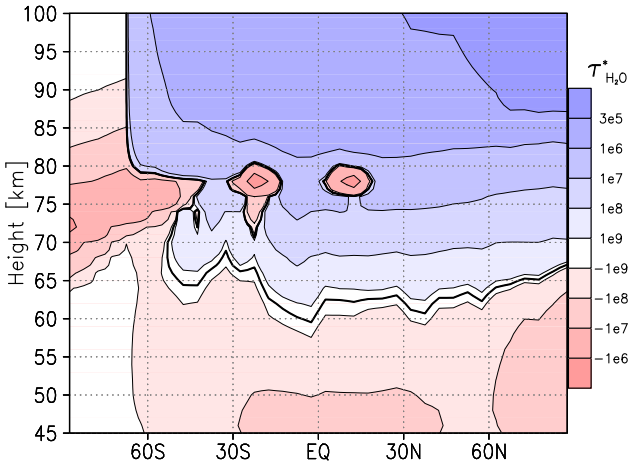

Figure 7.12: Latitudinal section of the effective characteristic chemical time [s] for H_2O for northern summer solstice computed according to equation 7.2. Isolated areas of strong production correspond to the downward directed wind cells which transport atomic hydrogen into deeper layers forming H_2O via HO_2 there. This figure has to be compared with figure 7.10 in order to understand the distribution of water vapour. Transport and chemistry are often processes of the same rank.

7.2 Ozone and the Oxygen Constituents

One of the most important species of the middle atmosphere is ozone. The heating due to the absorption of radiation in the stratosphere has a strong influence on the atmospheric motion in this region. For life on earth the absorption of the ultra violet radiation is very important.

The formation of an ozone layer was first published by *Chapman* [1930]. The components of a simple oxygen reaction system are O_2, O_3, $O(^1D)$, and $O(^3P)$. $O(^1D)$ is the most important form of excited atomic oxygen. It is produced by dissociation of O_2 ($\lambda < 175.9\,\mathrm{nm}$) or O_3 ($\lambda < 310\,\mathrm{nm}$), and is mainly deactivated by collisions with major species and forms ground state $O(^3P)$. O_3 is produced by the three body reaction

$$\mathrm{O} + \mathrm{O_2} + \mathrm{M} \longrightarrow \mathrm{O_3} + \mathrm{M} \quad .$$

In the stratosphere the amount of O_3 changes slowly although the characteristic time τ_{O_3} is in the order of hours. The characteristic time for odd-oxygen τ_{OX}, however, in the lower stratosphere is much longer (in the order of months). The number density M of the air is high enough to reproduce dissociated O_3 by the three body reaction immediately. The net source of atomic oxygen and therefore the source for ozone is the dissociation of O_2.

$$\begin{aligned} \mathrm{O_2} + h\nu &\longrightarrow 2\,\mathrm{O}(^3\mathrm{P}) \\ \mathrm{O_2} + h\nu(\lambda < 175.9\,\mathrm{nm}) &\longrightarrow \mathrm{O}(^1\mathrm{D}) + \mathrm{O}(^3\mathrm{P}) \end{aligned}$$

The loss of odd-oxygen occurs through the following reactions

$$\begin{aligned} \mathrm{O_3} + \mathrm{O} &\longrightarrow 2\,\mathrm{O_2} \\ \mathrm{O} + \mathrm{O} + \mathrm{M} &\longrightarrow \mathrm{O_2} \end{aligned}$$

and is increased by catalytic chain reactions with hydrogen-, nitrogen-, chlorine-, and bromine constituents, to note the most important.

$$\begin{array}{lrcrcl} & \mathrm{Y} + \mathrm{O_3} & \longrightarrow & \mathrm{YO} & + & \mathrm{O_2} \\ & \mathrm{O_3} + h\nu & \longrightarrow & \mathrm{O} & + & \mathrm{O_2} \\ & \mathrm{YO} + \mathrm{O} & \longrightarrow & \mathrm{Y} & + & \mathrm{O_2} \\ \hline \sum & 2\,\mathrm{O_3} & \longrightarrow & 3\,\mathrm{O_2} & & \end{array}$$

The primary absorption of ozone occurs in the Hartley bands (200–310 nm). The absorption cross section reaches a maximum value of $\sigma = 10^{-17}\,\mathrm{cm}^2$. In the Huggins

bands (310–370 nm) the absorption cross section decreases from $\sigma = 10^{-19}\,\mathrm{cm}^2$ to $\sigma = 10^{-21}\,\mathrm{cm}^2$. In the visible region of the spectrum, ozone absorbs in the Chappuis bands (450–800 nm) which contributes significantly to the photodissociation in the lower stratosphere, although the absorption cross section has a relative maximum in this wavelength range of only $\sigma = 5 \cdot 10^{-21}\,\mathrm{cm}^2$.

In the mesosphere the catalytic destruction by odd-hydrogen constituents is the most important loss cycle and therefore given here explicitly.

$$\begin{array}{rrcl} & \mathrm{OH} + \mathrm{O} & \longrightarrow & \mathrm{H} + \mathrm{O_2} \\ & \mathrm{H} + \mathrm{O_2} + \mathrm{M} & \longrightarrow & \mathrm{HO_2} + \mathrm{M} \\ & \mathrm{HO_2} + \mathrm{O} & \longrightarrow & \mathrm{OH} + \mathrm{O_2} \\ \hline \sum & 2\,\mathrm{O} & \longrightarrow & \mathrm{O_2} \end{array}$$

$$\begin{array}{rrcl} & \mathrm{OH} + \mathrm{O} & \longrightarrow & \mathrm{H} + \mathrm{O_2} \\ & \mathrm{H} + \mathrm{O_3} & \longrightarrow & \mathrm{OH} + \mathrm{O_2} \\ \hline \sum & \mathrm{O} + \mathrm{O_3} & \longrightarrow & 2\,\mathrm{O_2} \end{array}$$

Other hydrogen cycles which are important for oxygen destruction near the tropopause and in the stratosphere are not noted here. For more information about catalytic cycles involving ozone, see the book of *Brasseur and Solomon* [1986].

The interaction of oxygen and hydrogen constituents makes clear that diurnal variations are important. The photolysis of ozone and water vapour reduces the mixing ratio of ozone during daytime and enhances the mixing ratio of OH. This results in different efficiency of the cycles during day and night which has to be taken into account when an average efficiency of catalytic ozone destruction is calculated.

The typical height profiles of the oxygen constituents are demonstrated in figure 7.13 (analogue to figure 7.1). Up to about 60 km ozone shows no variation according to the large characteristic time of the oxygen family. The secondary maximum of ozone in the upper mesosphere and lower thermosphere contributes significantly to the chemical heating by the reaction with atomic hydrogen. In this height region atomic oxygen dominates the oxygen family.

A latitudinal section of atomic oxygen at northern summer solstice and local noon is shown in figure 7.14. The distribution is strongly dependent on the vertical wind. At lower latitudes the typical vertical wind cells from COMMA are reproduced in the distribution of atomic oxygen and hence in the distribution of ozone (figure 7.16). The local maximum of ozone at northern high latitudes depends on the high concentration of atomic oxygen and on the low temperature of the cold summer mesopause which increases the temperature dependent production of ozone. The small local maximum

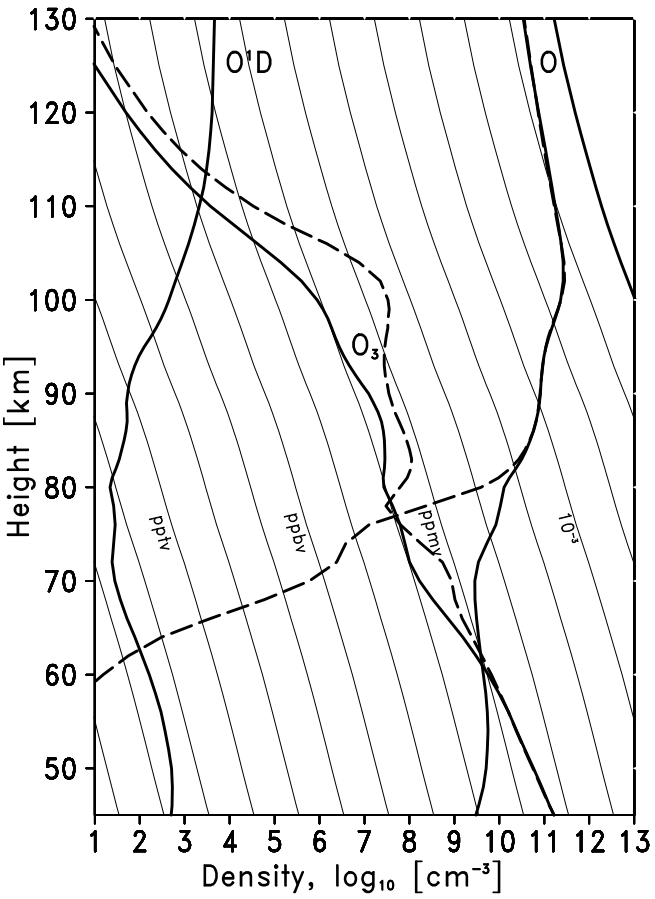

Figure 7.13: Height profile of different oxygen bearing constituents at 2.5° N for the northern summer solstice, noon (solid line) and midnight (dashed line). The thin lines represent levels of constant mixing ratio.

at 70 km altitude at the southern polar circle is more than a numerical artefact but not fully understood, yet.

Figures 7.15 and 7.17 show the same section at midnight. The difference in atomic oxygen at lower altitudes and the larger night time values of ozone in the height region of the secondary maximum are both due to ozone photolysis. At night the distribution of ozone reflects more strongly the distribution of atomic oxygen than by day.

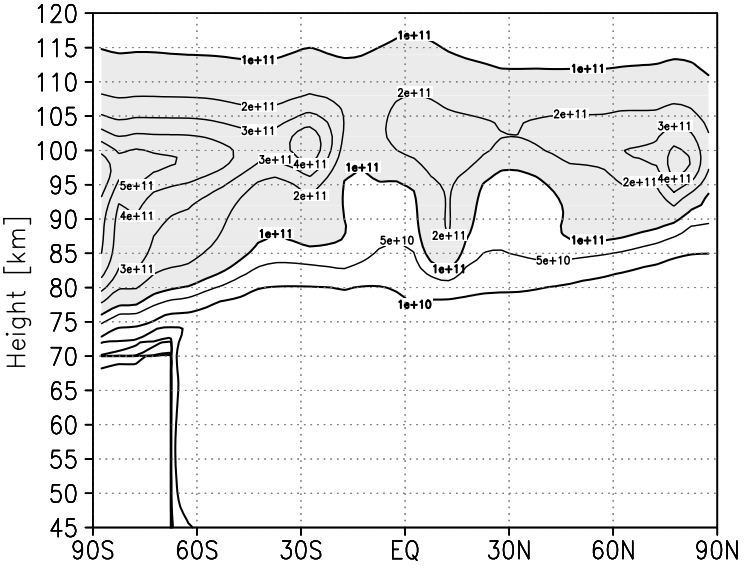

Figure 7.14: Latitudinal section of O [number density] at solstice, noon. Values larger than $1.10^{11}\,\mathrm{cm}^{-3}$ are shaded. The concentration of atomic oxygen is strongly dependent on the vertical wind structure.

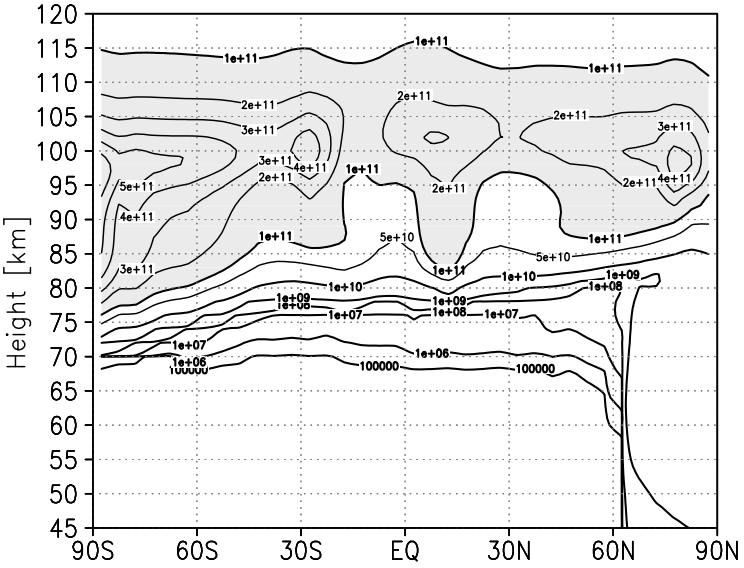

Figure 7.15: Latitudinal section of O [number density] at solstice, midnight. Values larger than $1.10^{11}\,\mathrm{cm}^{-3}$ are shaded.

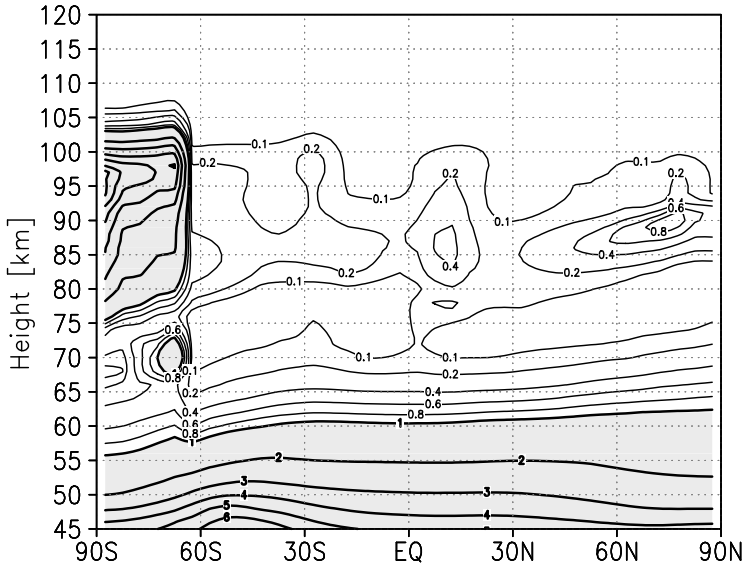

Figure 7.16: Latitudinal section of O_3 [ppmv] at solstice, noon. Values larger than 1 ppmv are shaded. The secondary ozone maximum is dependent on the concentration of atomic oxygen, and the temperature.

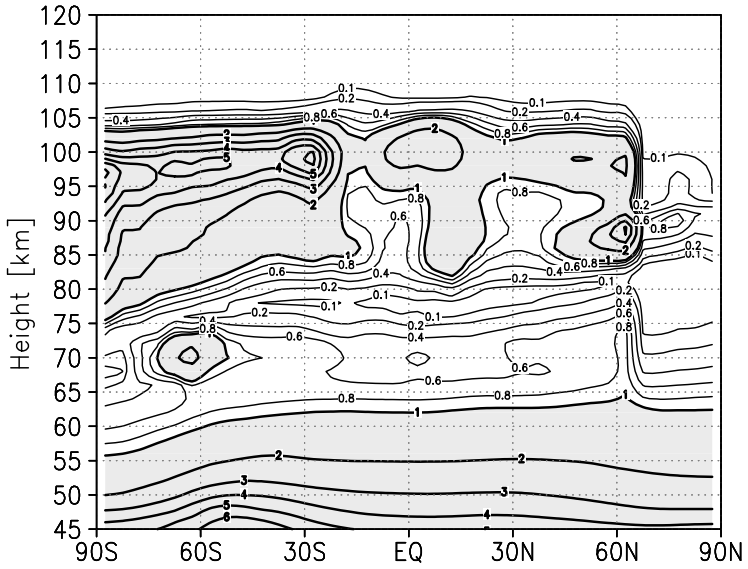

Figure 7.17: Latitudinal section of O_3 [ppmv] at solstice, midnight. Values larger than 1 ppmv are shaded. Without photolysis the ozone concentration increases during the night and reflects strongly the structure of the distribution of atomic oxygen.

Chapter 8

Flux Calculation for Hydrogen Constituents

8.1 Introduction

Total hydrogen in the stratosphere is related to the sum of H_2O and $2\,CH_4$ [*Gunson et al.*, 1990]. The mixing ratio of H_2 in the stratosphere is nearly constant at a value of ≈ 0.5 ppmv and total hydrogen is sometimes expressed by $H_{total} = H_2O + 2\,CH_4 + H_2 = const$. This term for total hydrogen is valid up to about 80 km altitude. Above this height the mixing ratio of atomic hydrogen increases strongly and cannot be neglected in the term for total hydrogen.

The freeze-drying process of water vapour at tropopause height leaves a mixing ratio of about 4 ppmv. CH_4 and H_2 pass the tropopause without any reduction by freeze-drying. The mixing ratio of CH_4 decreases with height due to oxidation which enhances finally the water vapour mixing ratio by the double amount. The methane oxidation leeds also to a small amount of molecular hydrogen which is oxidized by $O(^1D)$, too. Considering the net balance, the molecular hydrogen mixing ratio stays nearly constant and CH_4 seems to be entirely converted to $2\,H_2O$. In the mesosphere the amount of CH_4 is small and the mixing ratios of H_2O and H_2 balance each other.

The upwards directed flux of hydrogen resulting from the methane flux in the stratosphere is larger than the escape flux of hydrogen to space. A downward directed flux of H_2O from the stratosphere to the troposphere in global average is required to maintain the observed and modelled mixing ratios, or the stratosphere is filled up with water vapour resulting from the upwards directed flux of methane. However, this is a simplified look on the global average fluxes. Details about troposphere-stratosphere exchange can be found in the papers of *Dessler et al.* [1994], *Dessler et al.* [1995], *Holton et al.* [1995], and *Hintsa et al.* [1998].

At each moment one half of the earth is sunlit and it is to expect that the total flux

of hydrogen is nearly constant with small variations over the year due to the variation of the distance between earth and sun which varies by around 7 %. Storage effect may exist part time of the year in the stratosphere but the long-time, global average flux of hydrogen constituents through the tropopause and above should correspond to the hydrogen escape flux to space which is in the order of $10^8\,\mathrm{cm}^{-2}\,\mathrm{s}^{-1}$.

The main hydrogen bearing species have a much smaller molecular weight than the mean molecular weight of the surrounding air of about 29 amu, atomic mass units. Buoyant lift always acts on these species and even in the stratosphere and lower mesosphere the molecular diffusion has to be calculated for all hydrogen constituents in order to get precise flux results. The chemistry changes the partitioning of total hydrogen and the small scale turbulence, parametrized by eddy diffusion, smoothes the gradients of the distributions. Although these are the major influences on the distribution of the constituents, the sum of the fluxes should give the escape flux of hydrogen to space.

This points out that a high precision in all calculations is necessary and each loss of precision, for example by calculations in the chemistry module, will influence the total flux. One problem is still the advective transport. The wind fields have to be divergence free with high precision because large fluxes result from advective transport. As an example, the concentration of water vapour at 30 km altitude is about $10^{13}\,\mathrm{cm}^{-3}$. A local vertical wind of only 0.1 cm/s produces a flux of $10^{12}\,\mathrm{cm}^{-2}\,\mathrm{s}^{-1}$ which is four orders in magnitude higher than the hydrogen escape flux.

The basic approach of this work is to get the distribution of the hydrogen bearing constituents by an accurate calculation of the molecular diffusion at all height levels of the model. Together with the conversion of hydrogen constituents into one another by chemical reactions, this should result in a realistic distribution of total hydrogen. The sum of the fluxes of all hydrogen constituents should balance to the order of the escape flux to space in global average.

8.2 Atmospheric Escape

The atomic mass of hydrogen is so small, that there is a loss to space of atomic hydrogen by the fastest atoms of the Maxwellian velocity distribution. In the book by *Chamberlain and Hunten* [1987] the different escape mechanisms for earth and the planets are discussed in detail. The Jeans escape flux or thermal evaporation gives a lower limit to the escape flux, but other processes may work as well.

Hunten [1973] and *Maher* [1980] argue that the mesosphere can be thought as a bottleneck for the escape flux, which does not strongly depend on the exospheric temperature. This escape flux is the sum of three different escape processes. These are the thermal or Jeans escape flux (*Jeans* [1925], *Tinsley* [1973]), the escape flux due to charge transfer processes from hot hydrogen ions (protons) to cold neutral

hydrogen within the plasmasphere producing cold hydrogen ions and hot neutral hydrogen which can escape (this is maybe the most efficient escape process) (*Cole* [1966], *Maher* [1980]), and the so called polar wind which conveys protons along the magneto-tail into the interplanetary space (*Bauer* [1966], *Thomas and Vidal-Madjar* [1978]). The mean value of the escape flux is not well known. Older estimations yield values of $0.5 - 6 \cdot 10^8\,\mathrm{cm^{-2}\,s^{-1}}$ (*Liu and Donahue* [1974], *Hunten and Strobel* [1974], *Breig et al.* [1976], *Maher and Tinsley* [1977], and *Maher* [1980]). The newest publication in this listing [*Bishop*, 2001] quotes an estimated global mean total escape flux of roughly $3 \cdot 10^8\,\mathrm{cm^{-2}\,s^{-1}}$. The same value for the total hydrogen flux yields the CTM with standard boundary conditions. Bishop discusses past measurements and the difficulties of atomic hydrogen measurements. The sparseness of relevant data on the variation of atomic hydrogen with altitude is emphasized.

A demonstrative picture for the loss of hydrogen by the escape flux is the according loss of water from the oceans. Water has a mass of about $18\,\mathrm{g\,mol^{-1}}$. With the Avogadro number of $N_a = 6.022\ 10^{23}$ particles $\mathrm{mol^{-1}}$ the quantity of water molecules per cubic centimeter is obtained.

$$1\,\mathrm{cm^3} \mathrel{\hat{=}} 1\,\mathrm{g} \mathrel{\hat{=}} 3.345\ 10^{22}\,\mathrm{particles(H_2O)\,cm^{-3}} \mathrel{\hat{=}} 6.690\ 10^{22}\,\mathrm{particles(H)\,cm^{-3}} \quad (8.1)$$

The hydrogen flux is taken as $3 \cdot 10^8\,\mathrm{cm^{-2}\,s^{-1}}$. With the division of the particles per cubic centimeter by the flux, the time needed for the loss of one centimeter of the water column is obtained.

$$\frac{6.690\ 10^{22}\,\mathrm{cm^{-3}}}{3\ 10^8\,\mathrm{cm^{-2}\,s^{-1}}} = 2.23\ 10^{14}\,\mathrm{s\,cm^{-1}} \approx 7.07\ 10^6\,\mathrm{y\,cm^{-1}} \quad (8.2)$$

The oceans cover 70 % of the earth's surface at an average depths of 3700 m. With a constant hydrogen escape flux of $3\ 10^8\,\mathrm{cm^{-2}\,s^{-1}}$ takes the loss of one meter of their water column around 500 million years.

8.3 Boundary Conditions

The major hydrogen bearing constituents have fixed lower boundaries at established values. The bottom values in a dry atmosphere are set to 4 ppmv for water vapour, 1.7 ppmv for methane, and 0.55 ppmv for molecular hydrogen. Molecular hydrogen has a nearly constant mixing ratio all over the stratosphere and the amount of total hydrogen in the measure of H_2-equivalent is about 8 ppmv. The boundary values at the upper boundary are set to a mixing ratio of $2.0\ 10^{-5}$ for atomic hydrogen, and $1.0\ 10^{-5}$ for molecular hydrogen. The remaining hydrogen boundary conditions are set to zero flux through the according boundaries. The boundary conditions for atomic- and molecular hydrogen provide the same amount of hydrogen for both

species at a total of 20 ppmv H_2-equivalent at the upper boundary. At an altitude of 150 km the amount of total hydrogen is about 12 ppmv. The latter value can change slightly, because the model uses log-pressure coordinates and for the geometric scale the actual geopotential of the time step is used for the transformation of the height. The upper boundary is partly up to 170 km geometric height.

The flux calculations for this chapter are done with switched off advective transport. Small numerical errors in the calculation of the vertical wind by the condition of non-divergent wind fields can disturb seriously the flux balance in the lower regions, even in global average. Some more work has to be investigated into this point and with increased precision it should have the same quality for the global average flux. The eddy diffusion coefficient is therefore set to higher values in the mesosphere, compared to the case with advective transport, to reduce the time for the model to run into steady state. Permanent equinox is chosen for simplification because with switched off advective transport and with a one dimensional eddy diffusion coefficient, the three-dimensional standard distribution of the hydrogen bearing constituents at solstice cannot be obtained. Day-night variations in the photochemistry stay in their normal state and the three dimensional temperature field determines the number density of the air, according to the ideal gas law, and changes the coefficients for molecular diffusion. The discussed model runs are more than one-dimensional calculations of the fluxes, but the calculations of the global hydrogen fluxes for equinox and switched off advective transport under the use of three different eddy diffusion profiles.

8.4 Results

The initial values are taken from equinox of a standard model run with advective transport. Three model runs with the K-eddy profiles of figure 8.1 and switched off advective transport have been done. Each model run has been computed 180 model days. About half a year is needed because the distributions of the constituents undergo small changes when getting into a new equilibrium with constant flow of total hydrogen. Most of the time is needed for the lower model heights in the stratosphere. Without the enhancement of the K-eddy profile up to a constant value of $1\,m^2/s$ at 30–70 km the time until the model run would reach equilibrium would be two years and longer. The water vapour mixing ratios then could be expected to be slightly higher due to less intensive smoothing. The enhancement should compensate roughly the effect of the general circulation for a global, annual average mixing ratio of the constituents CH_4 and H_2O. The eddy diffusion coefficients needed for the parametrization of turbulent processes due to breaking gravity waves in the mesopause region have an extreme variability of up to two orders in magnitude. The eddy diffusion coefficient in this model is only used as a one-dimensional quantity and

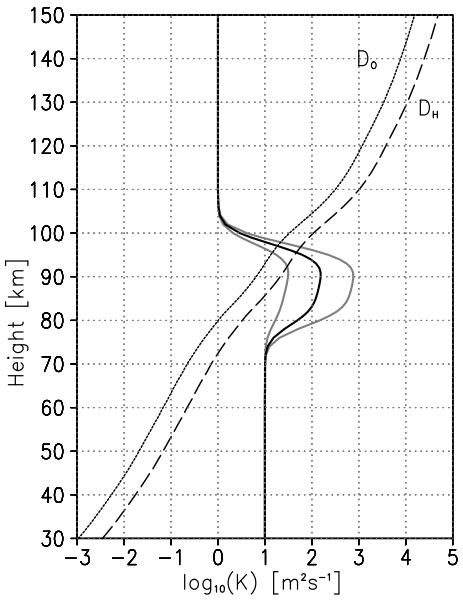

Figure 8.1: Eddy diffusion coefficient and global mean molecular diffusion coefficients for atomic hydrogen and atomic oxygen. One-dimensional, standard K_{zz} profile (black line) and variations of the K_{zz} profile in the region of the maximum by a factor of 5 (grey lines), with overestimated values in stratospheric heights to get shorter model runs into steady state with switched off advective transport.

is therefore an idealized standard profile based on results derived by *Lübken* [1997]. This profile is varied by a factor and quotient of five in the mesopause region, see figure 8.1, to get information about the influence of the eddy diffusion coefficient on total hydrogen.

The figures 8.2, 8.4, and 8.6 display the mixing ratios of the main hydrogen constituents and the sum given in equivalents of molecular hydrogen [ppmv]. The figures 8.3, 8.5, and 8.7 display the according fluxes. HX contains the constituents H, OH, HO_2, and H_2O_2 and is almost atomic hydrogen above 85 km.

The most marked result at the total hydrogen mixing ratio is the minimum at about 110 km height. In the height region where the eddy diffusion exceeds the molecular diffusion, the homosphere, the sum of the hydrogen constituents is expected to be constant with height. Above this height, in the heterosphere, the mixing ratios of the light hydrogen constituents should increase with height due to the buoyant forces by molecular diffusion. A minimum at any altitude is not expected. In the submitted paper by *Sonnemann and Körner* [2002] the modelled minimum is termed THYMRA (Total HYdrogen Mixing Ratio Anomaly).

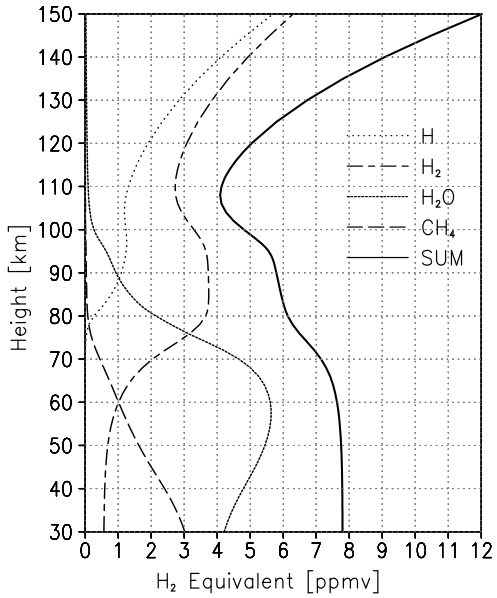

Figure 8.2: Global average mixing ratios of hydrogen constituents in a model run with the standard K_{zz} profile.

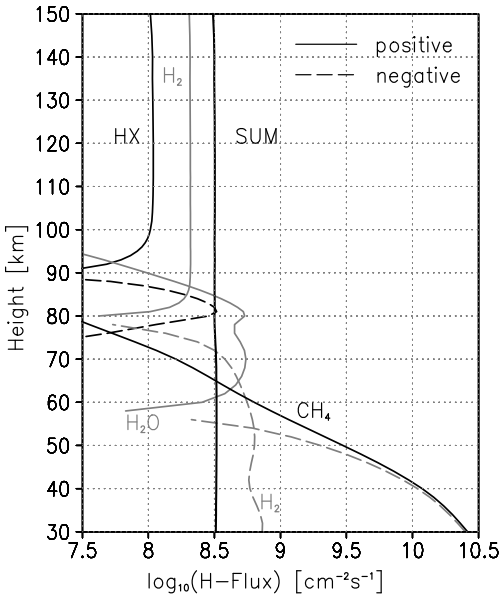

Figure 8.3: Global average hydrogen fluxes in a model run with the standard K_{zz} profile.

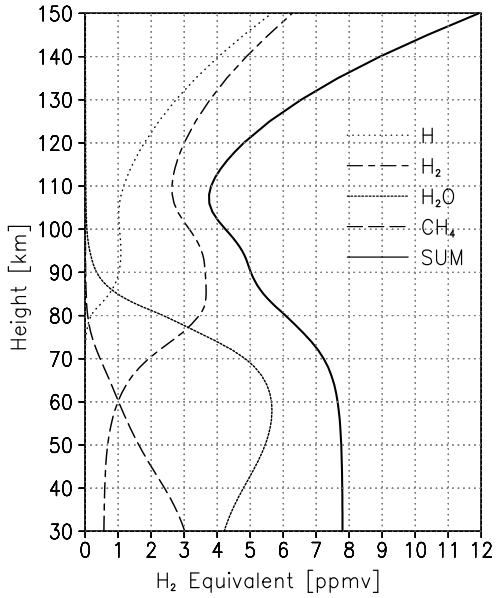

Figure 8.4: Global average mixing ratios of hydrogen constituents in a model run with the decreased K_{zz} profile.

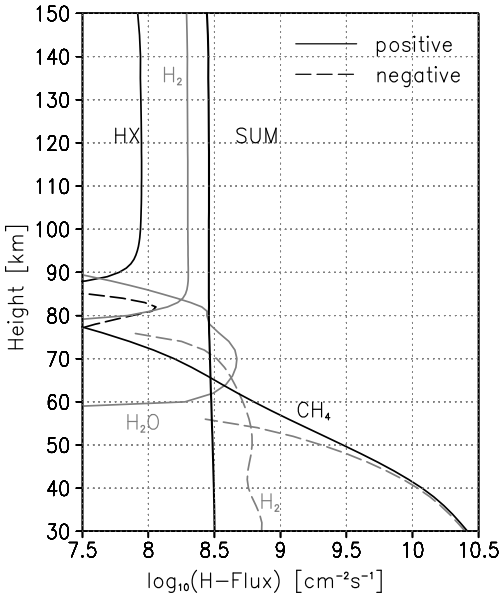

Figure 8.5: Global average hydrogen fluxes in a model run with the decreased K_{zz} profile.

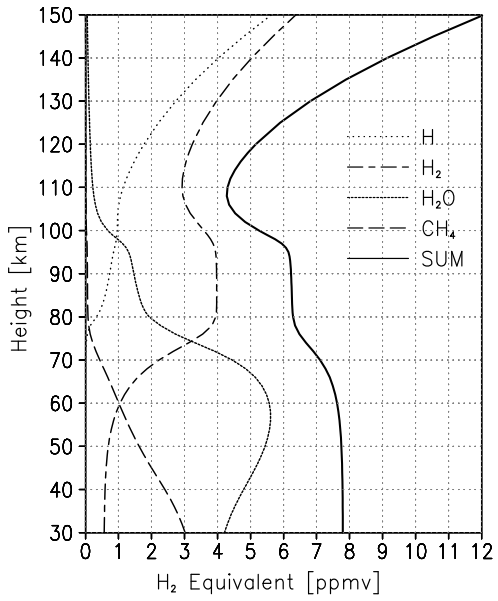

Figure 8.6: Global average mixing ratios of hydrogen constituents in a model run with the increased K_{zz} profile.

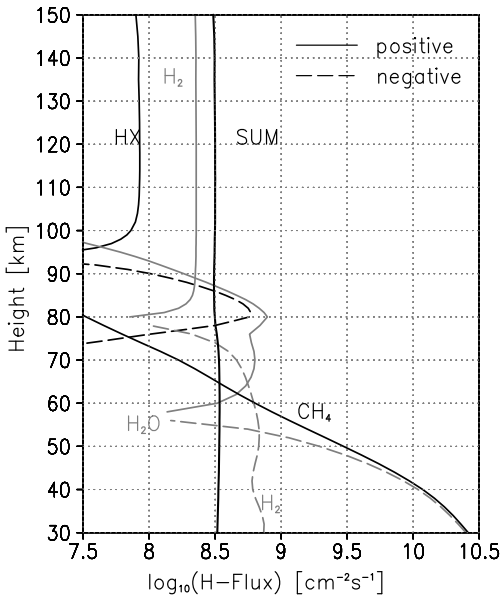

Figure 8.7: Global average hydrogen fluxes in a model run with the increased K_{zz} profile.

It is easy to think on errors in the partitioning of the hydrogen family. Especially, because the conversion of water vapour to molecular hydrogen at 60–80 km height takes place over the production of odd-hydrogen constituents which have much shorter life-times than H_2 and H_2O have. A significant violation of mass conservation, however, destroys easily the constant sum of the hydrogen fluxes.

The general picture, looking on the fluxes in the upper stratosphere and stratopause region up to about 50 km, is an upwards directed flux of methane which is balanced by a downwards directed flux of water vapour. Above the maximum in the H_2O mixing ratio the upwards directed flux is mainly carried by H_2O. Above about 85 km height this part is taken over by H_2 although it has a nearly constant mixing ratio between 80 and 95 km. It has to be kept in mind that H_2 has a very small molecular weight compared with the molecular weight of the surrounding air which results in an upwards directed flux by molecular diffusion, even with a constant mixing ratio.

The influence of the variation of the eddy diffusion coefficient on the mixing ratios is expressed most clearly in the mixing ratio equivalent of total hydrogen. A large value of the eddy diffusion coefficient is correlated to a small gradient of total hydrogen versus height. The mixing ratio of water vapour shows the same behaviour. The figures of the hydrogen fluxes display the strongest influence in the downwards

directed flux of odd-hydrogen (HX). Between the case of the decreased- and the increased eddy diffusion coefficient the flux varies by a factor of five at the maximum flux of HX. Surprisingly, the escape flux is relatively insensitive to changes of the upper boundary within realistic boundaries. A change by a factor or quotient of two in the upper boundary of atomic and molecular hydrogen has no significant effect on the escape flux. No figure but a short explanation for this result is given. The resulting flux of H and H_2 above about 100 km has two components. An upwards directed due to the small molecular weight and a downwards directed due to the positive gradient of the mixing ratios with height. An increase of the boundary values in the model gives an increase of the upwards directed, separating molecular flux and at the same time an increase of the downwards directed flux due to the steeper gradients. The resulting flux in the model stays at nearly the same value as before.

8.5 Total Hydrogen in the Middle Atmosphere

In height regions of the atmosphere where turbulence, described by eddy diffusion, is more important than decomposition by molecular diffusion, the amount of total hydrogen should be conserved. By chemistry only a conversion from one hydrogen containing constituent into another happens, which implicates that in the stratosphere and mesosphere the sum of $2\,CH_4 + H_2O + H_2$ should be constant. At the same time the total flux of all hydrogen components should be zero plus the hydrogen escape-flux to space.

Above 60 km the portion of methane in the distribution of total hydrogen is strongly decreased. The main part of the hydrogen molecules is bounded in the species H_2 and H_2O. At stratospheric heights, oxidized H_2O molecules are reproduced with the help of the three body reaction $H + O_2 + M \rightarrow HO_2 + M$, see the discussion about the characteristic times in section 7.1.3. Above about 70 km H_2O is destroyed very effectively by the photolysis through Lyman-α radiation. The reproduction from the resulting hydrogen radicals prefers the formation of H_2 in this height region, which leads to an effective flux of H_2, both down- and upwards directed.

In the region of transition from predominant turbulent diffusion to predominant molecular diffusion a strong decomposition of the heavier constituent H_2O into the light hydrogen constituents takes place. Additional, the temperature increases strongly with height above the mesopause. This causes the paradoxical behaviour of total hydrogen. The shape of the minimum in the distribution of total hydrogen versus height is then formed by the influence of the turbulent mixing, parametrized by the eddy diffusion.

Chapter 9

Chemical Heating

9.1 Introduction

The energy budget of the mesopause region is strongly affected by the release of heat from exothermic chemical reactions. As an example, the structure of the mesopause with two distinctive layers [*von Zahn et al.*, 1996], is influenced by the process of chemical heating.

An early one-dimensional model considering the heat deposition of exothermic reactions in the mesopause region was developed by *Crutzen* [1971]. Further studies of chemical heating are from *Brasseur and Offermann* [1986], *Mlynczak and Solomon* [1991a], *Mlynczak and Solomon* [1991b], *Mlynczak and Solomon* [1993], *Meriwether and Mlynczak* [1995]. The model used for the calculation of the heating rates in the paper of *Mlynczak and Solomon* [1993] is a two-dimensional model, [*Garcia and Solomon*, 1983] and [*Garcia and Solomon*, 1985]. A three-dimensional calculation of chemical heating rates was published by *Sonnemann et al.* [1997]. The diurnal variation of the mixing ratios of the constituents which contribute to the chemical heating implicate a diurnal variation of the heating rate itself. Especially ozone has a strong diurnal variation at mesopause heights. Three-dimensional modeling is therefore desirable to get results including the diurnal variations. In table 9.1 the seven major reactions are listed which contribute to the heat release in the middle atmosphere.

Results from the calculation of heating rates for individual processes indicate that the reaction of atomic hydrogen and ozone is potentially the largest single source of heat in the vicinity of the mesopause [*Mlynczak and Solomon*, 1993]. The heating can exceed the total immediate solar heating between 80 and 90 km. The formed hydroxyl is known to be initially highly vibrationally exited. There is sufficient energy released during the reaction to populate OH up to the vibrational $\nu = 9$ level in the ground electronic state. The chemical heating rate for the reaction of O_3 and H is reduced by

	Reaction			Heat of Reaction [kcal/mole]
R1	$O + O_3$	$\longrightarrow$	$2\ O_2$	-93.65
R2	$O + O + M$	$\longrightarrow$	$O_2 + M$	-119.40
R3	$O + OH$	$\longrightarrow$	$H + O_2$	-16.77
R4	$O + HO_2$	$\longrightarrow$	$OH + O_2$	-53.27
R5	$H + O_2 + M$	$\longrightarrow$	$HO_2 + M$	-49.10
R6	$O + O_2 + M$	$\longrightarrow$	$O_3 + M$	-25.47
R7	$H + O_3$	$\longrightarrow$	$OH + O_2$	-76.90

Table 9.1: Exothermic chemical reactions responsible for significant heating in the middle atmosphere

Meinel band emission and Mlynczak and Solomon recommend an efficiency of 60 %, constant with altitude.

The importance of the reaction $H + O_3 \rightarrow OH + O_2$ in the release of heat shows the relevance of ozone even in mesospheric heights. The lifetime of ozone, however, is much shorter than the lifetime of atomic oxygen. Each produced ozone molecule results from the reaction of atomic and molecular oxygen, reaction R6 of table 9.1, which releases one third of the heat compared with the reaction of ozone and atomic hydrogen, reaction R7. Atomic oxygen is also a reactant of the reactions R1–R4, with a quadratic dependence of reaction R2 on atomic oxygen. Under special condition, with downwards directed transport of high mixing ratios of atomic oxygen by vertical winds, the reaction $O + O + M \rightarrow O_2 + M$ can become the most important chemical heating source. For these reasons atomic oxygen is the central constituent for the treatment of chemical heating in the mesopause height region.

9.2 Modelling Results

Figure 9.1 displays the chemical heating rate [K/d] for northern summer solstice and local noon. The pattern of the secondary ozone maximum are mirrored in the heating rate. Corresponding structures can be found in the O and O_3 mixing ratios (figures 7.14 and 7.16). The heating rate in the winter hemisphere is strongly influenced by the downwards directed vertical wind and hence the increased number density of atomic

oxygen. The nightly heating rate in figure 9.2 shows increased values mainly caused by the increase of the nightly ozone mixing ratio, see the corresponding structures in the O and O_3 mixing ratios (figures 7.15 and 7.17). North of the northern polar circle there is only a small variation in the daily and nightly heating rates.

Mlynczak and Solomon showed heating rates for noon and nighttime condition at equinox [*Mlynczak and Solomon*, 1993]. The upper maximum of the daytime heating rate is located at around 90 km altitude with a rate of 6–8 K/d. The nighttime rate is increased with values of 13–16 K/d at around 87 km over the whole latitude range. The heating rates for equinox from Mlynczak and Solomon show higher values than the rates for solstice in this work. The daytime maximum is about 2 K/d higher, the nighttime maximum is about 6 K/d higher. It should be noted, however, that results from a two-dimensional calculation at equinox cannot be compared directly with results from a three-dimensional calculation at solstice. The heating rates of this work have a strong pattern structure caused by the vertical wind cells from figure 6.4 by the influence of advective transport on the constituents which are responsible for the main part of the heating rate.

These considerations show the relevance of the distribution of atomic hydrogen and the distribution of ozone and atomic oxygen for the heat balance of the mesopause region. The CTM computes a three-dimensional distribution and so the diurnal variation of the species which contribute to the chemical heating is naturally included. This allows the implementation of the diurnal variation of the chemical heating rates, with the recommended efficiency of 60 % for the reaction of ozone and atomic hydrogen, into the dynamic model COMMA-IAP.

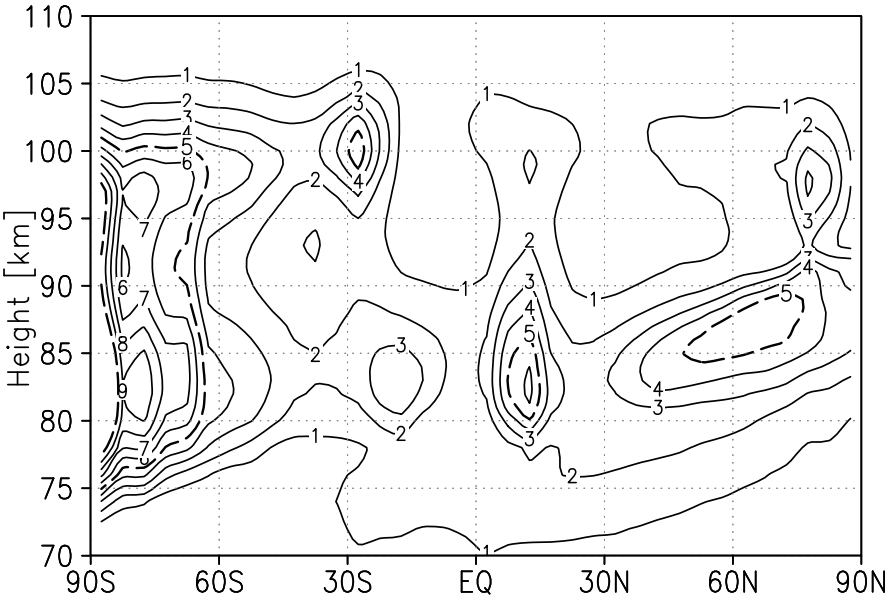

Figure 9.1: Latitudinal section of chemical heating rate [K/d] at solstice, noon (dashed lines for 5 and 10 K/d).

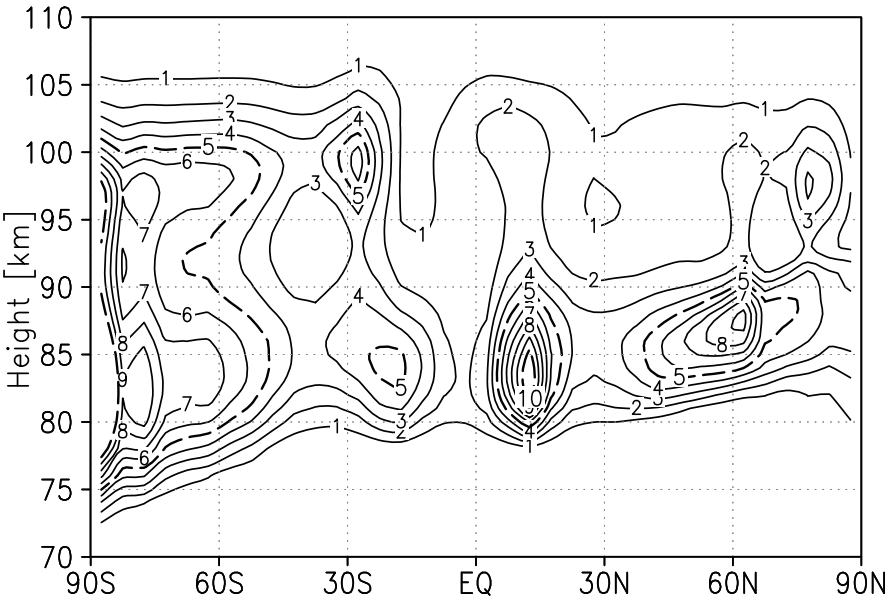

Figure 9.2: Latitudinal section of chemical heating rate [K/d] at solstice, midnight (dashed lines for 5 and 10 K/d).

Chapter 10

Summary

10.1 Summary

A three-dimensional chemistry-transport-model (CTM) was developed, starting from an existing model of middle atmospheric chemistry and transport. The Fortran source code of the model is highly vectorized and about two orders in magnitude faster than the code of the former model. The use of a new algorithm and a very efficient implementation make multiannual model runs possible.

The distribution of minor constituents in the middle atmosphere is computed with high precision. The results of the water vapour distribution agree well with microwave measurements at the ALOMAR Observatory, Norway. Water vapour is of special interest because it is the source of the hydrogen radicals which determine the catalytic loss of ozone in the mesosphere. A certain amount of water vapour is necessary for the formation of NLC and PSME at the polar summer mesopause. The calculation of the fluxes of the hydrogen constituents is precise enough that the estimation of a realistic escape flux to space at all height levels of the model is obtained. The minimum of the total hydrogen mixing ratio in the region of the upper mesosphere and lower thermosphere is a surprising but important result of this work, corroborated by the high precision of the flux calculation.

Three dimensional distributions of species like O, O_3, and the hydrogen constituents allow the computation of chemical heating with its diurnal variation. Implemented in the model COMMA-IAP the modelling of the mesopause region becomes much more realistic than before.

10.2 Future Tasks with the CTM

Interactive coupling with COMMA-IAP: An important task for the future is the interactive coupling of the CTM with the dynamic model COMMA-IAP.

To hand over a kind of climatology to the supplementary model in an iterative process is an important step but can never replace the full coupling of both parts of this complex model. Interactions in the points of chemical heating, absorber concentrations and other are to be expected.

Addition of Ion Chemistry: By the implementation of the most important ion reactions of the D- and E- layer, including water cluster ions, small scale changes in electron- and ion concentrations can be calculated. The background densities which are needed for the calculation of charged particles in a PMSE (Polar Mesospheric Summer Echo) can be provided. The chemistry of metals and sporadic metal layers interacts also with the ion chemistry and could be calculated with the derived background mixing ratios.

Addition of OH^* Deactivation Reactions: The reactions which describe the deactivation of excited OH molecules may be added. The model results should give a valuable view on the OH^*-airglow.

Bibliography

Alpers, M., M. Gerding, J. Höffner, and U. von Zahn, NLC particle properties from a five-color lidar observation at 54° N, *J. Geophys. Res.*, **105**, 12,235–12,240, 2000.

Arnold, N. F., and T. R. Robinson, Solar cycle changes to planetary wave propagation and their influence on the middle atmosphere circulation, *Ann. Geophys.*, **16**, 69–76, 1998.

Atkinson, R., D. L. Baulch, R. A. Cox, R. F. Hampson Jr., J. A. Kerr, and J. Troe, Evaluated Kinetic and Photochemical Data for Atmospheric Chemistry: Supplement IV, *Atmospheric Environment*, **26A**, 1187–1230, 1992.

Atkins, P. W., *Physical Chemistry*, Oxford University Press, Third Edition, 1986.

Banks, P. M., and G. Kockarts, *Aeronomy, Part A and B*, Academic, Orlando, Fla., 1973.

Balsley, B. B., W. L. Ecklund, D. A. Carter, and P. E. Johnson, The MST radar at Poker Flat, Alaska, *Radio Sci.*, **15**, 213–223, 1980.

Bauer, S. J., The constitution of the topside ionosphere, Electron Density Profiles in Ionosphere and Exosphere, ed. by J. Trihagen, North-Holland, Amsterdam, 1966.

Berger, U., Numerische Simulation klimatologischer Prozesse und thermischer Gezeiten in der mittleren Atmosphäre, *Dissertation*, Universität Köln, 1994.

Berger, U., and M. Dameris, Cooling of the upper atmosphere due to CO_2 increase: A model study, *Ann. Geophys.*, **11**, 809–819, 1993.

Berger, U., and U. von Zahn, The two-level structure of the mesopause: A model study, *J. Geophys. Res.*, **104**, 22,083–22,093, 1999.

Berger, U., and U. von Zahn, Icy particles in the summer mesopause region: 3-D modeling of their environment and 2-D modeling of their transport, *J. Geophys. Res.*, accepted 2001.

Bevilacqua, R. M., W. J. Wilson, W. B. Rickelts, R. Schwartz, and R. J. Howard, Possible seasonal variability of mesospheric water vapour, *Geophys. Res. Lett.*, **12**, 397–400, 1985.

Bevilacqua, R. M., D. L. Kriebel, T. A. Pauls, C. P. Aellig, D. E. Siskind, M. Daehler, J. J. Olivero, S. E. Puliafito, G. K. Hartmann, N. Kämpfer, A. Berg, and C. L. Croskey, MAS measurements of the latitudinal distribution of water vapour and ozone in the mesosphere and lower thermosphere, *Geophys. Res. Lett.*, **23**, 2317–2320, 1996.

Bevilacqua, R. M., J. J. Olivero, and C. L. Croskey, Mesospheric Water Vapour Measurements from Penn State: Monthly Mean Observations (1984–1987), *J. Geophys. Res.*, **94**, 12,807–12,818, 1989.

Bevilacqua, R. M., D. F. Strobel, M. E. Summers, J. J. Olivero, and M. Allen, The Seasonal Variation of Water Vapour and Ozone in the Upper Mesosphere: Implications for Vertical Transport and Ozone Photochemistry, *J. Geophys. Res.*, **95**, 883–893, 1990.

Bishop, J., Thermospheric atomic hydrogen densities and fluxes from dayside Lyman-α measurements *J. Atmos. Solar-Terr. Phys.*, **63**, 331–340, 2001.

Bott, A., A Positive Definite Advection Scheme Obtained by Nonlinear Renormalization of the Advective Fluxes, *Mon. Wea. Rev.*, **117**, 1006–1015, 1989.

Bott, A., Monotone Flux Limitation in the Area Preserving Flux-form Advection Algorithm, *Mon. Wea. Rev.*, **120**, 2592–2602, 1992.

Brasseur, G., and P. de Baets, Ions in the mesosphere and lower thermosphere: A two-dimensional model, *J. Geophys. Res.*, **91**, 4025–4046, 1986.

Brasseur, G., M. H. Hitchman, S. Walters, M. Dymek, E. Falise, and M. Pirre, An interactive chemical and dynamical radiative two-dimensional model of the middle atmosphere, *J. Geophys. Res.*, **95**, 5639–5655, 1990.

Brasseur, G., J. J. Orlando, and G. S. Tyndall, *Atmospheric Chemistry and Global Change*, Oxford University Press, Oxford New York, 1999.

Brasseur, G., and D. Offermann, Recombination of Atomic Oxygen Near the Mesopause: Interpretation of Rocket Data, *J. Geophys. Res.*, **91**, 10,818–10,824, 1986.

Brasseur, G., and S. Solomon, *Aeronomy of the Middle Atmosphere: Chemistry and Physics of the Stratosphere and Mesosphere*, D. Reidel Publishing Company, Dordrecht, Holland, Second revised edition, 1986.

Breig, E. L., W. B. Hanson, J. H. Hoffmann, and D. C. Kayser, In situ measurements of hydrogen concentration and flux between 160 and 300 km in the thermosphere, *J. Geophys. Res.*, **81**, 2677–2686, 1976.

Chapman, S., A theory of upper-atmospheric ozone, *Mem. Roy. Meteorol. Soc.*, **3**, 103–125, 1930.

Chamberlain, J. W., and D. M. Hunten, *Theory of Planetary Atmospheres, An Introduction to Their Physics and Chemistry*, Academic Press, Inc., San Diego, USA, Second edition, 1987.

Chen, L., H. Rabitz, D. B. Considine, C. H. Jackman, and J. A. Shorter, Chemical reaction rate sensitivity and uncertainty in a two- dimensional middle atmospheric model, *J. Geophys. Res.*, **102**, 16,201–16,214, 1997.

Cho, J. Y. N., and J. Röttger, An updated review of polar mesosphere summer echoes: Observation, theory, and their relationship to noctilucent clouds and subvisible aerosols, *J. Geophys. Res.*, **102**, 2001–2020, 1997.

Cole, K. D., Theory of some quiet magnetospheric phenomena relating to geomagnetic tail, *Nature*, **211**, 1385–1387, 1966.

Colegrove, F. D., Hanson, W. B., and Johnson, F. S., Eddy Diffusion and Oxygen Transport in the Lower Thermosphere, *J. Geophys. Res.*, **70**, 4931, 1965.

Courant, R., K. O. Friedrichs, and H. Lewy, Über die partiellen Differenzengleichungen der mathematischen Physik, *Math. Ann.*, **100**, 32, 1928.

Colegrove, F. D., Johnson, F. S., and Hanson, W. B., Atmospheric Composition in the Lower Thermosphere, *J. Geophys. Res.*, **71**, 2227, 1966.

Crutzen, P. J., Energy conversions and mean vertical motions in the high latitude summer mesosphere and lower thermosphere, in *Mesospheric Models and Related Experiments*, edited by G. Fiocco, *D. Reidel*, pp. 78–88 , Norwell, Mass., 1971.

Deguchi, S., and D. O. Muhleman, Mesospheric water vapour, *J. Geophys. Res.*, **87**, 1343–1346, 1982.

DeMore, W. B., S. P. Sander, D. M. Golden, M. J. Molina, R. F. Hampson, M. J. Kurylo, C. J. Howard, and A. R. Ravishankara, *Chemical Kinetics and Photochemical Data for Use in Stratospheric Modelling*, Jet Propulsion Laboratory, California Institute of Technology, Evaluation No. **9**, JPL Publication 90-1, 1990.

DeMore, W. B., S. P. Sander, D. M. Golden, R. F. Hampson, M. J. Kurylo, C. J. Howard, A. R. Ravishankara, C. E. Kolb, and M. J. Molina, *Chemical Kinetics and Photochemical Data for Use in Stratospheric Modelling*, Jet Propulsion Laboratory, California Institute of Technology, Evaluation No. **10**, JPL Publication 92–20, 1992.

DeMore, W. B., S. P. Sander, D. M. Golden, R. F. Hampson, M. J. Kurylo, C. J. Howard, A. R. Ravishankara, C. E. Kolb, and M. J. Molina, *Chemical Kinetics and Photochemical Data for Use in Stratospheric Modelling*, Jet Propulsion Laboratory, California Institute of Technology, Evaluation No. **11**, JPL Publication 94–26, 1994.

Dessler, A. E., and H. Kim, Determination of the amount of water vapour entering the stratosphere based on Halogen Occultation Experiment (HALOE) data, *J. Geophys. Res.*, **104**, 30,605–30,607, 1999.

Dessler, A. E., E. M. Weinstock, E. J. Hintsa, J. G. Anderson, C. R. Webster, R. D. May, J. W. Elkins, and G. S. Dutton, An examination of total hydrogen budget of the lower stratosphere, *Geophys. Res. Lett.*, **21**, 2563–2566, 1994.

Dessler, A. E., E. J. Hintsa, E. M. Weinstock, J. G. Anderson, and K. R. Chan, Mechanisms controlling water vapor in the lower stratosphere: "A tale of two stratospheres", *J. Geophys. Res.*, **100**, 23,167–23,172, 1995.

Ebel, A., U. Berger, and B. C. Krüger, Numerical simulations with COMMA, a global model of the middle atmosphere, *Simpo Newsl.*, **4**, No. 12, 22–32, Step Simul. Promotion Off., Japan, February, 1995.

Fichtelmann, B., and G. Sonnemann, On the Variation of Ozone in the Upper Mesosphere and Lower Thermosphere: A Comparison between Theory and Observation, *Z. Meteorol.*, **39**, 6, 297–308, 1989.

Fomichev, V. I., and G. M. Shved, Parametrization of the radiative flux divergence in the 9.6 μm O_3 band, *J. Atmos. Terr. Phys.*, **47**, 1037–1049, 1985.

Fomichev, V. I., J.-P. Blanchet, and D. S. Turner, Matrix parametrization of the 15 μm CO_2 band cooling in the middle and upper atmosphere for variable CO_2 concentrations, *J. Geophys. Res.*, **103**, 11,505–11,528, 1998.

Frederick, J. E., F. T. Huang, A. R. Douglas, and C. A. Reber, The distribution and annual cycle of ozone in the upper stratosphere, *J. Geophys. Res.*, **88**, 3,819–3,828, 1983.

Gadsden, M., and W. Schröder, *Noctilucent Clouds*, Springer-Verlag, New York, 1989.

Garcia, R. R., and S. Solomon, A numerical model of the zonally averaged dynamical and chemical structure of the middle atmosphere, *J. Geophys. Res.*, **88**, 1379–1400, 1983.

Garcia, R. R., and S. Solomon, The effect of breaking gravity waves on the dynamics and chemical composition of the mesosphere and lower thermosphere, *J. Geophys. Res.*, **90**, 3850–3868, 1985.

Garcia, R. R., F. Stordal, S. Solomon, and J. F. Kiehl, A numerical model of the middle atmosphere 1. Dynamics and transport of tropospheric source gases, *J. Geophys. Res.*, **97**, 12,967–12,991, 1992.

Gear, C. W., *Numerical initial value problems in ordinary differential equations*, Prentice Hall, Englewood Cliffs, N. J., 1971.

Gunson, M. R., C. B. Farmer, R. H. Norton, R. Zander, C. P. Rinsland, J. H. Shaw, and B.-C. Gao, Measurement of CH_4, N_2O, CO, H_2O, and O_3 in the middle atmosphere by the atmospheric trace molecule spectroscopy experiment on Spacelab 3, *J. Geophys. Res.*, **95**, 13,867–13,882, 1990.

Günther, G., Die numerische Simulation von Transportprozessen in der mittleren Atmosphäre, *Dissertation*, Universität Köln, 1995.

Haltiner, G., and R. Williams, *Numerical Prediction and Dynamic Meteorology*, 2nd Edition, John Wiley & Sons, 1980.

Hartogh, P., and C. Jarchow, Ground-based detection of middle atmospheric water vapour, Global Process Monitoring and Remote Sensing of the Ocean and Sea Ice, ed. by D. W. Deering and P. Gudmandsen, Vol. 2586 of Proc. SPIE, pp 188–195, 1995.

Hintsa, E. J., K. A. Boering, E. M. Weinstock, J. G. Anderson, B. L. Gary, L. Pfister, B. C. Daube, S. C. Wofsy, M. Loewenstein, J. R. Podolske, J. J. Margitan, and T. P. Bui, Troposphere-to-stratosphere transport in the lowermost stratosphere from measurements of H_2O, CO_2, N_2O and O_3, *Geophys. Res. Lett.*, **25**, 2655–2658, 1998.

Harries, J. E., J. M. Russell III, A. F. Tuck, L. L. Gordley, P. Purcell, K. Stone, R. M. Bevilacqua, M. Gunson, G. Nedoluha, and W. A. Traub, Validation of measurements of water vapour from the Halogen Occultation Experiment, HALOE, *J. Geophys. Res.*, **101**, 10,205–10,216, 1996a.

Harries, J. E., S. Ruth, and J. M. Russell III, On the distribution of mesospheric molecular hydrogen inferred from HALOE measurements of H_2O and CH_4, *Geophys. Res. Lett.*, **23**, 297–300, 1996b.

Hartmann, D. L., *Global Physical Climatology*, Academic Press, San Diego, 1994.

Holton, J. R., *An Introduction to Dynamik Meteorology*, Third Edition, Academic Press, San Diego, 1992.

Holton, J. R., P. H. Haynes, M. E. McIntyre, A. R. Douglass, R. Rood, and L. Pfister, Stratosphere-troposphere exchange, *Rev. Geophys.*, **33**, 403–439, 1995.

Holton, J. R., and X. Zhu, A further study of gravity wave induced drag and diffusion in the mesosphere, *J. Atmos. Sci.*, **41**, 2653–2662, 1984.

Hunten, D. M., The Escape of Light Gases from Planetary Atmospheres, *J. Atmos. Sci.*, **30**, 1481–1494, 1973.

Hunten, D. M., and D. F. Strobel, Production and Escape of Terrestrial Hydrogen, *J. Atmos. Sci.*, **31**, 305–317, 1974.

Jackman, C. H., A. R. Douglass, S. Chandra, R. S. Stolarski, J. E. Rosenfield, J. A. Kaye, and E. R. Nash, Impact of inter annual variability (1979–1986) of transport and temperature on ozone as computed using a two-dimensional photochemical model, *J. Geophys. Res.*, **96**, 5073–5079, 1991.

Jakobs, H. J., M. Bischof, A. Ebel, and P. Speth, Simulation of gravity wave effects under solstice conditions using a 3-D circulation model of the middle atmosphere, *J. Atmos. Terr. Phys.*, **48**, 1203–1223, 1986.

Jeans, J. H., *The dynamic theory of gases*, Cambridge University Press, 1925.

Jensen, E. J., G. E. Thomas, and B. B. Balsley, On the statistical correlation between polar mesospheric cloud occurrence and enhanced mesospheric radar echoes, *Geophys. Res. Lett.*, **15**, 315–318, 1988.

Jesse, O., Auffallende Abenderscheinung am Himmel, *Meteorol. Z.*, **2**, 311–312, 1885.

Kerridge, B. J., and E. E. Remsberg, Evidence from the Limb Infrared Monitor of the Stratosphere for Nonlocal Thermodynamic Equilibrium in the ν_2 Mode of Mesospheric Water Vapor and the ν_3 Mode of Stratospheric Nitrogen Dioxide, *J. Geophys. Res.*, **94**, 16,323–16,342, 1989.

Kirchhoff, V. W. J. H., B. R. Clemesha, and D. M. Simonich, Seasonal Variation of Ozone in the Mesosphere, *J. Geophys. Res.*, **86**, 1463–1466, 1981.

Kley, D., J. M. Russel III, and C. Phillips, editors, SPARC Assessment of Upper Tropospheric and Stratospheric Water Vapour, *WCRP*, **113**, WMO/TD No. 1043, SPARC Report No. 2, 2000.

Klinker, E., Die numerische Simulation der nahezu zweijährigen Schwingung des mittleren Zonalwindes in der äquatorialen Stratosphäre, *Dissertation*, Freie Universität Berlin, Berlin, 1981.

Ko, M. K. W., H. R. Schneider, R.-L. Shia, D. K. Weisenstein, and N.-D. Sze, A two-dimensional model with coupled dynamics, radiation, and photochemistry. 1. Simulation of middle atmosphere, *J. Geophys. Res.*, **98**, 20,429–20,440, 1993.

Körner U., and G. R. Sonnemann, Global three-dimensional modelling of the water vapour concentration of the mesosphere-mesopause region and implications with respect to the noctilucent cloud region, *J. Geophys. Res.*, **106**, 9639–9651, 2001.

Kockarts, G., Nitric oxide cooling in the terrestrial thermosphere, *Geophys. Res. Lett.*, **7**, 137–140, 1980.

Kremp, Ch., U. Berger, P. Hoffmann, D. Keuer, and G. R. Sonnemann, Seasonal variation of middle latitude wind fields of the mesopause region—a comparison between observation and model calculation, *Geophys. Res. Lett.*, **26**, 1279–1282, 1999.

Kutepov, A. A., and V. I. Fomichev, Application of the second order escape probability approximation to the solution of the NLTE vibrational-rotational band radiative transfer problem, *J. Atmos. Terr. Phys.*, **55**, 1–6, 1993.

Lacis, A. A., and J. E. Hansen, A parametrization for the absorption of solar radiation in the earth's atmosphere, *J. Atmos. Sci.*, **31**, 118–132, 1974.

Leslie, R., Sky glows, *Nature*, **32**, 245, 1885.

Lindemann, F. A., Discussion on radiation theory of chemical action, *Trans. Far. Soc.*, **17**, 598, 1922.

Liou, K.-N., *An Introduction to Atmospheric Radiation*, Academic, San Diego, Calif., 1980.

Liu, S. C., and T. M. Donahue, Realistic model of hydrogen constituents in the lower atmosphere and escape flux from the upper atmosphere, *J. Atmos. Sci.*, **31**, 2238–2242, 1974.

Lübken, F.-J., K. H. Fricke, and M. Langer, Noctilucent clouds and the thermal structure near the arctic mesopause in summer, *J. Geophys. Res.*, **101**, 9489–9508, 1996.

Lübken, F.-J., Seasonal variation of turbulent energy dissipation rates at high latitudes as determined by in situ measurements of neutral density fluctuations, *J. Geophys. Res.*, **102**, 13,441–13,456, 1997.

Lübken, F.-J., M. Rapp, T. Blix, and E. Thrane, Microphysical and turbulent measurements of the Schmidt number in the vicinity of polar mesosphere summer echoes, *Geophys. Res. Lett.*, **25**, 893–896, 1998.

Lübken, F.-J., Nearly zero temperature trend in the polar summer mesosphere, *Geophys. Res. Lett.*, **27**, 3603–3606, 2000.

Lübken, F.-J., M. Rapp, and P. Hoffmann, Neutral air turbulence and temperatures in the vicinity of polar mesopause summer echoes, *J. Geophys. Res.*, (submitted), 2001.

Maher, L. J. ,Jr., The latitudinal variation of the charge exchange induced atomic hydrogen escape flux, *J. Geophys. Res.*, **85**, 4621–4630, 1980.

Maher, L. J. , and B. A. Tinsley, Atomic hydrogen escape rate due to charge exchange with hot plasma ions, *J. Geophys. Res.*, **82**, 689–690, 1977.

Makhlouf, U. B., R. H. Picard, and J. R. Winick, Photochemical-dynamical modeling of the measured response of airglow to gravity waves 1. Basic model for OH airglow, *J. Geophys. Res.*, **100**, 11,289–11,311, 1995.

Marti, J., and K. Mauersberger, A survey and new measurements of ice vapour pressure at temperatures between 170 and 250 K, *Geophys. Res. Lett.*, **20**, 363–366, 1993.

McCormac, B. M. (Editor), *Atmospheres of Earth and the Planets*, D. Reidel Publishing Company, Dordrecht, Holland, 1975.

Meriwether, J., Jr., A review of the photochemistry of selected nightglow emissions from the mesopause, *J. Geophys. Res.*, **94**, 14,629–14,646, 1989.

Meriwether, J. W., and M. G. Mlynczak, Is chemical heating a major cause of the mesosphere inversion layer?, *J. Geophys. Res.*, **100**, 1379–1387, 1995.

Mlynczak, M. G., and S. Solomon, Middle atmosphere heating by exothermic chemical reactions involving odd-hydrogen species, *Geophys. Res. Lett.*, **18**, 37–40, 1991a.

Mlynczak, M. G., and S. Solomon, On the efficiency of solar heating in the middle atmosphere, *Geophys. Res. Lett.*, **18**, 1201–1204, 1991b.

Mlynczak, M. G., and S. Solomon, A detailed evaluation of the heating efficiency in the middle Atmosphere, *J. Geophys. Res.*, **98**, 10,517–10,541, 1993.

Morton, K. W., and D. F. Mayers, *Numerical Solution of Partial Differential Equations*, Cambridge University Press, 1994.

Nedoluha, G. E., L. M. Bevilacqua, R. M. Gomez, D. L. Thacker, W. B. Waltman, and T. A. Pauls, Ground-based measurements of water vapour in the middle atmosphere, *J. Geophys. Res.*, **100**, 2927–2939, 1995.

Nedoluha, G. E., L. M. Bevilacqua, R. M. Gomez, W. B. Waltman, B. C. Hicks, D. L. Thacker, and W. A. Matthews, Measurements of water vapor in the middle atmosphere and implications for mesospheric transport, *J. Geophys. Res.*, **101**, 21,183–21,193, 1996.

Nedoluha, G. E., R. M. Bevilaqua, R. M. Gomez, W. B. Waltmann, B. C. Hicks, D. L. Thacker, J. M. Russell III, M. Adams, H. C. Pumphrey, and B. J. Connor, A comparative study of mesospheric water vapor measurements from ground-based water vapor millimeter-wave spectroscopy and space-based instruments, *J. Geophys. Res.*, **102**, 16,647–16,661, 1997.

Nedoluha, G. E., R. M. Bevilaqua, R. M. Gomez, D. E. Siskind, B. C. Hicks, J. M. Russel III, and B. J. Connor, Increases in middle atmospheric water vapour as observed by the Halogen Occultation Experiment and the ground-based Water Vapour Millimeter-wave Spectrometer from 1991 to 1997, *J. Geophys. Res.*, **103**, 3531–3543, 1998a.

Nedoluha, G. E., D. E. Siskind, J. T. Bacmeister, and R. M. Bevilaqua, Changes in upper stratospheric CH_4 and NO_2 as measured by HALOE and implications for changes in transport, *Geophys. Res. Lett.*, **25**, 987–990, 1998b.

Nedoluha, G. E., R. M. Bevilacqua, R. M. Gomez, B. C. Hicks, and J. M. Russell III, Measurements of middle atmospheric water vapor from low altitudes and midlatitudes in the Northern Hemisphere, 1995–1998, *J. Geophys. Res.*, **104**, 19,257–19,266, 1999.

Ovarlez, J., P. van Velthoven, and H. Schlager, Water vapour measurements from the troposphere to the lowermost stratosphere: Some signatures of troposphere to stratosphere exchanges, *J. Geophys. Res.*, **104**, 16,973–16,978, 1999.

Pawson, S., U. Langematz, G. Radek, U. Schlese, and S. Strauch, The Berlin Troposphere-Stratosphere-Mesosphere GCM: Sensitivity to physical parametrizations, *Q. J. R. Meteorol. Soc.*, **124**, 1343–1371, 1998.

Peixoto, J. P., and A. H. Oort, The climatology of relative humidity in the atmosphere, *J. Climate*, **9**, 3443–3463, 1996.

Peter, R., K. Künzi, and G. K. Hartmann, Latitudinal survey of water vapour in the middle atmosphere using an airborne millimeter wave sensor, *Geophys. Res. Lett.*, **15**, 1173–1176, 1988.

Pumphrey, H. C., and R. S. Harwood, Water vapour and ozone in the mesosphere as measured by UARS MLS, *Geophys. Res. Lett.*, **24**, 1399–1402, 1997.

Prather, M. J., Numerical advection by conservation of second order moments, *J. Geophys. Res.*, **91**, 6671–6681, 1986.

Press, W. H., S. A. Teukolsky, W. T. Vetterling, and B. P. Flannery, *Numerical Recipes, The Art of Scientific Computing*, Second edition, Cambridge University Press, 1992.

Radford, H. E., M. M. Litvak, C. A. Gottlieb, E. W. Gottlieb, S. K. Rosenthal, an A. Lilley, Mesospheric water vapour measured from ground-based microwave observations, *J. Geophys. Res.*, **82**, 472–478, 1977.

Ramanathan, V., E. J. Pitcher, R. C. Malone, and M. L. Blackmon, The response of a spectral general circulation model refinements in radiative processes, *J. Atmos. Sci.*, **40**, 605–621, 1983.

Rapp, M., and F.-J. Lübken, Electron temperature control of PMSE, *Geophys. Res. Lett.*, **27**, 3285–3288, 2000.

Richmond, A. D., E. C. Ridley, and R. G. Roble, A thermospheric/ionospheric general circulation model with coupled electrodynamics, *Geophys. Res. Lett.*, **19**, 601–604, 1992.

Riegler, G. R., J. F. Drake, S. C. Liu, and R. J. Cicerone, Stellar Occultation Measurement of Atmospheric Ozone and Chlorine from OAO3, *J. Geophys. Res.*, **81**, 4997–5001, 1976.

Riegler, G. R., S. K. Atreya, T. M. Donahue, S. C. Liu, B. Wasser, and J. F. Drake, UV Stellar Occultation Measurements of Nighttime Equatorial Ozone, *Geophys. Res. Lett.*, **4**, 145–148, 1977.

Roble, R. G., and E. C. Ridley, A thermosphere - ionosphere - mesosphere - electrodynamics general circulation model (TIME - GCM): Equinox solar minimum simulation, 30–500 km, *Geophys. Res. Lett.*, **21**, 417–420, 1994.

Rose, K., On the influence of nonlinear wave-wave interaction in a 3-d primitive equation model for sudden stratospheric warmings, *Beitr. Phys. Atmosph,*, **56**, 14–41, 1983.

Röth, E.-P., Fast algorithm to calculate the photon flux in optically dense media for use in photochemical models, *Ber. Bunsenges. Phys. Chem.*, **96**, 417–420, 1992.

Russell, J. M., L. L. Gordley, J. H. Park, S. R. Drayson, W. D. Hesketh, R. J. Cicerone, A. F. Tuck, J. E. Frederick, J. E. Harries, and P. J. Crutzen, The Halogen Occultation Experiment, *J. Geophys. Res.*, **98**, 10,777–10,797, 1993.

Seele, C., and P. Hartogh, Water vapour of the polar middle atmosphere: Annual variation and summer mesosphere conditions as observed by ground-based microwave spectroscopy, *Geophys. Res. Lett.*, **26**, 1517–1520, 1999.

Seele, C., Bodengebundene Mikrowellenspektroskopie von Wasserdampf in der mittleren polaren Atmosphäre, *Dissertation*, Duehrkohp & Radicke, Göttingen, 2000.

Siskind, D. E., and M. E. Summers, Implications of enhanced mesospheric water vapor observed by HALOE, *Geophys. Res. Lett.*, **25**, 2133–2136, 1998.

Sivjee, G. G., Airglow hydroxyl emissions, *Planet. Space Sci.*, **40**, 235–242, 1992.

Shimazaki, T., *Minor constituents in the middle atmosphere*, D. Reidel Publishing Company, Dordrecht, Holland, 1985.

Smith, A. K., and G. P. Brasseur, Numerical Simulation of the Seasonal Variation of Mesospheric Water Vapour, *J. Geophys. Res.*, **96**, 7553–7563, 1991.

Smolarkiewicz P. K., A simple positive definite advection scheme with small implicit diffusion, *Mon. Wea. Rev.*, **111**, 479–486, 1983.

Sonnemann G., B. Fichtelmann, and K.-K. Ohle, An empirical ozone model of the mesosphere, *MAP Newsletter*, **3**, 5, 1984.

Sonnemann G., A. Ebel, C. Kremp, B. Fichtelmann, and U. Berger, The global NO distribution computed on the basis of a dynamic 3d-model and implications on the winter anomaly of the D-layer, *Adv. Space Res.*, **16(1)**, 133–136, 1995.

Sonnemann, G., C. Kremp, A. Ebel, and U. Berger, Calculation of the global chemical heating rates by means of a 3d-model of dynamics and chemistry, *Adv. Space Res.*, **20(6)**, 1153–1156, 1997.

Sonnemann, G., C. Kremp, A. Ebel, and U. Berger, A three-dimensional dynamic model of the minor constituents of the mesosphere, *Atmos. Environ.*, **32**, 3157–3172, 1998a.

Sonnemann, G., C. Kremp, A. Ebel, and U. Berger, The global 3-D calculation of the distribution of the plasma components within the 80 to 130 km height range, *Adv. Space Res.*, **21**, 887–890, 1998b.

Sonnemann, G. R., Feigin, A. M., Mol'kov, Ya. I., On the influence of diffusion upon the nonlinear behaviour of the photochemistry of the mesopause region, *J. Geophys. Res.*, **104**, 30,591–30,603, 1999.

Sonnemann, G. R., The photochemical effects of dynamically induced variations in solar insulation, *J. Atmos. Solar-Terr. Phys.*, **63**, 781–797, 2001.

Sonnemann, G. R., and U. Körner, The total hydrogen mixing ratio anomaly THYMRA around the mesopause region and implications concerning the evolution of the atmospheric oxygen level, *J. Geophys. Res.*, (submitted), 2001.

Strobel, D. F., Parametrization of the atmospheric heating rate from 15–120 km due to O_2 and O_3 absorption of solar radiation, *J. Geophys. Res.*, **83**, 6225–6230, 1978.

Strobel, D. F., M. E. Summers, R. M. Bevilaqua, M. T. DeLand, and M. Allen, Vertical Constituent Transport in the Mesosphere, *J. Geophys. Res.*, **92**, 6691–6698, 1987.

Summers, M. E., R. R. Conway, D. E. Siskind, R. M. Bevilaqua, and S. E. Zasadil, Mesospheric HO_x photochemistry: Constraints from recent satellite measurements of OH and H_2O, *Geophys. Res. Lett.*, **23**, 2097–2100, 1996.

Summers, M. E., R. R. Conway, D. E. Siskind, M. H. Stevens, D. Offermann, M. Riese, P. Preuse, D. F. Strobel, and J. M. Russel III, Implications of satellite OH observations for middle atmospheric H_2O and ozone, *Science*, **277**, 1967–1970, 1997a.

Summers, M. E., D. E. Siskind, R. R. Conway, S. E. Zasadil, and D. F. Strobel, The seasonal variation of middle atmospheric CH_4 and H_2O with a new chemical dynamical model, *J. Geophys. Res.*, **102**, 3503–3526, 1997b.

Summers, M. E., R. R. Conway, C. R. Englert, D. E. Siskind, M. H. Stevens, J. M. Russel III,L. L. Gordley, and M. J. McHugh, Discovery of a Water Vapour Layer in the Arctic Summer Mesosphere: Implications for Polar Mesospheric Clouds, *Geophys. Res. Lett.*, **28**, 3601–3604, 2001.

Sun, C., and C. Levoy, Ozone Variability in the Equatorial Middle Atmosphere, *J. Geophys. Res.*, **95**, 13,829–13,849, 1990.

Tinsley, B. A., The diurnal variation of atomic hydrogen, *Planet. Space Sci.*, **21**, 686–691, 1973.

Thomas, R. J., C. A. Barth, and S. Solomon, Seasonal Variations of Ozone in the Upper Mesosphere and Gravity Waves, *Geophys. Res. Lett.*, **11**, 673–676, 1984.

Thomas, R. J., Seasonal Ozone Variations in the Upper Mesosphere, *J. Geophys. Res.*, **95**, 7395–7401, 1990.

Thomas, R. J., Atomic Hydrogen and Atomic Oxygen Density in the Mesopause Region: Global and Seasonal Variations Deduced From Solar Mesosphere Explorer Near-Infrared Emissions, *J. Geophys. Res.*, **95**, 16,457–16,476, 1990.

Thomas, G. E., Mesospheric clouds and the physics of the mesopause region, *Rev. Geophys.*, **29**, 553–575, 1991.

Thomas, G. E., and Vidal-Madjar, Latitude variation of exospheric hydrogen and the polar wind, *Planet. Space Sci.*, **26**, 837, 1978.

Tsou, J.-J., J. J. Olivero, and C. L. Croskey, Study of variability of mesospheric H_2O during spring 1984 by ground-based microwave radiometric observations, *J. Geophys. Res.*, **93**, 5255–5266, 1988.

Ulwick, J. C., K. D. Baker, M. C. Kelley, B. B. Balsley, and W. L. Ecklund, Comparison of simultaneous MST radar and electron density probe measurements during STATE, *J. Geophys. Res.*, **93**, 6989–7000, 1988.

U. S. Standard Atmosphere 1976, U. S. Governement Printing Office, Washington, D. C. 20402, Stock No. 003-017-00323-0

von Cossart, G., J. Fiedler, and U. von Zahn, Size distributions of NLC particles as determined from 3-color observations of NLC by ground-based lidar, *Geophys. Res. Lett.*, **26**, 1513–1516, 1999.

von Zahn, U., J. Höffner, V. Eska, and M. Alpers, The mesopause altitude: Only two distinctive levels worldwide?, *Geophys. Res. Lett.*, **23**, 3231–3234, 1996.

von Zahn, U., G. von Cossart, and J. Fiedler, Tidal variations of noctilucent clouds measured at 69° N latitude by ground based lidar, *Geophys. Res. Lett.*, **25**, 1289–1292, 1998.

von Zahn, U., and J. Bremer, Simultaneous and common-volume observations of noctilucent clouds and polar mesosphere summer echoes, *Geophys. Res. Lett.*, **26**, 1521–1524, 1999.

Walcek, C. J., and N. M. Aleksic, A Simple but Accurate Mass Conservative, Peak-Preserving, Mixing Ratio Bounded Advection Algorithm with Fortran Code, *Atmos. Environ.*, **32**, 3863–3880, 1998.

Walcek, C. J., Minor flux adjustment near mixing ratio extremes for simplified yet highly accurate monotonic calculation of tracer advection, *J. Geophys. Res.*, **105**, 9335–9348, 2000.

Wayne, R. P., *Chemistry of atmospheres: an introduction to the chemistry of atmospheres of earth, the planets, and their satellites*, 2nd ed., Oxford University Press, Oxford, 1991.

Yang, H., E. Olaguer, and K. K. Tung, Simulation of the present day atmospheric ozone, odd nitrogen, chlorine and other species using a coupled 2-d model in isentropic coordinates, *J. Atmos. Sci.*, **98**, 442–471, 1991.

Acknowledgement

I would like to thank many colleagues for the time we worked together at the IAP.
Dr. G. Sonnemann for his very helpful assistance and collaboration in atmospheric chemistry and related fields.
Dr. C. Kremp for supply and assistance with the first version of the CTM and the work on the photolysis rates.
Dr. U. Berger for many discussions about COMMA which provided the insight for the new formulation of the diffusion module and for providing the initial data from COMMA-IAP for the CTM.
Prof. Dr. U. von Zahn and Prof. Dr. F.-J. Lübken as the directors of the IAP for their support and helpful discussions.
The members of the "optics" group, especially Prof. Dr. G. von Cossart, Dr. M. Alpers, Dr. J. Höffner, Dr. J. Schneider and many others. H. Körnich for many discussions about Grads and Unix, Dr. E. Becker, Dr. U. Achatz, Dr. M. Zecha, Dr. P. Hoffmann and other of the "theory" and "radar" groups.
R. Mehl, as the head of the library, for support with literature and encouraging. T. Linow and staff for support with hard- and software.
Most of all I want to thank my family ;-) .
This work was supported by the German Research Community DFG, grants So 268/3-1 and -2.